Fusobacterium nucleatum: Effects on Cancer and Oral Epithelial Cell PD-L1 Expression and Cell Viability

Inauguraldissertation

zur Erlangung des Grades eines Doktors der Zahnmedizin

des Fachbereichs Medizin

der Justus-Liebig-Universität Gießen

vorgelegt von Yuxi Zhou

aus Hunan, P.R. China

Giessen 2025

Aus dem Fachbereich Medizin der Justus-Liebig-Universität Gießen

Gutachterin: PD Dr. Gröger, Sabine

Gutachter: Prof. Dr. Gattenlöhner, Stefan

Tag der Disputation: 09.07.2025

To my family and loved ones

Abbreviations

Abbreviation	Definition
A. actinomycetemcomitans	*Aggregatibacter actinomycetemcomitans*
ADAM	A Disintegrin and Metalloproteinase
APCs	Antigen-presenting cells
ASC	Apoptosis-associated speck-like protein containing a C-terminal caspase activation and recruitment domain
APO	Adverse pregnancy outcome
ASP	Apoptosis-associated speck-like protein
BHI	Brain-heart infusion
CmpA	Coaggregation mediating protein A
CRC	Colorectal cancer
CTLA-4	Cytotoxic T-lymphocyte-associated protein 4
CTL	Cytotoxic T lymphocytes
DAMPs	Damage-associated molecular patterns
DMEM	Dulbecco's minimal essential medium
ECL	Enhanced Chemiluminescent
EGFR	Epidermal growth factor receptor
EMT	Epithelial–mesenchymal transition
ERK	Extracellular regulated protein kinases
FadA	Fusobacterial adhesion
FAD-I	*Fusobacterium*-associated defensing inducer
Fap2	Fusobacterium adhesin protein 2
F. nucleatum	*Fusobacterium nucleatum*
GFs	Gingival fibroblasts
HAT	Histone acetyltransferases
hBD	Human beta-defensin
HDAC	Histone deacetylases
HMGB1	High-mobility group box-1
HIF-1α	Hypoxia-induced transcription factor 1α
HNSCC	Head and neck squamous cell carcinoma
HSP	Heat shock protein

IBD	Inflammatory bowel disease
IL	Interleukin
JAK	Janus kinase
KCs	Keratinocytes
LAG3	Lymphocyte activation gene 3
LPS	Lipopolysaccharides
MMPs	Matrix metalloproteinase
MOI	Multiplicity of infection
MyD88	Myeloid differentiation primary response 88
NALP	Neutrophilic alkaline phosphatase
NF-κB	Nuclear factor kappa-light-chain-enhancer of activated B cells
NLRP	Nucleotide-binding oligomerization domain-like repeat protein
NLRX1	Nucleotide-binding domain and leucine-rich-repeat-containing family member X1
NSCLC	Non-small cell lung cancer
OMVs	Outer membrane vesicles
OSCC	Oral squamous cell carcinoma
PD-L1	Programmed death-ligand 1
P. gingivalis	*Porphyromonas gingivalis*
PHGK	Primary human gingival keratinocytes
PI	Popidium iodide
PTEN	Phosphatase and tensin homolog
RA	Rheumatoid arthritis
RAGE	Receptor of advanced glycation end-product
ROS	Reactive oxygen species
SCC	Squamous cell carcinoma
STAT	Signal transducer and activator of transcription
TIM-3	T-cell immunoglobulin 3
TIGIT	T-cell immunoreceptor with immunoglobulin and ITIM domains
TLRs	Toll-like receptors
TME	Tumor microenvironment

TNF-α	Tumor necrosis factor-α

Contents

1. Introduction

Fusobacterium nucleatum (*F. nucleatum)*, a Gram-negative obligate anaerobic bacterium, belongs to the genus *Fusobacterium* and is one of the most abundant species in the oral cavity in both diseased and healthy individuals[1]. Recently it has gained significant attention due to its association with various human diseases. *F. nucleatum* is implicated in various forms of periodontal diseases, including the mild reversible form of gingivitis and the advanced irreversible forms of periodontitis[1]. The prevalence of *F. nucleatum* increases with the severity of the disease, progression of inflammation, and pocket depth[2]. Moreover, emerging evidence suggests a potential role of *F. nucleatum* in systemic diseases, such as colorectal carcinoma (CRC), oral squamous cell carcinoma (OSCC), pancreatic, esophageal, and breast cancer[3]. Numerous studies investigated the mechanisms by which *F. nucleatum* contributes to disease pathogenesis. It can provoke pro-inflammatory responses and co-aggregation with other microorganisms, disrupt epithelial barrier integrity, activate cell proliferation, migration, and invasion, and modulate host immune responses[3; 4]. The understanding of *F. nucleatum*'s role in disease development and its intricate interactions with the host continuously evolves. This study aimed to unravel the impact of different strains of heatt-killed *F. nucleatum* on OSCC cells, CRC cells, and primary human gingival keratinocytes (PHGK) through immune checkpoint programmed death-ligand 1 (PD-L1) and cell proliferation to provide insights into the mechanisms of tumor immune evasion and potential therapeutic targets.

1.1 *Fusobacterium nucleatum*

In a dental plaque biofilm, *F. nucleatum* plays a structurally supportive role as a bridge organism, connecting primary colonizers such as *Streptococcus* species to the predominantly anaerobic secondary colonizers to which it can also bind, including *Porphyromonas gingivalis* (*P. gingivalis*) and *Aggregatibacter actinomycetemcomitans* (*A. actinomycetemcomitans*)[5; 6]. It can co-aggregate with nearly all bacterial species involved in oral plaque formation, triggering an inflammatory response that ultimately results in attachment loss and the destruction of periodontal tissues[7; 8]. Moreover, *F. nucleatum* can bind to and transport non-invasive bacterial species into host cells, acting as a shuttle[9]. *F. nucleatum* also mediates necessary biofilm-organizing behavior and interactions with host cells by expressing numerous adhesins. The best characterized fusobacterial adhesin is RadD, which can bind the *Streptococcus* mutans adhesin SpaP to mediate the co-aggregation of these two bacteria and support biofilm organization[5; 10; 11]. *F. nucleatum* is linked to periodontal diseases. Moreover, an elevated abundance of *F. nucleatum* has been reported in association with various cancers(Figure 1)[12]. *F. nucleatum* possesses several virulence factors that contribute to its pathogenicity and ability to cause disease.

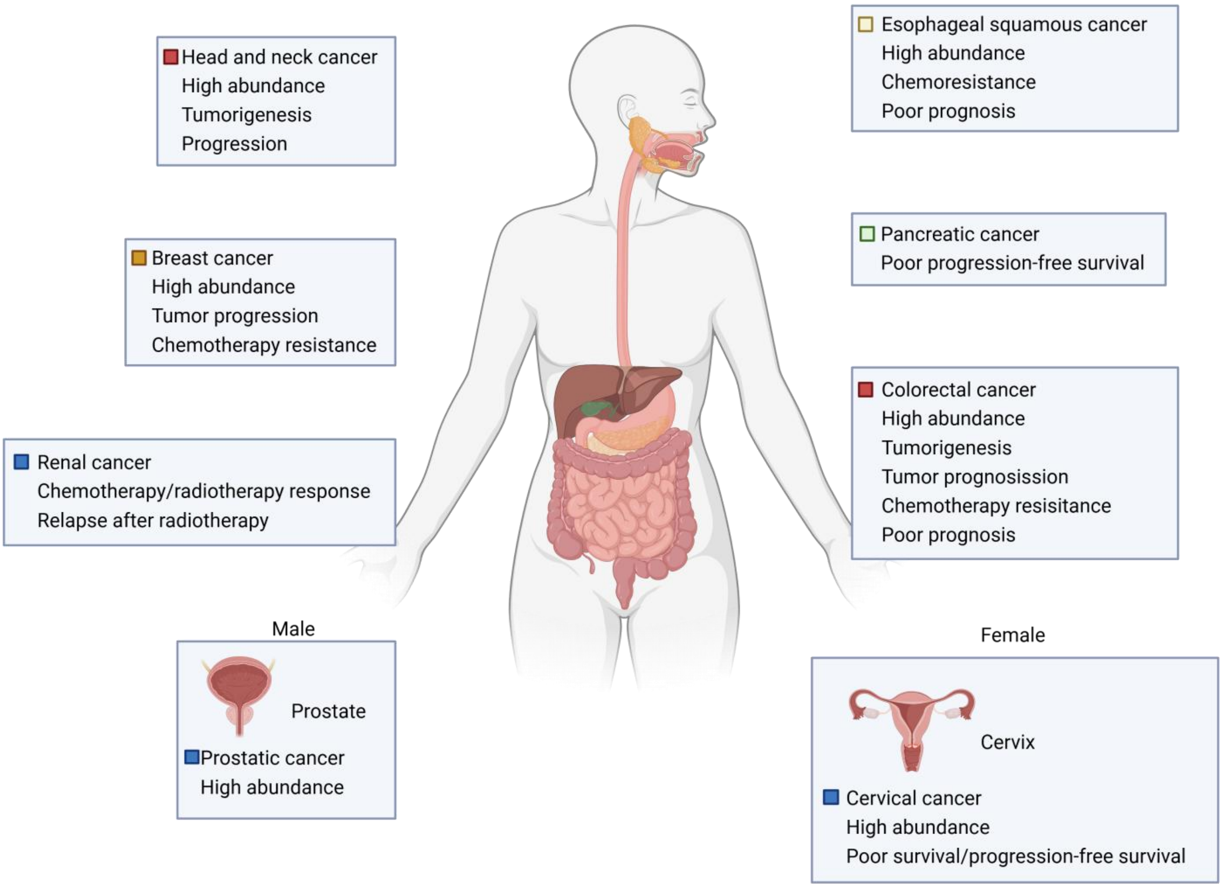

Figure 1. Different cancers associated with *F. nucleatum*[12].

Reproduced from "Fusobacterium nucleatum: a new player in regulation of cancer development and therapeutic response", by Zhao Tet al., *Cancer Drug Resist*. 2022, 5(2):436-450. Copyright 2022 by Zhao T, Wang X, Fu L, Yang K (https://creativecommons.org/licenses/by/4.0/).

1.1.1 Adhesins

F. nucleatum mediates important biofilm-organizing behavior and interactions with host cells through the expression of numerous adhesins, which promote colonization of various host tissues, such as oral epithelial cells and other bacteria. This enables the formation of polymicrobial biofilms. The repertoire of adhesins expressed by *F. nucleatum* includes the outer membrane protein RadD adhesin (RadD), the putative accessory protein Aid1, Fusobacterial adhesion (FadA), the porin FomA, the outer membrane protein coaggregation mediating protein A (CmpA). and Fusobacterium adhesin protein 2 (Fap2).

RadD functions as a facilitator of bacterial binding to host cells and extracellular matrix components, allowing co-aggregation between *F. nucleatum* and *Streptococcus mutans* through its interaction with the SpaP adhesin. This interaction contributes to the organization of biofilms[5; 10; 11]. Another co-aggregation phenomenon involving *F. nucleatum* has been identified with *Streptococcus gordonii* (*S. gordonii)*, mediated by CmpA[13]. In particular, FadA stands out as the only adhesin known to bind to host cells and remains the most extensively studied virulence factor in *F. nucleatum*[14]. FadA plays a critical role in eliciting tumorigenic responses, as demonstrated by the inhibition of such responses in colorectal cancer by the use of a synthetic peptide that prevents FadA from binding to E-cadherin[15]. FadA binding to E-cadherin leads to activation of the ß-catenin signaling pathway and differential regulation of inflammatory and oncogenic responses[15-18]. In addition, FadA binds to VE-cadherin, a cell junction molecule found on endothelial cells, leading to the repositioning of VE-cadherin away from cell-cell junctions[19]. Another small hypothetical protein characterized in *F. nucleatum* interspecies interactions is Aid1, which significantly facilitates RadD-mediated interaction with oral *streptococci*[20]. Fap2, an outer membrane protein expressed by *F. nucleatum*, functions as an adhesin by selectively interacting with receptors on host cell surfaces. In the oral cavity, Fap2 plays a pivotal role in co-adhesion with neighboring bacteria, bridging different species and increasing the diversity and stability of developing plaque[21]. In addition, Fap2 has the ability to bind Gal-GalNAc, a polysaccharide that is frequently overexpressed in colorectal cancer[21]. Besides, Fap2 can bind with T-cell immunoreceptor with immunoglobulin and ITIM domains (TIGIT), which inhibit natural killer (NK) cell cytotoxicity and T cell activation[22]. Besides Fap2, the nonspecific pore protein FomA, constituting about 30% of outer membrane proteins, contributes to cell adhesion and immunogenicity[23-25]. Martin-Gallausiaux et al. (2020) showed that FomA, present on extracellular vesicles from *F. nucleatum*, may be involved in nuclear factor kappa light chain enhancer of activated B cells (NF-κB) activation through toll-like receptor 2 (TLR2) signaling[23]. Figure 2 summarizes the structure and representative components of *F. nucleatum.*

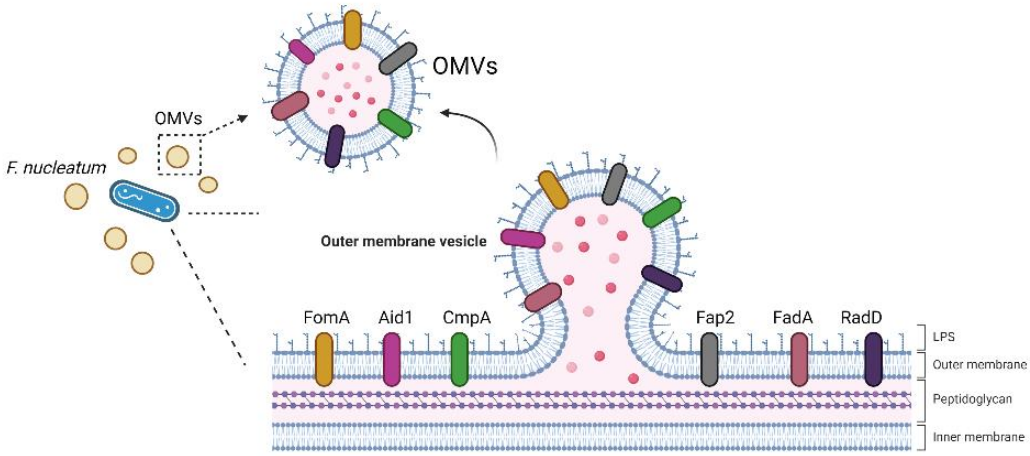

Figure 2. Virulence Factors and Adhesins of *Fusobacterium nucleatum*.

The bacterium is composed of cell membrane and genetic material. The outer layer of the cell membrane contains fimbriae, proteins, and channels. Notably, the prominent virulence factors of *F. nucleatum* are mainly derived from its intrinsic structural components, namely lipopolysaccharide (LPS), and fimbriae, and its secretory components, such as gingipains and outer membrane vesicles (OMVs). The repertoire of adhesins expressed by *F. nucleatum* includes the outer membrane protein RadD adhesin (RadD), the putative accessory protein Aid1, Fusobacterial adhesion (FadA), the porin FomA, the outer membrane protein coaggregation mediating protein A (CmpA) and Fusobacterium adhesin protein 2 (Fap2).CmpA: coaggregation mediating protein A; FadA: Fusobacterial adhesion;

1.1.2 Biofilm formation and polymicrobial interaction

F. nucleatum has the ability to form biofilms, which are complex communities of bacteria encased in a self-produced matrix. Biofilms provide protection against host immune defenses and antimicrobial agents, thereby facilitating the persistence of the bacteria in the oral cavity and at various sites of infection. The ability of *F. nucleatum* to interact with a wide range of bacteria is widely recognized. It exhibits adherence to other oral bacteria, thereby facilitating the formation of mixed-species biofilms. These polymicrobial communities contribute significantly to the initiation and progression of oral infections, including periodontitis. *F. nucleatum* acts as a central 'bridging' organism within naturally occurring plaque, co-aggregating with initial, early, and late colonizers such as *Streptococcus* species (via RadD), *P. gingivalis* (via Fap2), *Treponema denticola* and *A. actinomycetemcomitans*[3; 6]. These coaggregations confer resistance to displacement by saliva and gingival crevicular fluid, as shown in Figure 3.

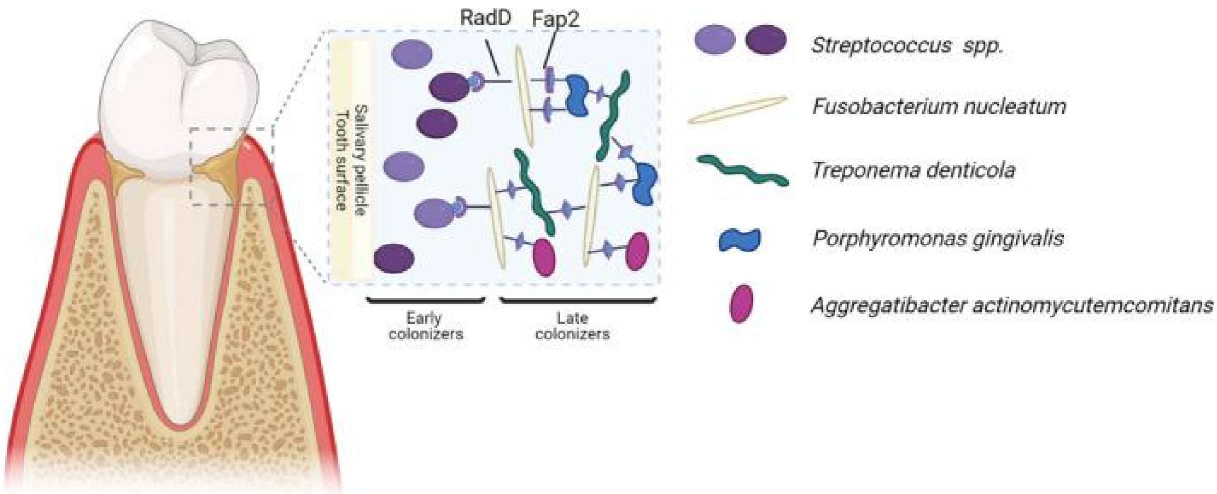

Figure 3. *F. nucleatum* acts as a bridging organism in dental plaques[3].

This diagram illustrates how *F. nucleatum* act as a “bridging” organism. Reprinted from “Fusobacterium nucleatum and cancer”, Copyright 2022 by Alon-Maimon T, Mandelboim O, Bachrach G. *Periodontology 2000* published by John Wiley & Sons Ltd.

1.1.3 Inflammatory response modulation and immune evasion

F. nucleatum has the ability to induce an inflammatory response in host tissues through the release of several molecules, including lipopolysaccharides (LPS), outer membrane proteins , and virulence factors. These bacterial components stimulate the production of pro-inflammatory cytokines and chemokines, which can contribute to tissue damage, chronic inflammation, and disease progression.

F. nucleatum exhibits potent stimulation of inflammatory cytokines such as Interleukin (IL)-6, IL-8, and tumor necrosis factor-α (TNF-α) [1; 26]. The binding of *F. nucleatum* to NK cells activates inflammatory responses associated with periodontal disease[27]. Moreover, infection of gingival epithelial cells by *F. nucleatum* also leads to activation of NF-κB, which translocates to the nucleus and stimulates the expression of pro-inflammatory genes, including those encoding pro-IL-1β [28; 29]. *F. nucleatum*-derived LPS is responsible for immune activation at the cellular level in periodontal disease, resulting in inflammatory and cytokine-mediated deleterious lesions in the gingiva[16; 30]. This activation further drives the production of inflammatory cytokines such as IL-1α, IL-1β, IL-6, IL-8, and matrix metalloproteinases (MMPs) through NF-κB activation and nuclear translocation[16; 31-33]. Krisanaprakornkit et al. (2000) demonstrated that human beta-defensin (hBD) 2 and IL-8 can be induced by LPS extracted from the cell wall of *F. nucleatum* and TNF- α [34]. Additionally, *F. nuleatum* can also enhance the production of TNF-α from gingival epithelial cells and macrophages, which plays a role in the generation of free radicals during sepsis[32; 35].

NLRP10, the smallest human nucleotide-binding oligomerization domain-like repeat protein (NLRP), has both anti-inflammatory and pro-inflammatory functions[36]. It is further involved in activating the extracellular regulated protein kinases (ERK) signaling pathway in human epithelial cells, when infected with *F. nucleatum* and it augments the pro-inflammatory cytokine IL-1 α levels[36].

TLRs are key pattern recognition receptors (PRRs) that recognize F. nucleatum and activate pro-inflammatory signaling pathways[16]. Specifically, TLR2 and neutrophilic alkaline phosphatase (NALP) 2 mediate the induction of hBD2 and hBD3 in oral epithelial cells following *F. nucleatum* infection[37; 38][39]. The *Fusobacterium*-associated defensing inducer (FAD-I) serves as the primary mediator of hBD2 induction in human oral epithelial cells by *F. nucleatum*, acting through both TLR-1/2 and TLR-2/6 pathways[40]. Beyond TLR activation, *F. nucleatum* also engages nucleotide-binding oligomerization domain (NOD)-like receptors (NLRs), particularly NLRX1, which promotes the formation of the NLRP3 inflammasome. This interaction results in the activation of, caspase-1, leading to the processing and release of IL-1β in gingival epithelial cells[28; 42]. Notably, *F. nucleatm* uniquely activates the inflammasome in gingival epithelial cells without the presence of exogenous damage-associated molecular patterns (DAMPs) such as ATP [28]. However, it has been shown to induce the release of other DAMPs involved in inflammasome activation, including HMGB1 and apoptosis-associated speck-like protein (ASP), with a time course similar to that of caspase-1 activation[28; 30; 43]. HMGB1, a DNA-binding nuclear protein, is actively released following cytokine stimulation as well as passively during cell death and has been implicated in several inflammatory disorders, cell adhesion, and migration [44]. It interacts with other molecules, including TLR ligands and cytokines, and activates cells through the differential engagement of multiple surface receptors, including TLR2, TLR4, and receptor of advanced glycation end-product (RAGE), leading to the activation of downstream pathways such as MAPKs, NF-κB, phosphatidylinositol 3-kinase (PI3K)/Akt, and JAK/STAT[44][30]. The interaction between HMGB1 and RAGE may contribute to oral inflammation and oral carcinogenesis[30].

Beyond its inflammatory effects, *F. nucleatum* employs various evasion strategies to interfere with immune cell activity, impair the production of pro-inflammatory cytokines, and modulate host immune signaling pathways, thereby facilitating its ability to evade clearance and establish chronic infections. One key mechanism involves the adhesin Fap2, which interacts with immune checkpoint molecules to induce apoptosis in lymphocytes[48; 49]. Kostic et al. (2013) demonstrated in an $Apc^{Min/}$+ mouse model of intestinal tumorigenesis that *F. nucleatum* increase tumor multiplicity and recruit tumor-infiltrating myeloid cells[50]. Furthermore, *F. nucleatum* can increase miR-21 level and decrease phosphatase and tensin homolog (PTEN) level in pancreatic cancer cells[51]. PTEN, a widely known tumor suppressor, plays a crucial role in the anti-cancer immune system. In addition, PTEN-deficient tumors have been associated with increased expression of indoleamine 2,3-dioxygenase 1 and PD-L1, which are known to dampen the activity of cytotoxic immune cells responsible for eliminating cancer cells[52]. Furthermore, *F. nucleatum* has been implicated in polymicrobial interactions that enhance pathogenicity. Coinfection with *F. nuleatum* can enhance the adhesion and invasion of *P. gingivalis* and *A. actinomycetemcomitans* to human gingival epithelial cells, as well as inhibition of the host's innate immune response[53].

1.1.4 Toxin production

F. nucleatum produces toxins, including ammonium, butyrate, and proteases. Bartoldet al. (1991) reported that many subgingival microflora release ammonium and butyrate, which inhibit fibroblast proliferation and potentially impede the process of tissue repair following bacterially induced periodontal destruction[54]. According to Bachrach et al. (2004), the 65 kDa protease identified in *F. nucleatum* has the ability to degrade natural proteins, which could potentially contribute to the nutritional and pathogenic functions of these periodontal microorganisms[55]. Enzymatic degradation of extracellular matrix proteins by bacterial enzymes may contribute to the detrimental breakdown of periodontal tissues. Additionally, the degradation of IgA by these bacteria may aid in evading the host immune system[55].

These toxins contribute to the pathogenic effects of *F. nucleatum* in various disease conditions.

1.1.5 Outer membrane vesicles

Outer membrane vesicles (OMVs) are small, spherical, bilayer lipid membrane nanostructures structures released by many Gram-negative bacteria, including *F. nucleatum*[56]. OMVs play a crucial role in bacterial communication, virulence, and interaction with the host. It is considered an important vehicle for the delivery of various bioactive molecules and virulence factors. OMVs of *F. nucleatum* usually consist of antigenic components capable of activating TLRs present on epithelial cells and immune cells[57]. Activation of TLRs triggers the activation of the NF-κB pathway, leading to the release of proinflammatory cytokines. According to a study by Engevik et al. (2021), *F. nucleatum subsp. polymorphum* was found to release OMVs that activate TLR4 and NF-κB, resulting in the stimulation of proinflammatory signals *in vitro*[57]. Understanding the role of *F. nucleatum* OMVs is crucial for unraveling the complex interactions between this bacterium and its host, and may provide insights for the development of novel therapeutic strategies to combat *F. nucleatum*-associated infections.

1.2 Effects of *F. nucleatum* on host systemic health

F. nucleatum is correlated with several diseases outside of the oral cavity. Figure 1 illustrates the diseases in which *F. nucleatum* can be isolated from clinical specimens. Detailed descriptions are below.

1.2.1 Adverse pregnancy outcome

Adverse pregnancy outcome (APO) encompasses a wide range of conditions, including preterm labor, chorioamnionitis, preterm premature rupture of membranes, preeclampsia, miscarriage, intrauterine growth retardation, low birth weight, stillbirth, neonatal sepsis, etc[58]. *F. nucleatum* stands out as one of the most prevalent species and the most prevalent oral species implicated in APO[59]. A case report presented evidence of a term stillbirth caused by oral *F. nucleatum*, providing the first instance in humans where the bacterium was found to originate from the mother's subgingival plaque[60]. The remarkable invasive properties of *F. nucleatum* facilitate its dissemination to various placental and fetal compartments, possibly explaining the frequent detection of this bacterium in paired samples of amniotic fluid and umbilical cord blood[61]. This hypothesis is supported by the results of animal studies. Han et al. (2004) intravenously injected *F. nucleatum* into pregnant CF-1 mice resulted in premature delivery, stillbirths, and non-sustained live births. The bacterium was initially detected in the blood vessels, then crossed the endothelium, proliferated in the surrounding tissues, and finally colonized the amniotic fluid[62]. The inflammatory response in the placenta exhibited a distinct spatiotemporal pattern. Activation of NF-κB was first observed in maternal endothelial cells, followed by its activation in decidual cells surrounding the endothelium, accompanied by induction of inflammatory cytokines and chemokines[63].

1.2.2 Atherosclerotic disease

Recently, numerous studies have confirmed that the development of cardiovascular disease is closely related to periodontal pathogens. Periodontal pathogens can evade host immune defense and reach and colonize atherosclerotic plaques and thrombi through blood circulation[64]. A study has shown that the heat-shock protein GroEL of *F. nucleatum* triggers atherosclerotic risk factors both *in vivo* and *in vitro*, providing evidence for the link between periodontal pathogens and atherosclerosis[65].

1.2.3 Rheumatoid arthritis

Rheumatoid arthritis (RA) is an autoimmune disease characterized by chronic inflammation. Periodontitis and RA share some common pathogenic mechanisms, such as chronic inflammation caused by inflammatory cytokines, connective tissue breakdown, and bone loss, and periodontal pathogens are also involved in the pathogenesis of RA[66]. Periodontal pathogens can enter the circulation, colonize tissues and organs, and induce an autoimmune response that promotes the development of rheumatoid arthritis. Ebbers et al. (2018) found that oral inoculation of *F. nuleatum* accelerated the subsequent development and progression of arthritis in mice[67]. Hong et al. (2023) observed that *F. nucleatum* was enriched in RA patients and positively associated with RA severity[68]. Observation of OMVs containing

FadA and increased expression of Rab5a-YB-1, a key regulator of inflammatory mediators, were observed in RA patients compared to the control[68].

1.2.4 Inflammatory bowel disease

Inflammatory bowel disease (IBD) is closely associated with oral disease. As early as 1945, Bergen demonstrated that a group of bacteria present in dental lesions, non-hemolytic streptococci, could cause colitis that rapidly resolved when the dental lesions were removed and the patient was given an appropriate amount of autologous vaccine[69]. Intestinal dysbiosis plays an important role in the pathogenesis of IBD, and many highly invasive strains of *F. nucleatum* have been detected in the intestine of patients with IBD[70; 71]. IBD is a risk factor for colorectal cancer, thus *F. nucleatum* infection in the intestine may be a common pathogenesis for both diseases[1].

1.2.5 Other organ inflammations and abscesses

F. nucleatum is associated with a wide range of infections and abscesses including infections of the head and neck, brain, lungs, abdomen, pelvis, bones, joints, and blood[1]. One study reported that *F. nucleatum* caused Lemierre's syndrome in a previously healthy 19-year-old male[72]. Moreover, *F. nucleatum* has also been detected in a pyogenic liver abscess site and infective appendicitis[73; 74].

1.2.6 *F. nucleatum* and its impact on tumorigenesis in OSCC and CRC

The concept of a microbial role in cancer is not new — bacteria, parasites, and viruses are all associated with potentiating cancer[5]. Around 15-20% of all cancer cases are preceded by infection, chronic inflammation, or autoimmunity at the same tissue or organ site[75-77]. *F. nucleatum*'s ability to modulate the tumor microenvironment and contribute to cancer progression is increasingly recognized, with mechanisms involving immune evasion, inflammation, and modulation of key signaling pathways.

Head and neck squamous cell carcinoma (HNSCC), derived from the squamous epithelium of the upper aerodigestive tract, is the most common malignancy in the head and neck region with over 600,000 new cases diagnosed every year[78]. The majority of HNSCCs are cancers of the oral cavity and oropharynx[16]. OSCC remains a major cause of morbidity and mortality[79]. An estimated 354,864 new cases and 177,384 deaths from oral cavity cancer (including lip cancer) occurred in 2018 worldwide[80]. Oral cancer and epithelial precursor lesions have been associated with bacteria belonging to various genera, including *Fusobacterium*, *Veillonella*, *Actinomyces*, *Clostridium*, *Haemophilus*, and *Enterobacteriaceae*[81]. *F. nucleatum* has been reported that it likely plays a role in the development of gastrointestinal cancer and oral cancer[82]. Chang et al. (2019) study found that *P. gingivalis* and *F. nucleatum* were present in higher amounts in OSCC tissue compared to normal tissue [83], consistent with Nagy's (1998) and Schmidt's (2014) results[81; 84]. Studies have provided epidemiological evidence linking *F. nucleatum* with OSCC, further confirming its potential as a carcinogen.[85; 86]. Several studies reported that *F. nucleatum* can induce the production of inflammatory cytokines, as well as cell proliferation and cellular invasion, in OSCC by various mechanisms. Such *F. nucleatum*-driven inflammation contributes to disease progression in a model of oral tumorigenesis[29]. By utilizing a murine model of periodontitis-associated oral tumorigenesis, Gallimidi et al. (2015) reported that chronic bacterial infection promotes OSCC and that augmented signaling along the IL-6-STAT3 axis underlies this effect[29]. *P. gingivalis* and *F. nuleatum* stimulate tumorigenesis via direct interaction with oral epithelial cells via TLRs[29]. Moreover, *F. nucleatum* could potentially enhance cancer cell invasiveness, survival, and epithelial-mesenchymal transition (EMT) when present in the oral tumor microenvironment[87].

CRC is the third most commonly diagnosed malignancy and the fourth leading cause of cancer-related deaths worldwide[88]. It remains associated with a poor prognosis and low rates of long-term survival in patients with advanced disease[89]. However, the 5-year survival rate of patients treated at the early stages of CRC is encouraging[89]. The exact cause of CRC is not fully understood, but it is believed to result from a combination of genetic and environmental factors, including age, family history, lifestyle choices (such as smoking, diet, and physical activity, and certain medical conditions (such as inflammatory bowel disease). *F. nucleatum* has been found to be enriched in CRC tissues[90]. The presence of *F. nucleatum* DNA in CRC tissue is associated with shorter survival and may serve as a prognostic biomarker[91].

Moreover, *F. nucleatum* has been linked to the CRC recurrence, and its high abundance contributes to the development of chemoresistance[92]. The same strains of *F. nucleatum* have been detected in CRC and saliva specimens of CRC patients, suggesting an oral origin for *F. nucleatum* in CRC [93]. Mechanistically, *F. nucleatum*'s adaptation to oral life influences colorectal tumorigenesis. It recognizes Gal-GalNAc, which is overexpressed in CRC, through the Gal-GalNAc lectin Fap2[21]. *F. nucleatum* can activate the β-catenin and Wnt pathway by binding the adhesion protein FadA to the E-cadherin on the surface of CRC cells[94]. *F nucleatum* also activates TLR4 signaling to myeloid differentiation primary response 88 (MyD88), leading to NF-κB activation and increased expression of microRNA21[95]. This mechanism enhances the proliferation and invasion of colon cancer cells. During tumor development, *F. nucleatum* induces a pro-inflammatory microenvironment and suppresses host immunity, thereby supporting CRC progression. Furthermore, during oncological treatment, *F. nucleatum* has the potential to heighten the risk of relapse and promote chemoresistance by interfering with specific microRNAs critical for autophagy regulation. Recent research has demonstrated that *F. nucleatum* orchestrates a complex interplay between TLR4-MyD88 signaling, miR18a*, miR4802, and the ULK1/ATG7 autophagy network, exerting a biocontrol effect on CRC chemoresistance[92]. Additionally, *F. nucleatum* can migrate from the oral cavity to CRC sites, compromising the therapeutic efficacy of radiotherapy and adversely impacting the overall prognosis of patients[96].

In summary, *F. nucleatum* plays a pivotal role in the tumorigenesis of both OSCC and CRC. By inducing chronic inflammation, immune modulation, and activation of key oncogenic pathways, *F. nucleatum* contributes to cancer progression. Given the significant role of *F. nucleatum* in altering the tumor microenvironment, it is crucial to understand the immune evasion mechanisms that are often exploited by tumors. One key player in this process is PD-L1, an immune checkpoint molecule that plays a central role in tumor immune evasion.

1.3 PD-L1

In 1992, Ishida et al. found that the activation of the PD-1 gene may be associated with classical types of programmed cell death[97]. It was not until 1999 that a similar B7 homolog (now called PD-L1) was discovered as an inhibitor of human T-cell responses *in vitro*[98]. PD-L1, also known as immune-regulatory B7-H1 receptor, plays an important role in the cell-mediated immune response. It is expressed on macrophages, antigen-presenting cells (APCs) like dendritic cells (DCs), and is induced on activated T cells, B cells, smooth muscle cells, endothelial cells, and epithelial cells under inflammatory conditions[99-104]. Under normal conditions, the interaction of PD-1 and PD-L1 may play a role in preventing autoimmunity and modulating inflammatory responses in target organs or providing autoimmune protection in peripheral tissues[105]. The presence of PD-L1 in healthy tissues suggests a role in preventing autoimmunity and modulating inflammatory responses in target organs[106]. PD-L1 limits T cell activity in peripheral tissues in the inflammatory response and limits autoimmune disease[107]. Groeger et al. (2017) proved that *P. gingivalis* can up-regulate PD-L1 expression in SCC-25 as well as primary and immortalized human gingival keratinocytes[109; 110]. It was demonstrated that the total membrane fraction of *P. gingivalis* induced the highest up-regulation in PD-L1 expression, followed by the outer and inner membrane, whereas cytosolic proteins and LPS did not[109]. Adel-khattab et al. (2021) found that peptidoglycan (PDG) of *P. gingivalis* plays a major role in PD-L1 up-regulation in colon cancer cells[111]. When infected with viable or heat-killed *P. gingivalis* membrane fractions, upregulation of PD-L1 has also been demonstrated in prostate cancer cells[112]. Furthermore, isolated PDG from *P. gingivalis* was found to induce PD-L1 upregulation, and this upregulation was mediated through the NOD1/NOD2 signaling pathway[112]. These results indicate that epithelial PD-L1 expression is induced by inflammatory stimuli.

1.3.1 PD-L1 in cancer

However, PD-L1 overexpression is seen in a variety of malignancies. Groeger et al. (2017) examined 15 tissue samples from patients with OSCC and observed the expression of B7-H1 and B7-DC in OSCC *in vivo*[113]. Tumor cells use the PD-1/PD-L1 axis to suppress immunity and evade immune surveillance, thereby enhancing tumorigenesis and tumor aggressiveness[114].

1.3.1.1 PD-L1 overexpression

PD-L1 expression in cancer cells is subject to complex regulations, possibly due to aberrant activation of signaling pathways, genetic alterations, or regulatory deficits in transcriptional, translational, or post-translational stages[105]. (Figure 4.)

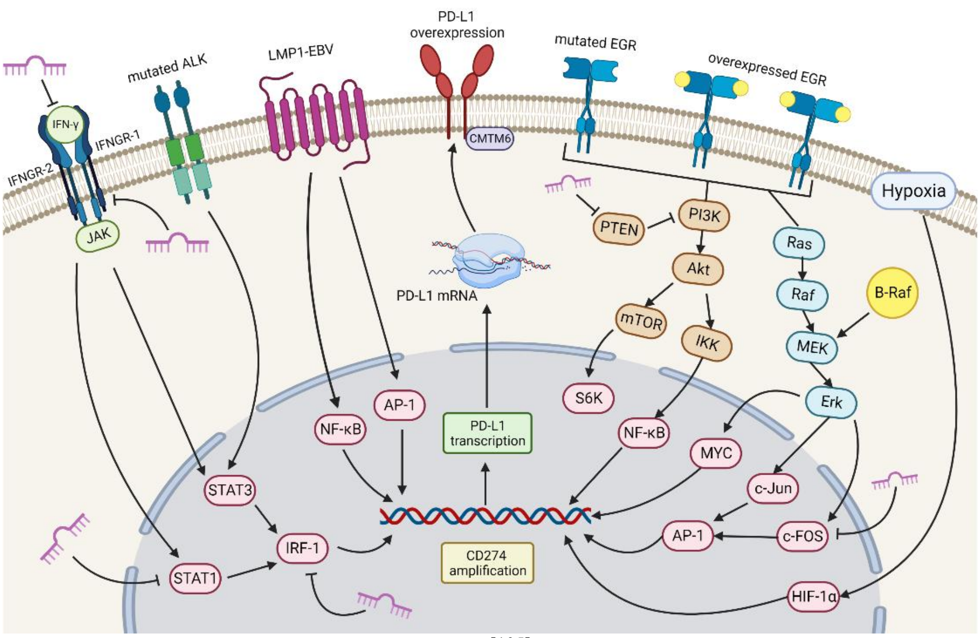

Figure 4. Mechanisms of overexpression of PD-L1[105].

miRNAs and their respective targets (IFN-γ, IFNGR-1, PD-L1, PTEN, c-Fos, STAT1, IRF-1) regulate PD-L1 production. Mutations in these miRNAs may cause a loss of function resulting in increased PD-L1 expression. 1 Mutations in PD-L1 upstream receptors may result in PD-L1 overexpression; 2 Epstein–Barr viral oncoproteins signaling may increase PD-L1 production; 3 overexpression of PD-L1 pathway receptors; 4 Amplification of the PD-L1 gene: CD274; 5 proteins stabilizing PD-L1; 6 overexpressed PD-L1. Figure modified, with permission, from Ref. 118 © 2019 John Wiley & Sons A/S.

1.3.1.2 Signaling pathways and transcriptional regulation

Various oncogenic pathways lead to PD-L1 overexpression. The MAPK/Erk, JAK/STAT, MyD88/IKK/NF-κB, and PI3K/Akt pathways are known to play a key role in promoting cell survival and proliferation and are also involved in immune evasion through the upregulation of PD-L1 (CD274) [115; 116]

MAPK signaling is one of the most well-defined pathways in cancer biology, and its over-activation is responsible for more than 40% of human cancer cases[117]. RNA sequencing analysis data from non-small cell lung cancer (NSCLCs) have revealed a correlation between CD274 gene expression in lung adenocarcinoma and the signaling pathways of IFN-γ, EGFR, and MAPK[118]. Specifically, it has been observed that the activation of IFN-γ, EGFR, and MAPK signaling is associated with increased CD274 gene expression[118]. It has been found that inhibiting the MAPK pathway using EGFR inhibitors like cetuximab and erlotinib, or MEK 1 and 2 inhibitors such as selumetinib, can effectively block the upregulation of CD274 mRNA and PD-L1 protein, as well as the membrane expression of PD-L1 induced by EGF and IFN-γ[118]. Bone marrow cells play a significant role in facilitating immune evasion by pancreatic cancer cells through the EGFR/MAPK signaling pathway, which regulates the expression of PD-L1 on tumor cells[119].

PTEN serves as a negative regulator of the PI3K/AKT pathway. Alterations in this pathway, along with a decrease or loss of PTEN expression, are observed in human SCC, indicating its significance in disease development[116]. Furthermore, in human glioma, the loss of PTEN has been associated with an increased expression of PD-L1[120]. The upregulation of miR-20b, -21, and -130b in CRC, leads to overexpression of PD-L1 in colorectal cancer by suppressing PTEN expression[121]. PTEN knockdown leads to significantly higher cell surface PD-L1 expression and PD-L1 transcripts[122]. LY294002 (PI3K inhibitor) reduced PD-L1 levels in gastric cancer cells[123].

Janus kinase (JAK) and signal transducer and activator of transcription (STAT) are the major signaling pathways mediating interferon-induced gene expression[124]. The JAK/STAT pathway plays a crucial role in cellular processes, including cell proliferation, migration, differentiation, and inflammation. Garcia-Diaz et al. (2017) reported that PD-L1 is mainly regulated by the type II interferon receptor singling pathway through JAK1 and JAK2, several STATs, and other modulators of the pathway and converged on the binding of IRF1 to the PD-L1 promoter[124]. Study has shown that intracellular JAK/STAT pathways are involved in the upregulation of PD-L1 in prostate cancer[125]. In NCSLC, PD-L1 and JAK2 genes were amplified simultaneously through the JAK-STAT signaling pathway, and PD-L1 protein expression was upregulated[126].

One of the most frequently mutated oncogenes in patients with NSCLC is the epidermal growth factor receptor (EGFR) gene. Recent reports have shown that EGFR-driven lung tumors suppress anti-tumor immunity by activating the PD-1/PD-L1 pathway to inhibit T-cell function and increase levels of pro-inflammatory cytokines[127].

While NF-κB is a well-known transcription factor involved in the regulation of PD-L1, the precise mechanisms underlying this regulation remain relatively unexplored. Upon stimulation with IFN-γ, the NF-κB transcription factor facilitates the upregulation of PD-L1 expression by transient phosphorylation of ERK1/2 and PI3K signaling pathways[128].

1.3.1.3 Inflammatory factors and cytokines

Inflammatory factors and cytokines, such as IFN-γ and TNF-α, have been widely reported to upregulate PD-L1 expression in various cell types. These factors are believed to promote PD-L1 expression directly or indirectly by activating related signaling pathways or transcription factors. The biological functions of IFN-γ include increasing antigen presentation and promoting Th1 differentiation, which leads to cellular immunity[129]. For instance, IL-17 and TNF-α upregulate PD-L1 expression in HCT116 cells via NF-κB and ERK1/2 signaling pathways individually but not synergistically[131]. Additionally, in OSCC, IL-10 concentrations in the tumor microenvironment directly correlate with PD-L1 levels in tumor-associated macrophages[132]. Hypoxia promotes tumor immune escape of cytotoxic T lymphocytes (CTL) through this mechanism[133]. Exposure of human or mouse cancer cells to hypoxia for 24 hours results in the up-regulation of PD-L1 in a manner dependent on hypoxia-induced transcription factor 1α (HIF-1α)[133].

1.3.1.4 Epigenetic regulation of PD-L1

Epigenetic regulation such as methylation and histone acetylation also determine the expression of PD-L1. DNA methylation typically occurs at cytosine residues within CpG dinucleotides, resulting in the addition of a methyl group. Hypermethylation of the PD-L1 gene promoter region can lead to transcriptional silencing and reduced PD-L1 mRNA expression in various malignancies[134; 135]. Micevic et al. (2019) found that hypermethylation of PD-L1 in melanoma was associated with reduced PD-L1 expression and shorter overall patient survival[136].

Histones are proteins around which DNA is wrapped, forming a structure known as chromatin. Specific histone modifications, such as acetylation, methylation, and phosphorylation, can either promote or inhibit PD-L1 gene transcription. Acetylation is the reversible modification of the lysine residue ε-amino group and is controlled by two groups of enzymes: histone acetyltransferases (HAT) and histone deacetylases (HDAC)[137]. HDAC inhibitors upregulate PD-L1 expression in melanoma[138]. HDAC3 overexpression inhibits PD-L1 expression, which largely reverses the inhibition of $CD3^{+}$T cell proliferation *in vitro*[139]. PD-L1 expression was significantly upregulated in MCF-7 and BT-549 cancer cells and in tumorspheres, a solid, spherical formation derived from the proliferation of a cancer stem/progenitor cell, and this upregulation was partially dependent on PD-L1 promoter demethylation[140]. Furthermore, Darvin et al. (2019) suggested that the lower distribution of repressive histones in the PD-L1 promoter region and over expression of histone acetylases also lead to PD-L1 up-regulation in tumorspheres[140].

As important determinants of post-transcriptional regulation, microRNAs (miRNAs) are not only involved in cancer development and progression, but also regulate anti-cancer immune responses[128]. Many miRNAs are involved in the production of PD-L1 as epigenetic control points. miR-513 regulates PD-L1 translation and participates in IFN-γ-induced PD-L1 expression in human bile duct cells[141]. In acute myeloid leukemia, a negative correlation was observed between PD-L1 and miR-34a expression[142]. miR-155 is a key component of the inflammation-induced regulatory circuit that controls PD-L1 expression in primary cells[143]. Xie et al. (2018) observed decreased expression of miR-140 and elevated expression of PD-L1 and cyclin E in NSCLC cells[144]. The up-regulation of miR-93 and miR-106b, either through the use of miRNA mimics or treatment with an epigenetic reader domain (BET) inhibitor, led to a reduction in the expression of CXCL12 and PD-L1[145]. In addition to tumor-intrinsic miRNAs, exosome-containing miRNAs such as miR-27A, miRAN-15A, and miRNA-16 can also target and regulate PD-L1 expression[146]. Overall, the epigenetic regulation of PD-L1 involves DNA methylation, histone modifications, and miRNAs, which collectively influence the expression levels of PD-L1 in various cell types. Understanding the epigenetic mechanisms governing PD-L1 expression can provide insights into its dysregulation in diseases such as cancer and potentially guide the development of novel therapeutic strategies targeting these epigenetic modifications.

1.3.2 Clinical significance of PD-L1 over-expression in OSCC and CRC

Increased PD-L1 is associated with poor prognosis in a variety of cancers, including melanoma, ovarian, lung, nasopharyngeal, and renal cell cancers[115]. Meta-analysis studies reported in OSCC, females were associated with a higher PD-L1 level[147; 148]. Lenouvel et al. (2020) presented evidence that the overexpression of PD-L1 in the cell membrane has a negative impact on the prognosis of OSCCs, especially in disease specific survival and disease-free survival[148]. These studies underscore the complexity of PD-L1 regulation and its varying roles in different cancers. While epigenetic regulation, such as promoter methylation, plays a central role in melanoma, influencing both immune activation and prognosis, membrane-bound PD-L1 overexpression in OSCC is associated with immune escape and worse clinical outcomes. This apparent divergence reflects the cancer type-specific mechanisms underlying PD-L1 regulation and highlights the importance of tailoring therapeutic strategies to the unique biological context of each cancer. In freshly isolated squamous cell carcinoma (SCC) of the head and neck, PD-L1 expression was detected in 66% of cases[149]. Increased frequencies of PD-1(+) expressing $CD4^+$ and $CD8^+$ T cells were observed in OSCC samples, accompanied by strong PD-L1 expression[150]. Kouketsu et al. (2019) identified a potential association between PD-L1 and PD-1 immunohistochemical status and the development, progression, and prognosis of oral epithelial lesions[151]. Hirai et al. (2017) reported higher PD-L1 expression in a low-grade invasive OSCC cell line compared to a high-grade invasive OSCC cell line, suggesting a potential relationship between PD-L1 expression and the EMT[152]. Differences in PD-L1 expression between tumor sites have been reported. PD-L1 expression was found to be significantly more frequent in cancers arising from mandibular structures and the tongue compared to those originating in the maxilla or soft palate[153].

The correlation between PD-L1 expression and clinicopathological features and the prognosis of CRC patients is still controversial[154]. Meta-analysis reported that PD-L1 expression was significantly positively correlated with lymphatic metastasis and tumor diameter, but negatively correlated with differentiation and vascular invasion in CRC[154]. PD-L1 expression independently predicts poor prognosis in CRC[154; 155]. Patients with advanced cancer or lymphatic invasion are more likely to express PD-L1, but not correlative with patients' gender, microsatellite instability, or tumor location[156].

1.4 Aims of the study

F. nucleatum has been strongly linked to CRC, with increasing evidence supporting its role in tumor progression, PD-L1 is a key immune checkpoint molecule that contributes to immune evasion in various malignancies, including colorectal cancer[157]. However, the CRC tumor sample which contained high amout of *F. nucleatum* was not significantly associated with PD-L1 expression status[158]. What's more, the role of *F. nucleatum* in OSCC remains largely unexplored.

There are three *F. nucleatum* strains (*subspecies [subsp.] nucleatum* ATCC 25586, *subsp. polymorphum* ATCC 10953, *subsp. vincentii* ATCC 49256) that have been associated with periodontal disease and oral cancer[85; 159-162]. Previous research has demonstrated that *F. nucleatum* ATCC 25586 activates STING signaling in CRC cells, thereby regulating PD-L1 expression through NF-κB transcription[163]. Another study reported that this strain stimulates PD-L1 protein expression through m^6A modification of IFIT1[164]. Despite these findings, no studies to date have explored the relationship between PD-L1 and *F. nucleatum* in oral epithelial cells and OSCC. It remains unclear how *F. nucleatum* regulates PD-L1 expression in oral epithelial cells, OSCC, and CRC. Therefore, we aimed to investigate the effect of these three different strains of heat-killed *F. nucleatum* on OSCCs, CRC and PHGK viability, and PD-L1 expression. By evaluating strain- and cell type-specific responses, this study provides insights into the potential immunomodulatory role of *F. nucleatum* in these contexts.

2. Materials and Methods

2.1. Cells culture

2.1.1 Cell line

The human squamous cell carcinoma cell lines SCC-25 and the colon carcinoma cell line CL-11 were purchased from the DSMZ (German Collection of Microorganisms and Cell Cultures, Braunschweig, Germany, DSMZ numbers ACC 617 and ACC 467). PHGK were obtained from gingival biopsies of healthy volunteers.

2.1.2 Cell recovery, passage, and freezing

(1) Cells recovery and passage: The human SCC-25 were cultured in a medium containing Dulbecco's minimal essential medium (DMEM): Ham's F12 (4:1), Hepes buffer, penicillin/streptomycin (Invitrogen, Karlsruhe, Germany) and 10% fetal calf serum (FCS, Greiner, Frickenhausen, Germany). CL-11 cells were cultured in DMEM medium: Hams's F12 (1:1) and 20% fetal calf serum (FCS. PHGK were cultured in a serum-free medium containing DMEM: Ham's F12 (4:1), Hepes buffer, and penicillin/streptomycin as basal substances (The composition of various cell culture media is detailed in Table 1). The cells were seeded in T75 culture flasks. When cell density up to 80%, discard the medium, use 2 ml trypsin to digest for 3-5 min, and then added 4 ml culture medium. Cells were softly and carefully resuspended, then diluted with the cell culture medium at the ratio of 1:3 and place it in the cell incubator (5% CO_2, 37 °C).

Table 1. Composition of cell culture media of SCC-25 and CL-11

Stock solution	SCC-25	CL-11
DMEM	88 ml	80 ml
Ham F-12	88 ml	80 ml
FCS	20 ml	40 ml
1M HEPES	2 ml	--
PenStrep (10^4 U/ml)	2 ml	--

Hydrocortison (10µg/ml)	8µg	--
Total volume	200 ml	200 ml

Table 2. Composition of cell culture media of PHGK

Stock solution	PHGK
DMEM	145.05 ml
HAM's F12	48.35 ml
Hydrocortison (10µg/ml)	8 µl
PenStrep (10^4 U/ml)	2 ml
Gentamicin (50µg/ml)	0.4 ml
HEPES-Buffer (1M)	2 ml
Insulin-Transferrin-Selenium-X Supplement, 100x	2 ml
Human-Epidermal Growth Factor (1µg/ml)	2 µl
Choleratoxin (10^{-7}M/ml)	0.2 ml
Total volume	200 ml

(2) Cell freezing: Collected cell suspension according to passage method, centrifugated at 2000 g for 5 min, and the supernatant was discarded. The freezing medium (media:FCS: DMSO=8:1:1) was added to resuspend the cells, then the suspension was aliquoted 1 ml each in 1.5 ml freezing tubes and frozen at -80 °C.

2.2. Bacterial culture

2.2.1 Bacterial strains

F. nucleatum strains *subsp. nucleatum* ATCC 25586, *subsp. polymorphum* ATCC 10953, and *subsp. vincentii* ATCC 49256 were purchased from the DSMZ(German Collection of

Microorganisms and Cell Cultures, Braunschweig, Germany. DSMZ numbers are DSM 15463, DSM 20482 and DSM 19507, seperately).

2.2.2 Bacterial culture conditions and heat-killing

Bacterial were cultured in Brain-heart infusion (BHI) broth supplemented with 5μg/ml of hemin and 1 μg/ml of vitamin K and incubated at 37°C anaerobically in 5% CO_2 conditions for 48h. Bacterial suspensions were centrifuged 3 times (1000 rpm, 10 min), and then pellets were resuspended in PBS to a final working concentration of 1×10^9 bacteria/ml[159; 165]. The bacterial concentration of the suspension was determined by measuring the optical density using a spectrophotometer (HACH DR/2000) at 600 nm. Before measurements, the spectrophotometer was calibrated using PBS as the blank control. The resuspended bacterial solution was then heat-killed by incubation in a water bath for 10 min at 100°C[166; 167]. Heat-killing was confirmed by plating the bacteria on agar to ensure no viable colonies. Aliquots of the heat-killed bacteria were stored at -80°C until used.

2.3. Infection model

1×10^6 cells/ml SCC-25, CL-11, and PHGK cells were grown in 6-well plates in growth medium separately and infected with heat-killed *F. nucleatum* at the multiplicity of infection (MOI) (10, 50, 100, 200) for 4h, 8h, 24h, 48h. Cells without heat-killed *F. nucleatum* were used as control. As a reference condition, cells were treated with human IFN- γ (Miltenyi Biotec) at a concentration of 100 U/ml.

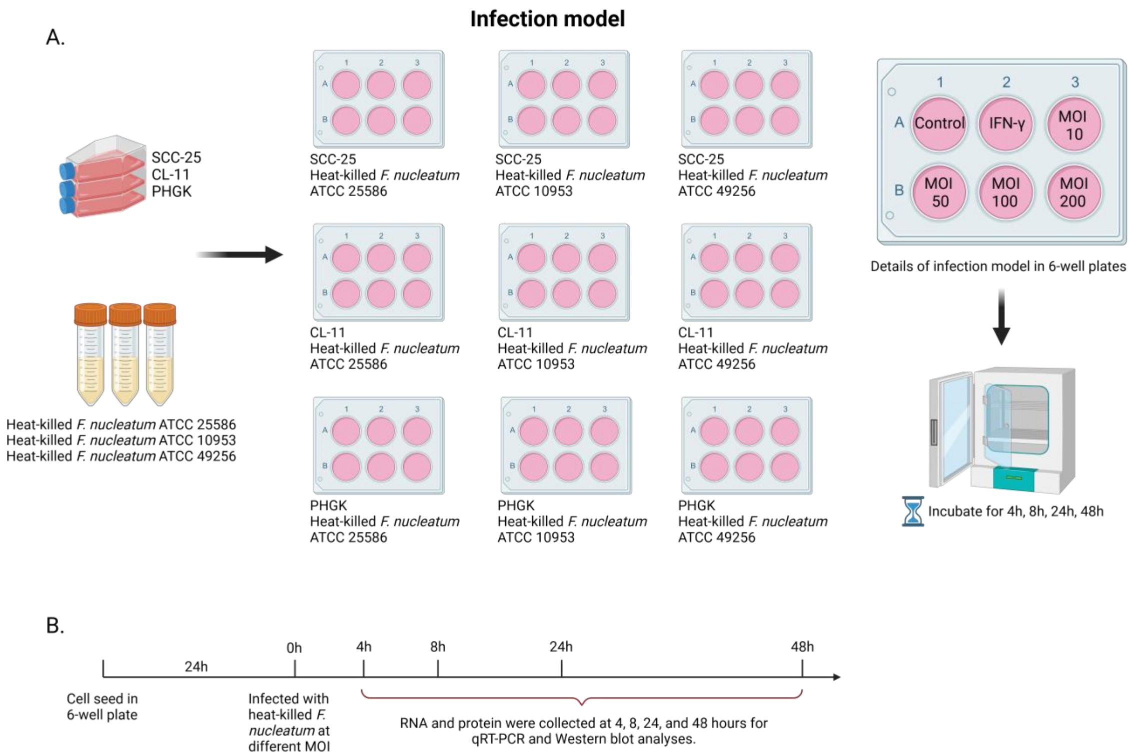

Figure 5. Experimental Design

A. Details of the Inflammatory Model: SCC-25, CL-11, and PHGK cells were co-cultured with heat-killed *F. nucleatum* strains ATCC 25586, 10953, and 49256 for 4h, 8h, 24h, and 48 h. B. Experimental timeline: The timeline of the experiment is illustrated, highlighting key steps and sampling intervals.

2.4. Cell viability assay

When the cell confluency reached approximately 80% in T75 flasks, the medium was discarded, and 2 ml of trypsin was added to digest the cells for 3 – 5 minutes. After digestion, 4 ml of culture medium was added to neutralize the trypsin. The cells were gently and carefully resuspended and transferred into a 15 ml centrifuge tube. The suspension was centrifuged at 1000 rpm for 5 minutes. The cell pellet was then resuspended carefully in 2 ml of fresh culture medium. Next, 10 µL of the cell suspension was transferred to a cell counter, and the cells were counted under a microscope. The cell suspension was adjusted to a density of 50000cells/ml, and 100 µl of the prepared cell suspension was added to each well of a 96-well plate. Cells were incubated for 4 h, 8 h, 24 h, and 48 h at 37°C and infected with heat-killed *F. nucleatum* at a MOI of 10, 50, 100, and 200. Cells without heat-killed *F. nucleatum* were used as the negative control. After the incubation period, 10 µl cell countin kit (CCK)-8 solution was added to each well and cells were incubated for 2 h at 37°C. The absorbance at 450 nm was measured using a microplate reader (Berthold LB940). The viability of cells was calculated as cell viability = (OD of treatment − OD of blank control)/(OD of control − OD of blank control)[168; 169]. All experiments were performed at least three times to ensure reproducibility.

2.5. Western blot analysis

2.5.1 Buffers and solutions

Composition of buffers:

10 x SDS running buffer: 30.3 g Tris, 144 g Glycine, 10 g SDS, pH 8.3.

Lower gel buffer: 187 g Tris Base pH 8.8 with HCL, 4 g SDS, dH_2O to 1L.

Upper gel buffer: 60.5 g Tris Base pH6.8 with HCL,4 g SDS, dH_2O to 1L.

5 x Loading buffer: 10% w/v SDS, 10 mM Dithiothreitol or beta-mercapto-ethanol, 20% v/v Glycerol, 0.2 M Tris-HCL pH6.8, 0.05% w/v Bromophenolblue.

10% w/v Ammonium persulfate (AP): 10 g ammonium persulfate dissolved in 10 ml dH_2O.

2.5.2 Sample preparation and quantification

The SCC-25, CL-11, PHGK cells in 6-well plates were washed with ice-cold PBS and lysed with 100 µL RIPA buffer (Thermo Fisher Scientific) per well containing 1% Halt™ Protease-Inhibitor-Ccktail (Thermo Fisher Scientific). The cell lysates were kept on ice for 30 min and then centrifuged at 14000 rpm 4°C for 20 min. The protein concentration was measured using the Pierce™ BCA Protein Assay Kits (Thermo Fisher Scientific, 23227). Transfer supernatant to new tube. Mix BCA solution A and B 50:1. Mix 30 µl Protein sample with 570 µl BCA solution (A+B). Incubate tubes for 30 min at 37°C. Put tubes on ice. Measure OD562 on Spectrophotometer--HACH DR/2000 (Use Water as Blank). Calculate protein concentration of samples using protein standards and a standard curve. Adjust protein concentration to 1 µg/µl (20 µg protein/lane). The samples were then mixed with loading buffer (5 x) and heated at 95°C for 5 min, followed by cooling on ice. Load 20 µl proteins onto 12% SDS-PAGE gel (10 cm x 10 cm), with a running condition of 80V for stacking gel and 120V for the separating gel. The resolved proteins were electroblotted onto polyvinylidene difluoride membranes and stained with Ponceau S to visualize protein bands. After washing the membrane with TBS containing 0.1% Tween-20 (TBST) three times to remove the Ponceau S, the membrane was blocked with 2% non-fat milk in TBST for 1 h at room temperature. Subsequently, the membrane was incubated with specific antibodies (dilutions shown in Table 3) in 2% non-fat milk in TBST for 1 h at room temperature. Following three washes with TBST, the membrane was incubated with Anti-Host IgG, HRP-linked antibody (dilutions shown in Table 3) in 2% non-fat milk in TBST for 1 h at room temperature. After another three washes with TBST, signals were detected using the Enhanced Chemiluminescent kit (BIO-RAD, Germany). β-actin was used as control. All experiments were performed at least three times to ensure reproducibility.

Table 3. The antibody dilutions for western blot

Sample	Catalog	Dilution	Company
PD-L1	PA5-20343	1:2000	Thermo Fisher Scientific
Beta-actin	AM4302	1:2000	Thermo Fisher Scientific
anti-rabbit-IgG-HRP	32460	1:750	Thermo Fisher Scientific
anti-mouse-IgG-HRP	32430	1:750	Thermo Fisher Scientific

2.6. Quantitative real-time PCR

Before starting, the workspace was cleaned using ROTI®Nukleinsäurefrei (Roth, HP69.1) to prevent contamination from exogenous DNA or RNA. The SCC-25, CL-11, and PHGK cells cultured in 6-well plates were carefully aspirated to removde the medium and lysed using RNAprotect Cell Reagent (Qiagen, 76526). Adherent cells were gently scraped using a cell scraper to ensure complete detachment and lysis. The cell lysate was transferred into 1.5 ml EP tubes and centrifuged for 5 min at 5000 × g. The supernatant was carefully removed. Total RNA was isolated using NucleoSpin® RNA plus columns (Machery-Nagel, 740984.250) following the manufacturer's instructions. 350 µL of Buffer LBP was added to each sample and mixed thoroughly. The homogenized lysate was then transferred into a NucleoSpin® gDNA Removal Column placed in a 2 ml Collection Tube. The column was centrifuged at 11,000 × g for 30 seconds, and the flowthrough was discarded. To remove residual genomic DNA, 100 µL of binding solution was added to the flowthrough and mixed well by vortexing or pipetting up and down several times. The entire lysate (~450 µL) was then transferred to a

NucleoSpin® RNA Plus Column reassembled with a new collection tube. The column was centrifuged at 11,000 × g for 15 seconds, and the flowthrough was discarded. Following this, 200 µL of Buffer WB1 was added to the RNA Plus Column and centrifuged for 15 seconds at 11,000 × g. The flowthrough was discarded, and the column was placed into a new 2 ml Collection Tube. Then, 600 µL of Buffer WB2 was added to the RNA Plus Column and centrifuged for 15 seconds at 11,000 × g. The flowthrough was discarded, and the column was returned to the collection tube. To remove any remaining contaminants, 250 µL of Buffer WB2 was added to the column and centrifuged for 2 minutes at 11,000 × g to completely dry the membrane. The RNA Plus Column was then placed into a nuclease-free Collection Tube, and 30 µL of RNase-free H_2O was added to the membrane. After centrifuging at 11,000 × g for 1 minute, the elution was repeated with another 30 µL of RNase-free H_2O. Finally, 1 µL of the eluted RNA was taken for quantification using a NanoDrop spectrophotometer, and the instrument was calibrated with RNase-free H_2O before measurement. After measuring the RNA concentration, the RNA was diluted to a final concentration of 100 ng/µL using RNase-free H_2O .

The following pairs of primers were used: QuantiTect Primer Assay (Qiagen, Hilden, Germany) Hs_CD274_1_SG (PD-L1), QuantiTect Primer Assay (Qiagen, Hilden, Germany) Hs_ACTB_1_SG (beta-actin) as a housekeeping gene (Table 4). cDNA was prepared by reverse transcription using the Verso cDNA synthesis kit (Thermo Fisher, AB1453A). The preparation of the cDNA reaction mix was performed on an ice box, and the specific composition is detailed in Table 5. The reverse transcription cycling program is provided in Table 6.

qRT-PCR using the SYBR Green Assay was performed with SensiFast no ROX STBR Green Mix (Meridian bioscience, BIO-98005) according to the manufacturer’s recommendations. Prepare a PCR master mix as descibed in Table 7. Bio-RAD CFX96TMReal-Time System was operated using a 3-step cycling program (Table 8). The Ct values obtained from different samples were compared using the $2^{-\Delta\Delta Ct}$ method. All experiments were performed at least three times to ensure reproducibility.

Table 4. The primer for quantitative real-time PCR

Gene Name	Product Name	GeneGlobe ID	Website
PD-L1	Hs_CD274_1_SG	QT00082775	https://geneglobe.qiagen.com/de/product-groups/quantitect-primer-assays?q=Hs_CD274_1_SG
Beta-actin	Hs_ACTB_1_SG	QT00095431	https://geneglobe.qiagen.com/de/product-groups/quantitect-primer-assays?q=Hs_ACTB_1_SG

Table 5. cDNA reaction mix preparation

Component	Volume	Final Concentration
5X cDNA Synthesis Buffer	4 µL	1X
dNTP Mix	2 µL	500 µM each
RNA Primer*	1 µL	
RT Enhancer	1 µL	
Verso Enzyme Mix	1 µL	
Template (RNA)	2 µL	1 ng
Water	9 µL	
Total volume	20 µL	

Table 6. Reverse transcription cycling program

Component	Temperature	Time	Number of cycles
cDNA synthesis	42℃	30 min	1 cycle
Inactivation	95℃	2 min	1 cycle

Table 7. Reaction mix composition

Reagent	Volume	Final concentration
2x SensiFAST SYBR	10 μL	1x
Primer	1.6 μL	
Template	1 μL	
Water	7.4 μL	
Final volume	20μL	

Table 8. 3-step cycling

Cycles	Temperature	Time
1	95℃	2 min
40	95℃	5s
	60℃	10s
	72℃	5-20s

2.7. Statistical analysis

All data are expressed as mean ± standard deviation (SD). Statistical analyses were conducted using GraphPad Prism 10.4.0. The normality of data distribution was assessed with the Shapiro-Wilk test, and homogeneity of variances was evaluated using Brown-Forsythe test. For data that did not meet normality or homogeneity assumptions, non-parametric tests (e.g., Kruskal-Wallis test) were applied. For comparisons among more than two groups, one-way or two-way ANOVA was performed when assumptions of normality and homogeneity were met, followed by Dunnett's post-hoc test, depending on the study design. For non-parametric analyses, post-hoc pairwise comparisons were conducted using Dunn's test with multiple comparisons correction as implemented in GraphPad Prism 10.4.0. All experiments were repeated at least three times independently, and statistical significance was defined as $P < 0.05$.

3. Results

3.1 Protein expression of PD-L1 in cells stimulated with heat-killed *F. nucleatum*

3.1.1 PD-L1 protein expression in SCC-25 Cells in response to heat-killed *F. nucleatum* ATCC 49256

The expression of PD-L1 protein in SCC-25 cells in response to heat-killed *F. nucleatum* ATCC 49625 infection was evaluated at multiple time points (4, 8, 24, and 48 hours) and across different multiplicities of infection (MOI: 10, 50, 100, 200) (Figure 6). The mean PD-L1 expression levels (relative to control) at different time points are summarized in Table 9.

At the 4-hour time point, PD-L1 expression showed a dose-dependent increase with higher MOI. The MOI 50, 100, and 200 groups exhibited significant upregulation of PD-L1 (MOI 50: 2.925 ± 0.5990, p = 0.0154; MOI 100: 2.864 ± 1.037, p = 0.0188; MOI 200: 2.760 ± 0.5977, p = 0.0264), However, MOI 10 did not reach statistical significance (p = 0.0886), suggesting that a lower bacterial load may not be sufficient to trigger a strong PD-L1 response within this short exposure period. By 8 hours, PD-L1 expression remained elevated in the MOI 200 group (1.427 ± 0.1862, p = 0.0279). Lower MOIs (10, 50, 100) did not reach statistical significance, suggesting that the early activation of PD-L1 may require both higher bacterial loads and prolonged exposure. At 24 hours, the effects of heat-killed *F. nucleatum* became more pronounced (Figure 6.B.3). Significant upregulation of PD-L1 was observed across multiple bacterial MOIs, with MOI 10 (p = 0.0022), MOI 50 (p = 0.0008), MOI 100 (p = 0.0009), and MOI 200 (p = 0.0024) all showing statistically significant increases compared to control. The MOI 50 group exhibited the highest PD-L1 expression (1.433 ± 0.2060), indicating a strong bacterial-induced immune regulatory response in SCC-25 cells at this time point. By 48 hours, PD-L1 expression levels returned to near baseline across all groups, with no significant differences observed compared to the control ($p > 0.05$ for all groups). This suggests that the bacterial-induced upregulation of PD-L1 may be transient and could be subject to post-translational regulation or immune adaptation over time.

These findings (Figure 6, Table 9) indicate that *F. nucleatum* ATCC 49625 induces PD-L1 expression in SCC-25 cells in a time- and dose-dependent manner, with the most significant effects observed at 24 hours, particularly at MOI 50, 100, and 200. The response appears to peak at 24 hours and subsequently decline by 48 hours, suggesting a potential regulatory mechanism that limits sustained PD-L1 up-regulation.

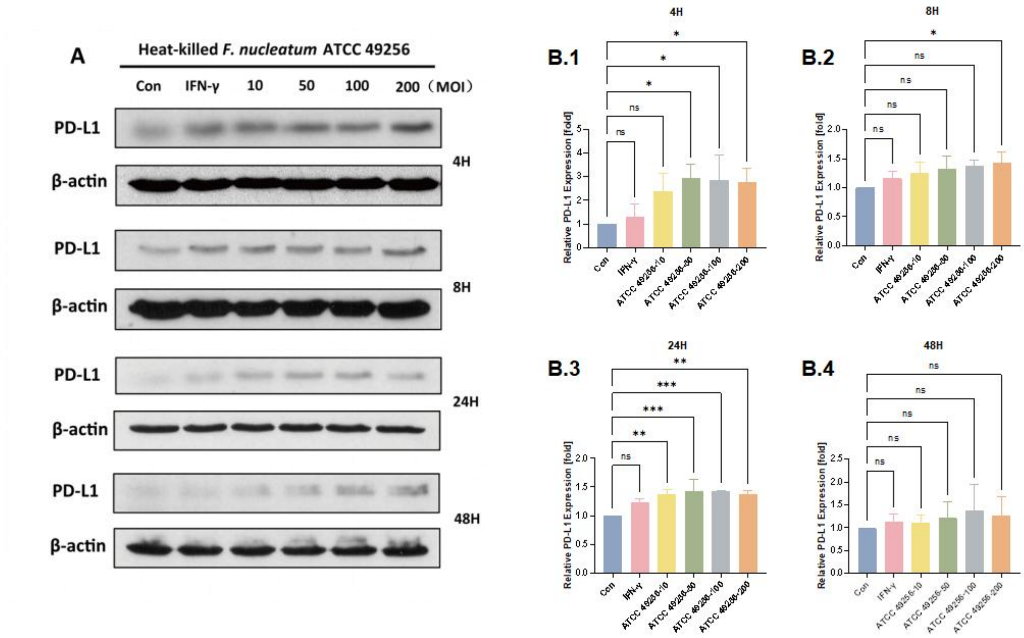

Figure 6. The protein expression of PD-L1 in response to heat-killed *F. nucleatum* ATCC 49625 infection in SCC-25.

A.Western blot assays detecting PD-L1 protein expression in SCC-25 cells treated with heat-killed *F. nucleatum* ATCC 49256 (MOI=10, 50, 100, and 200), IFN-γ, and medium control. B. Quantitative analysis of the blots after 4-hour (B.1), 8-hour (B.2), 24-hour (B.3), and 48-hour (B.4). The expression of PD-L1 was normalized to ß-actin and the relative fold change was compared with the control group. The relative PD-L1 expression was presented as the mean ± standard deviation of at least three independent assays. * $p < 0.05$, ** $p < 0.01$, *** $p < 0.001$.

Table 9. Statistical summary of PD-L1 protein expression in SCC-25 cells infected with heat-killed *F. nucleatum* ATCC 49625 at different MOIs and time points.

Time Point	Group	Mean ± SD	N (Sample Size)	Test Type	Adjusted P Value (vs Control)
4 hours	Control	1.000 ± 0.000	3	ANOVA	N/A

	IFN- γ	1.318 ± 0.5347	3	ANOVA	0.9616
	MOI 10	2.387 ± 0.7357	3	ANOVA	0.0886
	MOI 50	2.925 ± 0.5990	3	ANOVA	0.0154
	MOI 100	2.864 ± 1.037	3	ANOVA	0.0188
	MOI 200	2.760 ± 0.5977	3	ANOVA	0.0264
8 hours	Control	1.000 ± 0.000	3	ANOVA	N/A
	IFN- γ	1.165 ± 0.1256	3	ANOVA	0.6172
	MOI 10	1.246 ± 0.2004	3	ANOVA	0.2772
	MOI 50	1.317 ± 0.2320	3	ANOVA	0.1187
	MOI 100	1.370 ± 0.1133	3	ANOVA	0.0595
	MOI 200	1.427 ± 0.1862	3	ANOVA	0.0279
24 hours	Control	1.000 ± 0.000	3	ANOVA	N/A
	IFN- γ	1.224 ± 0.07494	3	ANOVA	0.0634
	MOI 10	1.381 ± 0.07996	3	ANOVA	0.0022
	MOI 50	1.433 ± 0.2060	3	ANOVA	0.0008
	MOI 100	1.423 ± 0.02308	3	ANOVA	0.0009
	MOI 200	1.375 ± 0.06510	3	ANOVA	0.0024
48 hours	Control	1.000 ± 0.000	3	ANOVA	N/A
	IFN- γ	1.139 ± 0.1610	3	ANOVA	0.9794
	MOI 10	1.104 ± 0.1704	3	ANOVA	0.9942
	MOI 50	1.223 ± 0.3381	3	ANOVA	0.8793
	MOI 100	1.383 ± 0.5703	3	ANOVA	0.5234
	MOI 200	1.258 ± 0.4309	3	ANOVA	0.8114

3.1.2 PD-L1 protein expression in SCC-25 cells in response to heat-killed *F. nucleatum* ATCC 10953 infection

Western blot analysis (Figure 7) demonstrated that heat-killed *F. nucleatum* ATCC 10953 modulated PD-L1 protein expression in SCC-25 cells in a time- and dose-dependent manner. The mean PD-L1 expression levels at different time points are summarized in Table 10.

At the 4-hour time point (Figure 7.B.1), PD-L1 expression was significantly increased in the MOI 10 (1.649 ± 0.1898, $p = 0.0212$) and MOI 50 (1.610 ± 0.3717, $p = 0.0305$) groups compared to the control. However, the MOI 100 and MOI 200 groups did not show significant increases, indicating that at this early stage, lower bacterial doses might be more effective at inducing PD-L1 expression in SCC-25 cells. At 8 hours (Figure 7.B.2), PD-L1 expression continued to rise in response to bacterial stimulation, with MOI 50 (1.550 ± 0.5271, $p = 0.0572$) and MOI 100 (1.887 ± 1.290, $p = 0.1927$) showing higher PD-L1 levels compared to the control, although these increases were not statistically significant. The variability in response at this time point suggests that PD-L1 induction may be influenced by bacterial adaptation or host cell regulatory mechanisms. At 24 hours (Figure 7.B.3), MOI 100 showed the most pronounced PD-L1 upregulation (1.695 ± 0.4365, $p = 0.0229$), reaching statistical significance. MOI 50 also demonstrated an increasing trend (1.578 ± 0.2876, $p = 0.0572$), but the effect was not significant. The MOI 10 and MOI 200 groups did not show significant differences from the control, suggesting that an intermediate bacterial dose (MOI 100) may be optimal for inducing PD-L1 expression in SCC-25 cells at this stage. At 48 hours (Figure 7.B.4), PD-L1 expression remained elevated across all treatment groups but did not reach statistical significance compared to the control ($P > 0.05$ for all MOIs). This trend aligns with the 24-hour data, indicating that PD-L1 expression may peak at intermediate time points and stabilize over prolonged exposure.

These findings (Figure 7, Table 10) suggest that heat-killed *F. nucleatum* ATCC 10953 induces PD-L1 expression in SCC-25 cells in a time-dependent manner, with the most significant increase observed at 24 hours in the MOI 100 group. Unlike *F. nucleatum* ATCC 49625 (Figure 6), where MOI 50 and MOI 200 induced the strongest responses, the ATCC 10953 strain exhibited its peak effect at MOI 100. Additionally, the statistical significance of

PD-L1 induction varied across time points, suggesting that strain-specific differences may play a role in immune modulation.

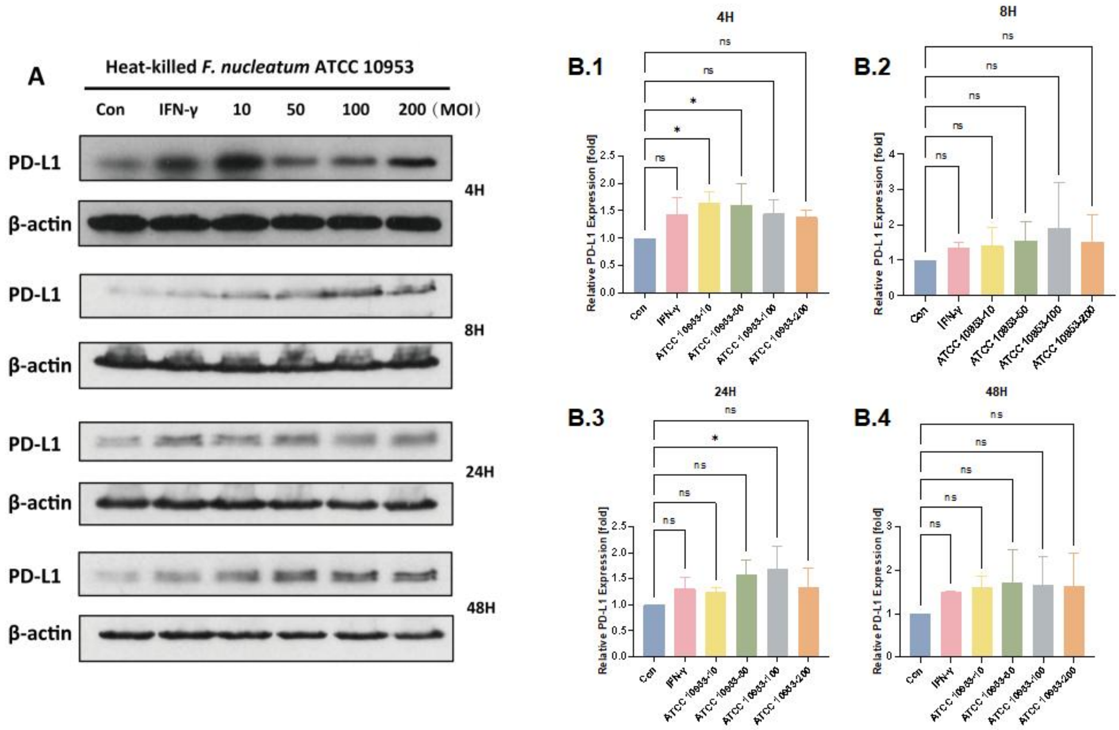

Figure 7. The protein expression of PD-L1 in response to heat-killed *F. nucleatum* ATCC 10953 infection in SCC-25.

A.Western blot assays detecting PD-L1 protein expression in SCC-25 cells treated with heat-killed *F. nucleatum* ATCC 10953 (MOI=10, 50, 100, and 200), IFN-γ, and medium control. B. Quantitative analysis of the blots after 4-hour (B.1), 8-hour (B.2), 24-hour (B.3), and 48-hour (B.4). The expression of PD-L1 was normalized to ß-actin and the relative fold change was compared with the control group. The relative PD-L1 expression was presented as the mean ± standard deviation of at least three independent assays. * $p < 0.05$.

Table 10. Statistical summary of PD-L1 protein expression in SCC-25 cells infected with heat-killed *F. nucleatum* ATCC 10953 at different MOIs and time points.

Time Point	Group	Mean ± SD	N (Sample Size)	Test Type	Adjusted P Value (vs Control)
4 hours	Control	1.000 ± 0.000	3	ANOVA	N/A
	IFN- γ	1.422 ± 0.2900	3	ANOVA	0.1380

	MOI 10	1.649 ± 0.1898	3	ANOVA	0.0212
	MOI 50	1.610 ± 0.3717	3	ANOVA	0.0305
	MOI 100	1.444 ± 0.2466	3	ANOVA	0.1357
	MOI 200	1.401 ± 0.1088	3	ANOVA	0.1965
8 hours	Control	1.000 ± 0.000	3	Kruskal-Wallis Test	N/A
	IFN- γ	1.345 ± 0.1645	3	Kruskal-Wallis Test	0.0876
	MOI 10	1.430 ± 0.5055	3	Kruskal-Wallis Test	0.3295
	MOI 50	1.550 ± 0.5271	3	Kruskal-Wallis Test	0.0572
	MOI 100	1.887 ± 1.290	3	Kruskal-Wallis Test	0.1927
	MOI 200	1.504 ± 0.7911	3	Kruskal-Wallis Test	0.6269
24 hours	Control	1.000 ± 0.000	3	Kruskal-Wallis Test	N/A
	IFN- γ	1.315 ± 0.2224	3	Kruskal-Wallis Test	0.6269
	MOI 10	1.255 ± 0.06764	3	Kruskal-Wallis Test	0.3295
	MOI 50	1.578 ± 0.2876	3	Kruskal-Wallis Test	0.0572
	MOI 100	1.695 ± 0.4365	3	Kruskal-Wallis Test	0.0229
	MOI 200	1.347 ± 0.3588	3	Kruskal-Wallis Test	0.5378
48 hours	Control	1.000 ± 0.000	3	Kruskal-Wallis Test	N/A
	IFN- γ	1.494 ± 0.03324	3	Kruskal-Wallis Test	0.0710
	MOI 10	1.606 ± 0.2560	3	Kruskal-Wallis Test	0.0876

MOI 50	1.728 ± 0.7431	3	Kruskal-Wallis Test	0.2770
MOI 100	1.662 ± 0.6524	3	Kruskal-Wallis Test	0.3899
MOI 200	1.647 ± 0.7396	3	Kruskal-Wallis Test	0.3295

3.1.3 PD-L1 protein expression in SCC-25 cells in response to heat-killed *F. nucleatum* ATCC 25586 infection

Figure 8 presents the WB analysis of PD-L1 protein expression in SCC-25 cells following exposure to heat-killed *F. nucleatum* ATCC 25586. While an initial increase in PD-L1 expression was observed at 4 hours, this effect diminished over time, contrasting with the more sustained upregulation seen in ATCC 49625 and ATCC 10953. The detailed quantitative analysis is provided in Table 11.

At the 4-hour time point (Figure 8.B.1), PD-L1 expression was significantly increased in MOI 10 (p = 0.0039), MOI 50 (p = 0.0043), and MOI 100 (p = 0.0032) groups compared to the control, suggesting an early upregulation of PD-L1 at moderate infection doses. However, MOI 200 did not reach statistical significance (p = 0.0849), indicating that higher bacterial loads may not further enhance PD-L1 expression at this early stage. At 8 hours (Figure 8.B.2), PD-L1 expression showed no significant differences across all groups ($P > 0.05$), suggesting that the early upregulation observed at 4 hours may be transient, and the bacterial stimulation did not sustain PD-L1 induction at this time point. At 24 hours (Figure 8.B.3), PD-L1 expression remained relatively stable, with no statistically significant differences across all groups ($P > 0.05$). Unlike ATCC 49625 and ATCC 10953, where MOI 50–100 showed significant upregulation at this time point, ATCC 25586 did not elicit a strong PD-L1 response in SCC-25 cells. At 48 hours (Figure 8.B.4), PD-L1 expression remained similar to control levels in all treatment groups, with no significant upregulation observed ($P > 0.05$). This suggests that PD-L1 induction by ATCC 25586 is not sustained over prolonged bacterial exposure, in contrast to the other two strains.

The results (Figure 8, Table 11) indicate that heat-killed *F. nucleatum* ATCC 25586 induces PD-L1 expression in SCC-25 cells, but the response is weaker and more transient compared to the effects observed with ATCC 49625 and ATCC 10953. A statistically significant increase in PD-L1 expression was observed at 4 hours in MOI 10, 50, and 100, but this effect disappeared at later time points, with no significant changes detected at 8, 24, or 48 hours. This suggests that ATCC 25586 may have a weaker immunomodulatory effect on SCC-25 cells compared to the other strains.

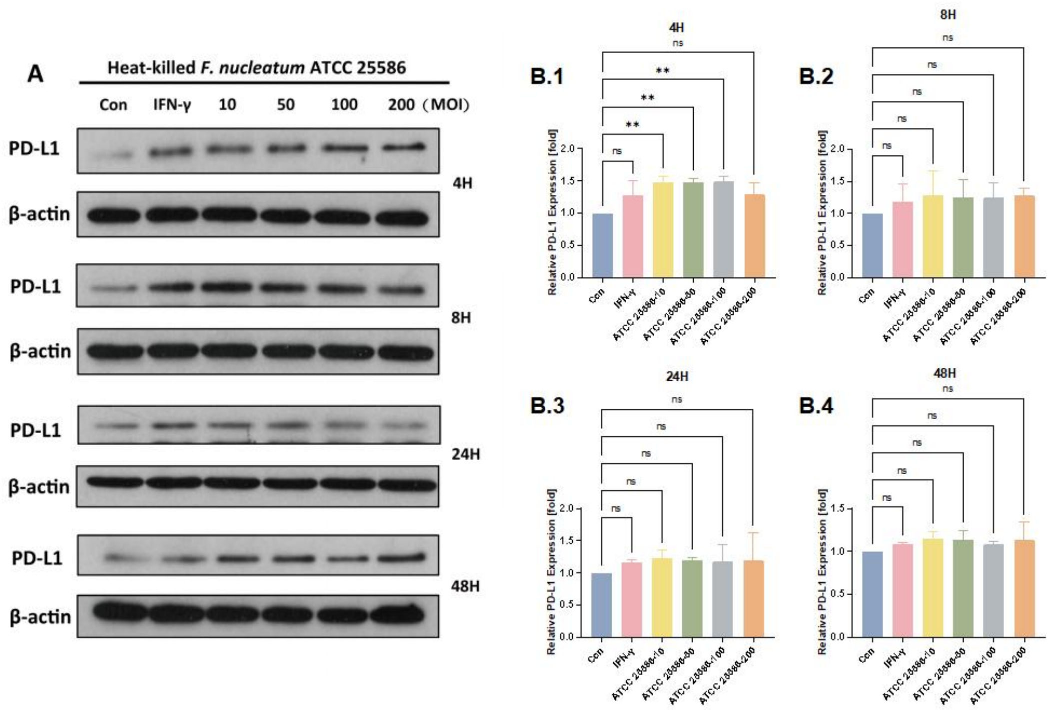

Figure 8. The protein expression of PD-L1 in response to heat-killed *F. nucleatum* ATCC 25586 infection in SCC-25.

A. Western blot assays detecting PD-L1 protein expression in SCC-25 cells treated with heat-killed *F. nucleatum* ATCC 25586 (MOI=10, 50, 100, and 200), IFN-γ, and medium control. B. Quantitative analysis of the blots after 4-hour (B.1), 8-hour (B.2), 24-hour (B.3), and 48-hour (B.4).The expression of PD-L1 was normalized to ß-actin and the relative fold change was compared with the control group. The relative PD-L1 expression was presented as the mean ± standard deviation of at least three independent assays. * $p < 0.05$, ** $p < 0.01$.

Table 11. Statistical summary of PD-L1 protein expression in SCC-25 cells infected with heat-killed *F. nucleatum* ATCC 25586 at different MOIs and time points.

Time Point	Group	Mean ± SD	N (Sample Size)	Test Type	Adjusted P Value (vs Control)
4 hours	Control	1.000 ± 0.000	3	ANOVA	N/A
	IFN- γ	1.269 ± 0.2297	3	ANOVA	0.1100
	MOI 10	1.480 ± 0.09333	3	ANOVA	0.0039
	MOI 50	1.472 ± 0.06734	3	ANOVA	0.0043
	MOI 100	1.491 ± 0.07765	3	ANOVA	0.0032
	MOI 200	1.286 ± 0.1924	3	ANOVA	0.0849
8 hours	Control	1.000 ± 0.000	3	Kruskal-Wallis Test	N/A
	IFN- γ	1.187 ± 0.2728	3	Kruskal-Wallis Test	>0.9999
	MOI 10	1.275 ± 0.3866	3	Kruskal-Wallis Test	0.6269
	MOI 50	1.246 ± 0.2793	3	Kruskal-Wallis Test	0.2770
	MOI 100	1.257 ± 0.2161	3	Kruskal-Wallis Test	0.1595
	MOI 200	1.288 ± 0.1036	3	Kruskal-Wallis Test	0.1076
24 hours	Control	1.000 ± 0.000	3	ANOVA	N/A
	IFN- γ	1.159 ± 0.04327	3	ANOVA	0.8286
	MOI 10	1.230 ± 0.1186	3	ANOVA	0.5374
	MOI 50	1.203 ± 0.03739	3	ANOVA	0.6678

	MOI 100	1.173 ± 0.2689	3	ANOVA	0.7787
	MOI 200	1.191 ± 0.4270	3	ANOVA	0.7129
48 hours	Control	1.000 ± 0.000	3	ANOVA	N/A
	IFN- γ	1.084 ± 0.01671	3	ANOVA	0.7706
	MOI 10	1.152 ± 0.08120	3	ANOVA	0.2933
	MOI 50	1.137 ± 0.1104	3	ANOVA	0.3827
	MOI 100	1.088 ± 0.03215	3	ANOVA	0.7389
	MOI 200	1.132 ± 0.2062	3	ANOVA	0.4148

3.1.4 PD-L1 protein expression in CL-11 cells in response to heat-killed *F. nucleatum* ATCC 49256 infection

WB analysis (Figure 9) showed that heat-killed *F. nucleatum* ATCC 49256 induced PD-L1 expression in CL-11 cells, but the response was weaker and more delayed compared to SCC-25 cells. The mean PD-L1 expression levels at different time points are summarized in Table 12.

At the 4-hour time point (Figure 9.B.1), PD-L1 expression exhibited a slight increase in response to increasing MOI levels, but none of the conditions reached statistical significance ($P > 0.05$ for all MOIs). The highest increase was observed in MOI 200 (1.305 ± 0.1235, $p = 0.1765$), indicating that heat-killed *F. nucleatum* ATCC 49256 exposure alone may not be sufficient to induce a strong PD-L1 response in CL-11 cells within this short timeframe. At 8 hours (Figure 9.B.2), a trend toward increased PD-L1 expression was observed, particularly in the MOI 100 (2.218 ± 1.215, $p = 0.2441$) and MOI 10 (1.856 ± 0.9023, $p = 0.4707$) groups. However, due to variability within the data, these differences were not statistically significant. At 24 hours (Figure 9.B.3), PD-L1 expression remained moderately elevated in the MOI 10 (1.660 ± 0.2096, $p = 0.1753$) and MOI 200 (1.537 ± 0.4877, $p = 0.3232$) groups, though no significant differences were detected ($P > 0.05$ for all MOIs). At 48 hours (Figure 9.B.4), MOI 200 exhibited a statistically significant increase in PD-L1 expression

(1.549 ± 0.2221, p = 0.0290), while MOI 100 (1.493 ± 0.3328, p = 0.0572) approached significance. This suggests that prolonged exposure to heat-killed *F. nucleatum* ATCC 49256 may be necessary to induce PD-L1 upregulation in CL-11 cells.

The results (Figure 9, Table 12) indicate that heat-killed *F. nucleatum* ATCC 49256 induced PD-L1 expression in CL-11 cells, but the response was more gradual and less pronounced compared to SCC-25 cells. Unlike SCC-25, which exhibited early PD-L1 upregulation at 4 hours, CL-11 cells showed the most notable increase at 48 hours, particularly in the MOI 200 group (p = 0.0290). These findings suggest that PD-L1 induction in colon cancer cells may follow a different kinetic profile compared to oral squamous cell carcinoma cells.

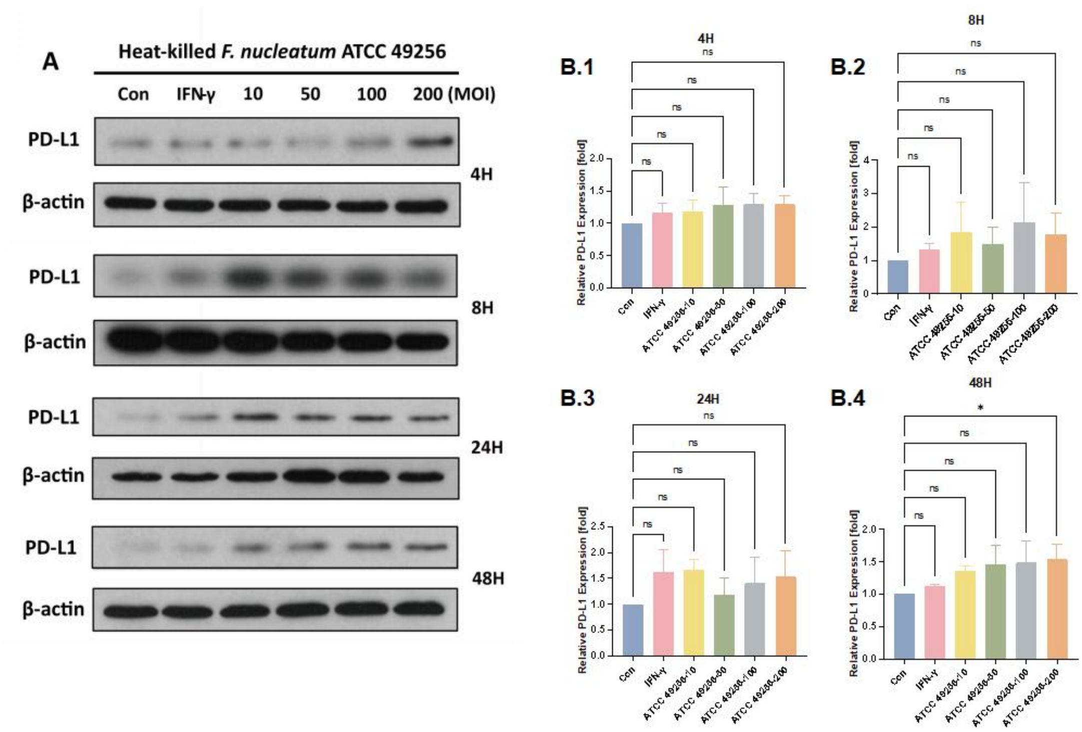

Figure 9. The protein expression of PD-L1 in response to heat-killed *F. nucleatum* ATCC 49256 infection in CL-11.

A. Western blot assays detecting PD-L1 protein expression in CL-11 cells treated with heat-killed *F. nucleatum* ATCC 49256 (MOI=10, 50, 100, and 200), IFN-γ, and medium control. B. Quantitative analysis of the blots after 4-hour (B.1), 8-hour (B.2), 24-hour (B.3), and 48-hour (B.4). The expression of PD-L1 was normalized to ß-actin and the relative fold change was compared with the control group. The relative PD-L1 expression was presented as the mean ± standard deviation of at least three independent assays. * $p < 0.05$ (vs. con group).

Table 12. Statistical summary of PD-L1 protein expression in CL-11 cells infected with heat-killed *F. nucleatum* ATCC 49625 at different MOIs and time points.

Time Point	Group	Mean ± SD	N (Sample Size)	Test Type	Adjusted P Value (vs Control)
4 hours	Control	1.000 ± 0.000	3	ANOVA	N/A
	IFN- γ	1.167 ± 0.1395	3	ANOVA	0.6602
	MOI 10	1.177 ± 0.1867	3	ANOVA	0.6125
	MOI 50	1.280 ± 0.2905	3	ANOVA	0.2329
	MOI 100	1.304 ± 0.1619	3	ANOVA	0.1979
	MOI 200	1.305 ± 0.1235	3	ANOVA	0.1765
8 hours	Control	1.000 ± 0.000	3	ANOVA	N/A
	IFN- γ	1.315 ± 0.2050	3	ANOVA	0.9721
	MOI 10	1.856 ± 0.9023	3	ANOVA	0.4707
	MOI 50	1.505 ± 0.5054	3	ANOVA	0.8478
	MOI 100	2.218 ± 1.215	3	ANOVA	0.2441
	MOI 200	1.779 ± 0.6513	3	ANOVA	0.5514
24 hours	Control	1.000 ± 0.000	3	ANOVA	N/A
	IFN- γ	1.614 ± 0.4437	3	ANOVA	0.224
	MOI 10	1.660 ± 0.2096	3	ANOVA	0.1753
	MOI 50	1.175 ± 0.3305	3	ANOVA	0.9660
	MOI 100	1.410 ± 0.5015	3	ANOVA	0.5553
	MOI 200	1.537 ± 0.4877	3	ANOVA	0.3232
48 hours	Control	1.000 ± 0.000	3	Kruskal-Wallis Test	N/A
	IFN- γ	1.123 ± 0.03344	3	Kruskal-Wallis	>0.9999

			Test	
MOI 10	1.358 ± 0.07914	3	Kruskal-Wallis Test	0.1595
MOI 50	1.454 ± 0.2987	3	Kruskal-Wallis Test	0.1313
MOI 100	1.493 ± 0.3328	3	Kruskal-Wallis Test	0.0572
MOI 200	1.549 ± 0.2221	3	Kruskal-Wallis Test	0.0290

3.1.5 PD-L1 protein expression in CL-11 cells in response to heat-killed *F. nucleatum* ATCC 10953 i-nfection

WB analysis (Figure 10) showed that heat-killed *F. nucleatum* ATCC 10953 induced PD-L1 protein expression in CL-11 cells, following a time- and dose-dependent pattern. The mean PD-L1 expression levels at different time points are summarized in Table 13. Compared to ATCC 49256 (Figure 9), ATCC 10953 induced a stronger and more sustained increase in PD-L1 expression, particularly at 24 and 48 hours.

At the 4-hour time point (Figure 10.B.1), PD-L1 expression showed a moderate but statistically insignificant increase across all MOI conditions ($P > 0.05$). The MOI 200 group exhibited the highest mean value (1.867 ± 0.8353, $p = 0.1933$), but the variability limited its statistical significance. At 8 hours (Figure 10.B.2), a trend toward increased PD-L1 expression was observed, particularly in MOI 10 (2.779 ± 2.200, $p = 0.3139$) and MOI 100 (2.078 ± 0.7939, $p = 0.7257$). However, due to high variability, these differences did not reach statistical significance. At 24 hours (Figure 10.B.3), PD-L1 expression was significantly upregulated in the MOI 50 ($p = 0.0482$), MOI 100 ($p = 0.0400$), and MOI 200 ($p = 0.0178$) groups. The highest PD-L1 expression was observed at MOI 200, indicating that prolonged exposure to a high bacterial load enhances PD-L1 upregulation in CL-11 cells. At 48 hours (Figure 10.B.4), PD-L1 expression remained elevated, with MOI 100 ($p = 0.0377$) and MOI 200 ($p = 0.0324$) maintaining statistical significance compared to control. The increasing trend observed at 24 hours was sustained, reinforcing the idea that ATCC 10953 induces a more prolonged PD-L1 response in CL-11 cells compared to ATCC 49256.

The results (Figure 10, Table 13) indicate that heat-killed *F. nucleatum* ATCC 10953 induces PD-L1 expression in CL-11 cells in a time- and dose-dependent manner, with significant upregulation observed at 24 and 48 hours, particularly in the MOI 100 and 200 groups. Compared to ATCC 49256, which exhibited a delayed and weaker effect, ATCC 10953 induced a more robust and sustained PD-L1 response.

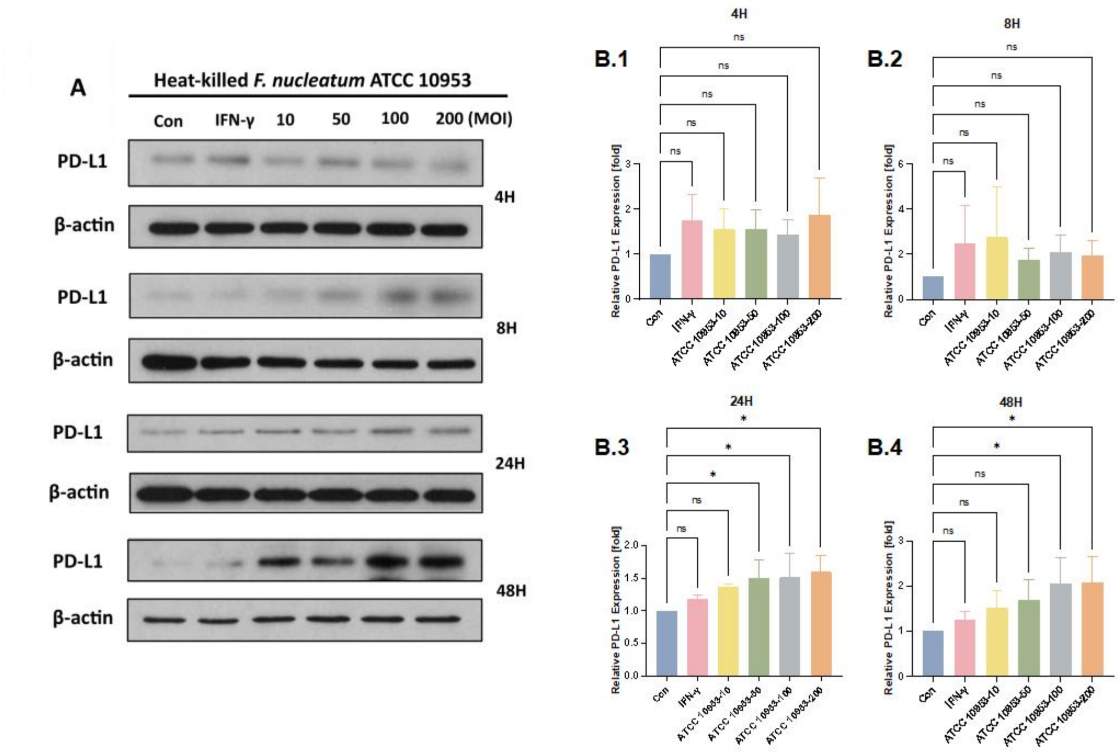

Figure 10. The protein expression of PD-L1 in response to heat-killed *F. nucleatum* ATCC 10953 infection in CL-11.

A. Western blot assays detecting PD-L1 protein expression in CL-11 cells treated with heat-killed *F. nucleatum* ATCC 10953 (MOI=10, 50, 100, and 200), IFN-γ, and medium control. B. Quantitative analysis of the blots after 4-hour (B.1), 8-hour (B.2), 24-hour (B.3), and 48-hour (B.4).The expression of PD-L1 was normalized to ß-actin and the relative fold change was compared with the contrl group. The relative PD-L1 expression was presented as the mean ± standard deviation of at least three independent assays. * $p < 0.05$ (vs. con group).

Table 13. Statistical summary of PD-L1 protein expression in CL-11 cells infected with heat-killed *F. nucleatum* ATCC 10953 at different MOIs and time points.

Time Point	Group	Mean ± SD	N (Sample Size)	Test Type	Adjusted P Value (vs Control)
4 hours	Control	1.000 ± 0.000	3	ANOVA	N/A
	IFN- γ	1.744 ± 0.5851	3	ANOVA	0.3033
	MOI 10	1.566 ± 0.4447	3	ANOVA	0.5363
	MOI 50	1.560 ± 0.4187	3	ANOVA	0.5494
	MOI 100	1.425 ± 0.3475	3	ANOVA	0.7570
	MOI 200	1.867 ± 0.8353	3	ANOVA	0.1933
8 hours	Control	1.000 ± 0.000	3	ANOVA	N/A
	IFN- γ	2.502 ± 1.661	3	ANOVA	0.4575
	MOI 10	2.779 ± 2.200	3	ANOVA	0.3139
	MOI 50	1.738 ± 0.5541	3	ANOVA	0.9123
	MOI 100	2.078 ± 0.7939	3	ANOVA	0.7257
	MOI 200	1.933 ± 0.6840	3	ANOVA	0.8146
24 hours	Control	1.000 ± 0.000	3	ANOVA	N/A
	IFN- γ	1.188 ± 0.04854	3	ANOVA	0.7189
	MOI 10	1.363 ± 0.05323	3	ANOVA	0.1916
	MOI 50	1.504 ± 0.2758	3	ANOVA	0.0482
	MOI 100	1.522 ± 0.3534	3	ANOVA	0.0400
	MOI 200	1.601 ± 0.2480	3	ANOVA	0.0178
48 hours	Control	1.000 ± 0.000	3	ANOVA	N/A
	IFN- γ	1.270 ± 0.1754	3	ANOVA	0.8913

MOI 10	1.514 ± 0.3965	3	ANOVA	0.4605
MOI 50	1.699 ± 0.4386	3	ANOVA	0.2127
MOI 100	2.051 ± 0.5911	3	ANOVA	0.0377
MOI 200	2.080 ± 0.5748	3	ANOVA	0.0324

3.1.6 PD-L1 protein expression in CL-11 cells in response to heat-killed *F. nucleatum* ATCC 25586 infection

Figure 11 demonstrated that heat-killed *F. nucleatum* ATCC 25586 modulated PD-L1 protein expression in CL-11 cells, but its effect was less consistent and largely non-significant across different time points. The mean PD-L1 expression levels at different conditions are summarized in Table 14. Compared to ATCC 10953 (Figure 10), ATCC 25586 elicited a weaker and less sustained induction of PD-L1 expression in CL-11 cells, with significant upregulation observed only at 48 hours in the MOI 50 group.

At the 4-hour time point (Figure 11.B.1), PD-L1 expression exhibited slight increases across all bacterial MOI conditions, but none of the changes reached statistical significance ($P > 0.05$ for all groups). The MOI 10 group showed the highest mean value (1.446 ± 0.3496, p = 0.2363), while MOI 50, 100, and 200 displayed only minor changes compared to the control. These results suggest that ATCC 25586 does not induce a strong early PD-L1 response in CL-11 cells. At 8 hours (Figure 11.B.2), PD-L1 expression displayed greater variability, with MOI 10 and MOI 50 reaching the highest levels (2.789 ± 1.730 and 2.793 ± 2.224, respectively), though these increases were not statistically significant ($P > 0.05$). MOI 100 and MOI 200 groups exhibited lower mean values, suggesting that PD-L1 induction at this stage is highly variable and not dose-dependent. At 24 hours (Figure 11.B.3), PD-L1 expression showed a moderate increasing trend, with the MOI 200 group reaching the highest value (1.943 ± 0.3405, p = 0.1942). However, none of the bacterial-treated groups showed significant upregulation compared to the control ($P > 0.05$), indicating that ATCC 25586-induced PD-L1 expression in CL-11 cells remains inconsistent even at this later time point. At 48 hours (Figure 11.B.4), MOI 50 was the only group that exhibited a statistically significant increase in PD-L1 expression (2.558 ± 0.7337, p = 0.0180). Other groups (MOI 10, 100, and 200) showed a trend toward increased PD-L1 expression, but these changes were not statistically significant (P > 0.05). This suggests that ATCC 25586 may only induce PD-L1 upregulation in CL-11 cells under specific conditions, with a delayed and dose-selective effect.

The results (Figure 11, Table 14) indicate that heat-killed *F. nucleatum* ATCC 25586 has a limited and inconsistent effect on PD-L1 expression in CL-11 cells. Unlike ATCC 10953, which showed a strong and sustained PD-L1 induction at 24 and 48 hours, ATCC 25586 only significantly upregulated PD-L1 at 48 hours in the MOI 50 group. The lack of significant effects at earlier time points and across most MOI conditions suggests that ATCC 25586 may not be as potent in modulating immune checkpoint responses in CL-11 cells compared to other *F. nucleatum* strains.

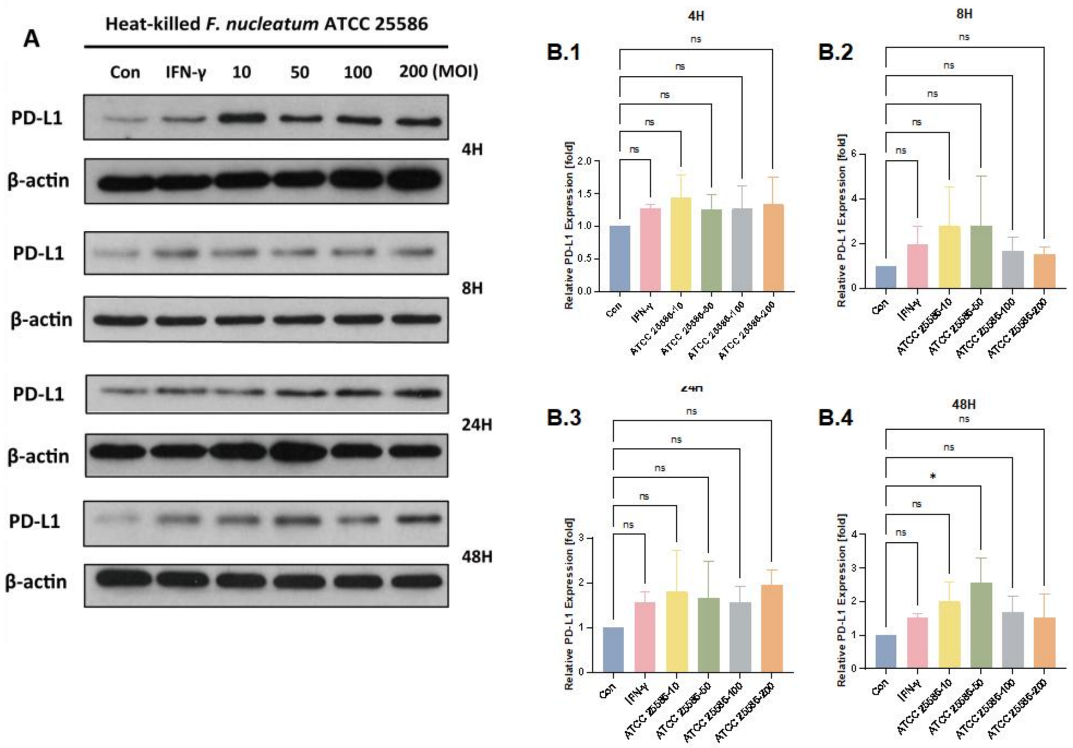

Figure 11. The protein expression of PD-L1 in response to heat-killed *F. nucleatum* ATCC 25586 infection in CL-11.

A. Western blot assays detecting PD-L1 protein expression in CL-11 cells treated with heat-killed *F. nucleatum* ATCC 25586 (MOI=10, 50, 100, and 200), IFN-γ, and medium control. B. Quantitative analysis of the blots after 4-hour (B.1), 8-hour (B.2), 24-hour (B.3), and 48-hour (B.4).The expression of PD-L1 was normalized to ß-actin and the relative fold change was compared with the control group. The relative PD-L1 expression was presented as the mean ± standard deviation of at least three independent assays. * $p < 0.05$ (vs. con group).

Table 14. Statistical summary of PD-L1 protein expression in CL-11 cells infected with heat-killed *F. nucleatum* ATCC 25586 at different MOIs and time points.

Time Point	Group	Mean ± SD	N (Sample Size)	Test Type	Adjusted P Value (vs Control)
4 hours	Control	1.000 ± 0.000	3	ANOVA	N/A
	IFN- γ	1.279 ± 0.5501	3	ANOVA	0.6252
	MOI 10	1.446 ± 0.3496	3	ANOVA	0.2363
	MOI 50	1.268 ± 0.2134	3	ANOVA	0.6572
	MOI 100	1.274 ± 0.3438	3	ANOVA	0.6409
	MOI 200	1.340 ± 0.4154	3	ANOVA	0.4572
8 hours	Control	1.000 ± 0.000	3	ANOVA	N/A
	IFN- γ	1.979 ± 0.8059	3	ANOVA	0.7892
	MOI 10	2.789 ± 1.730	3	ANOVA	0.3115
	MOI 50	2.793 ± 2.224	3	ANOVA	0.3097
	MOI 100	1.684 ± 0.5935	3	ANOVA	0.9336
	MOI 200	1.536 ± 0.3256	3	ANOVA	0.9740
24 hours	Control	1.000 ± 0.000	3	ANOVA	N/A
	IFN- γ	1.571 ± 0.2228	3	ANOVA	0.6017
	MOI 10	1.807 ± 0.9170	3	ANOVA	0.3064
	MOI 50	1.654 ± 0.8279	3	ANOVA	0.4855
	MOI 100	1.574 ± 0.3569	3	ANOVA	0.5961

	MOI 200	1.943 ± 0.3405	3	ANOVA	0.1942
48 hours	Control	1.000 ± 0.000	3	Kruskal-Wallis Test	N/A
	IFN- γ	1.516 ± 0.1329	3	Kruskal-Wallis Test	>0.9999
	MOI 10	2.008 ± 0.5717	3	Kruskal-Wallis Test	0.1927
	MOI 50	2.558 ± 0.7337	3	Kruskal-Wallis Test	0.0180
	MOI 100	1.697 ± 0.4705	3	Kruskal-Wallis Test	0.6269
	MOI 200	1.524 ± 0.7094	3	Kruskal-Wallis Test	0.9634

3.1.7 PD-L1 protein expression in PHGK in response to heat-killed *F. nucleatum* ATCC 49256 infection

The response of PHGK cells to heat-killed *F. nucleatum* ATCC 49256 was relatively mild, with no significant PD-L1 upregulation detected at any time point (Figure 12, Table 15). Compared to SCC-25 and CL-11 cells, where PD-L1 expression exhibited more pronounced changes, PHGK cells showed only subtle variations, with high variability across replicates.

At 4 hours (Figure 12.B.1), PD-L1 levels remained stable across all bacterial treatment groups, with no significant differences compared to the control ($P > 0.9999$). The MOI 10 and MOI 200 groups displayed slightly lower PD-L1 levels than control, while MOI 50 and MOI 100 showed mild, non-significant increases. At 8 hours (Figure 12.B.2), a moderate increase in PD-L1 expression was observed in MOI 10 and MOI 50 groups (1.983 ± 0.9819 and 1.881 ± 0.7963, respectively), though this trend lacked statistical significance ($P > 0.05$). MOI 200 remained comparable to the control, further indicating that PHGK cells may not respond to *F. nucleatum* stimulation in the same manner as SCC-25 and CL-11 cells. At 24 hours (Figure 12.B.3), MOI 10, MOI 50, and MOI 100 groups exhibited a slight upward trend, with PD-L1 expression reaching 2.035 ± 1.493, 2.051 ± 1.306, and 1.797 ± 1.568, respectively. However, none of these increases were statistically significant ($P > 0.05$). The MOI 200 group showed no notable changes, further reinforcing the weaker response of PHGK cells. At 48 hours (Figure 12.B.4), MOI 50 exhibited the highest PD-L1 expression (1.976 ± 0.6809, $p = 0.0572$), approaching statistical significance, while other groups remained largely unchanged. This suggests that PHGK cells may require extended bacterial exposure for PD-L1 induction, though the effect remains inconsistent.

Overall, PHGK cells exhibited limited PD-L1 induction in response to heat-killed *F. nucleatum* ATCC 49256, with no significant upregulation at any time point (Figure 12, Table 15). Unlike SCC-25 and CL-11 cells, which showed distinct increases in PD-L1 expression, PHGK cells displayed high variability and weak responses to bacterial stimulation. The only condition approaching significance was MOI 50 at 48 hours, suggesting that PHGK cells may have a higher activation threshold for PD-L1 expression. These findings further highlight the differential immune regulatory responses between normal and cancerous epithelial cells.

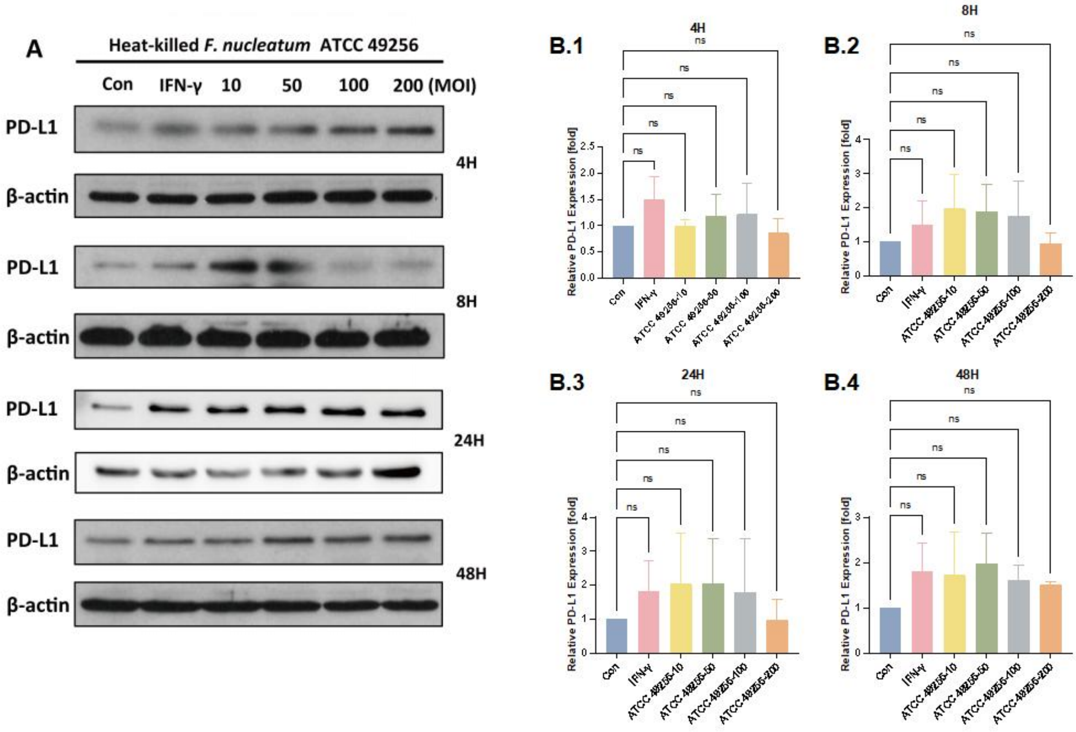

Figure 12. The protein expression of PD-L1 in response to heat-killed *F. nucleatum* ATCC 49256 infection in primary human gingival keratinocytes (PHGK).

A.Western blot assays detecting PD-L1 protein expression in PHGK cells treated with heat-killed *F. nucleatum* ATCC 49256 (MOI=10, 50, 100, and 200), IFN-γ, and medium control. B. Quantitative analysis of the blots after 4-hour (B.1), 8-hour (B.2), 24-hour (B.3), and 48-hour (B.4). The expression of PD-L1 was normalized to ß-actin and the relative fold change was compared with the control group. The relative PD-L1 expression was presented as the mean ± standard deviation of at least three independent assays.

Table 15. Statistical summary of PD-L1 protein expression in PHGK infected with heat-killed *F. nucleatum* ATCC 49625 at different MOIs and time points.

Time Point	Group	Mean ± SD	N (Sample Size)	Test Type	Adjusted P Value (vs Control)
4 hours	Control	1.000 ± 0.000	3	ANOVA	N/A
	IFN- γ	1.495 ± 0.4361	3	ANOVA	0.3899
	MOI 10	0.9970 ± 0.1157	3	ANOVA	>0.9999
	MOI 50	1.176 ± 0.4138	3	ANOVA	>0.9999
	MOI 100	1.228 ± 0.5841	3	ANOVA	>0.9999
	MOI 200	0.8627 ± 0.2760	3	ANOVA	>0.9999
8 hours	Control	1.000 ± 0.000	3	ANOVA	N/A
	IFN- γ	1.507 ± 0.6770	3	ANOVA	0.8589
	MOI 10	1.983 ± 0.9819	3	ANOVA	0.3745
	MOI 50	1.881 ± 0.7963	3	ANOVA	0.4696
	MOI 100	1.765 ± 1.012	3	ANOVA	0.5902
	MOI 200	0.9487 ± 0.3197	3	ANOVA	>0.9999
24 hours	Control	1.000 ± 0.000	3	ANOVA	N/A
	IFN- γ	1.816 ± 0.9114	3	ANOVA	0.8390
	MOI 10	2.035 ± 1.493	3	ANOVA	0.6973
	MOI 50	2.051 ± 1.306	3	ANOVA	0.6823
	MOI 100	1.797 ± 1.568	3	ANOVA	0.8503

	MOI 200	0.9808 ± 0.5969	3	ANOVA	>0.9999
48 hours	Control	1.000 ± 0.000	3	Kruskal-Wallis Test	N/A
	IFN- γ	1.794 ± 0.6443	3	Kruskal-Wallis Test	0.1927
	MOI 10	1.734 ± 0.9501	3	Kruskal-Wallis Test	0.3899
	MOI 50	1.976 ± 0.6809	3	Kruskal-Wallis Test	0.0572
	MOI 100	1.608 ± 0.3390	3	Kruskal-Wallis Test	0.2770
	MOI 200	1.507 ± 0.0638	3	Kruskal-Wallis Test	0.1927

3.1.8 PD-L1 protein expression in PHGK in response to heat-killed *F. nucleatum* ATCC 10953 infection

PD-L1 expression in PHGK cells following stimulation with heat-killed *F. nucleatum* ATCC 10953 exhibited a more dynamic response compared to ATCC 49256, with significant upregulation detected at specific time points and bacterial concentrations (Figure 13, Table 16). However, the pattern remained inconsistent, and only select conditions demonstrated statistical significance.

At 4 hours (Figure 13.B.1), MOI 10 induced a notable increase in PD-L1 expression (2.801 ± 1.369, p = 0.0366), whereas other bacterial-treated groups showed only moderate changes that did not reach statistical significance (P > 0.05). This suggests that early PD-L1 upregulation in PHGK cells may be dependent on specific bacterial concentrations rather than following a linear dose-response pattern. At 8 hours (Figure 13.B.2), PD-L1 levels exhibited a downward adjustment, with no significant differences among bacterial-treated groups (P > 0.05). MOI 100 and MOI 50 showed slightly increased expression (1.621 ± 0.1739 and 1.497 ± 0.3401, respectively), but these changes were not statistically significant. The loss of PD-L1 induction after 8 hours suggests that PHGK cells may exhibit a transient response to ATCC 10953, with an initial spike followed by stabilization. At 24 hours (Figure 13.B.3), PD-L1 levels significantly increased in the MOI 50 (p = 0.0229) and MOI 100 (p = 0.0459) groups, whereas MOI 10 and MOI 200 did not exhibit significant changes (P > 0.05). These findings indicate that prolonged exposure to moderate bacterial loads (MOI 50 – 100) may be required to sustain PD-L1 induction in PHGK cells. At 48 hours (Figure 13.B.4), MOI 200 showed a significant increase in PD-L1 expression (p = 0.0459), while MOI 100 approached significance (p = 0.0572). Other groups remained close to baseline levels, suggesting that longer exposure and higher bacterial loads may be necessary to maintain PD-L1 upregulation in PHGK cells.

The results (Figure 13, Table 16) indicate that heat-killed *F. nucleatum* ATCC 10953 elicits a more variable PD-L1 response in PHGK cells compared to ATCC 49256. While PD-L1 induction was observed at 4 hours (MOI 10), 24 hours (MOI 50, 100), and 48 hours (MOI 200), the response did not follow a clear dose-dependent pattern. These findings suggest that PHGK cells may require specific bacterial concentrations and exposure durations to activate PD-L1 expression, further emphasizing the distinct immune regulation patterns in normal versus cancerous epithelial cells.

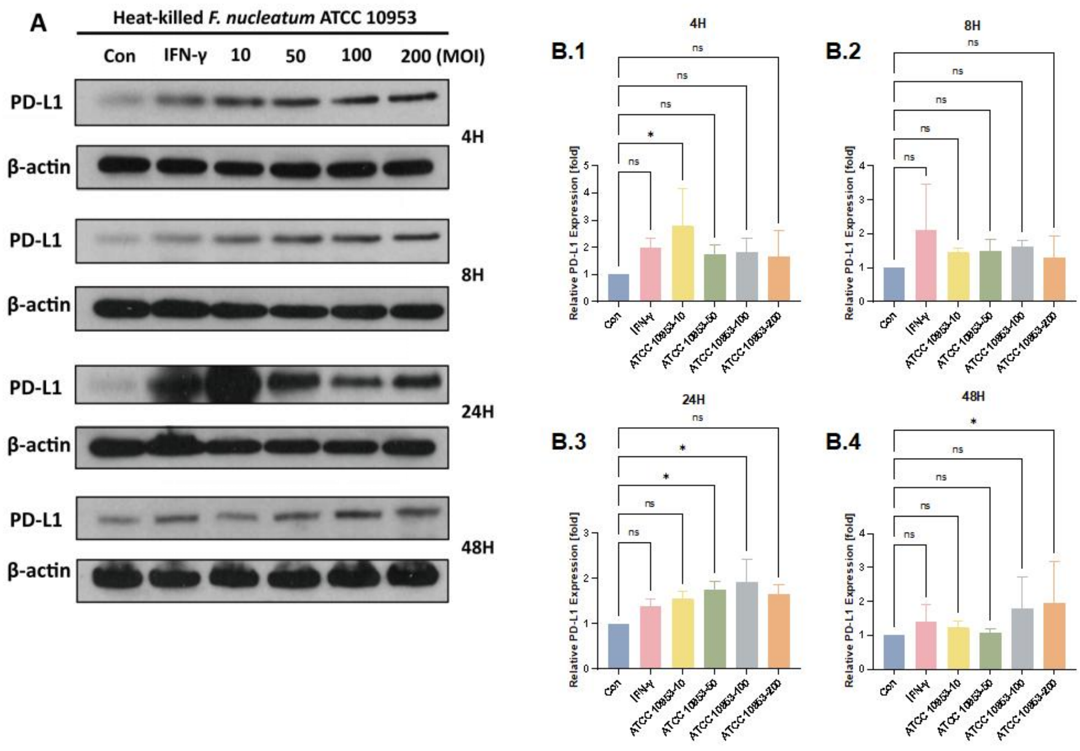

Figure 13. The protein expression of PD-L1 in response to heat-killed *F. nucleatum* ATCC 10953 infection in primary human gingival keratinocytes (PHGK).

A. Western blot assays detecting PD-L1 protein expression in PHGK cells treated with heat-killed *F. nucleatum* ATCC 10953 (MOI=10, 50, 100, and 200), IFN-γ, and medium control. B. Quantitative analysis of the blots after 4-hour (B.1), 8-hour (B.2), 24-hour (B.3), and 48-hour (B.4). The expression of PD-L1 was normalized to ß-actin and the relative fold change was compared with the control group. The relative PD-L1 expression was presented as the mean ± standard deviation of at least three independent assays. * $p < 0.05$ (vs. con group).

Table 16. Statistical summary of PD-L1 protein expression in PHGK infected with heat-killed *F. nucleatum* ATCC 10953 at different MOIs and time points.

Time Point	Group	Mean ± SD	N (Sample Size)	Test Type	Adjusted P Value (vs Control)
4 hours	Control	1.000 ± 0.000	3	Kruskal-Wallis Test	N/A
	IFN- γ	1.987 ± 0.3432	3	Kruskal-Wallis Test	0.1595
	MOI 10	2.801 ± 1.369	3	Kruskal-Wallis Test	0.0366
	MOI 50	1.736 ± 0.3425	3	Kruskal-Wallis Test	0.7270
	MOI 100	1.818 ± 0.5347	3	Kruskal-Wallis Test	0.6269
	MOI 200	1.654 ± 0.9448	3	Kruskal-Wallis Test	>0.9999
8 hours	Control	1.000 ± 0.000	3	ANOVA	N/A
	IFN- γ	2.096 ± 1.373	3	ANOVA	0.1914
	MOI 10	1.451 ± 0.1166	3	ANOVA	0.8517
	MOI 50	1.497 ± 0.3401	3	ANOVA	0.8021
	MOI 100	1.621 ± 0.1739	3	ANOVA	0.6513
	MOI 200	1.307 ± 0.6284	3	ANOVA	0.9615
24 hours	Control	1.000 ± 0.000	3	Kruskal-Wallis	N/A

				Test	
	IFN- γ	1.391 ± 0.1620	3	Kruskal-Wallis Test	>0.9999
	MOI 10	1.567 ± 0.1383	3	Kruskal-Wallis Test	0.3295
	MOI 50	1.752 ± 0.1886	3	Kruskal-Wallis Test	0.0229
	MOI 100	1.922 ± 0.5034	3	Kruskal-Wallis Test	0.0459
	MOI 200	1.640 ± 0.2130	3	Kruskal-Wallis Test	0.2316
48 hours	Control	1.000 ± 0.000	3	Kruskal-Wallis Test	N/A
	IFN- γ	1.416 ± 0.4760	3	Kruskal-Wallis Test	0.4591
	MOI 10	1.224 ± 0.1985	3	Kruskal-Wallis Test	0.6269
	MOI 50	1.068 ± 0.1370	3	Kruskal-Wallis Test	>0.9999
	MOI 100	1.798 ± 0.9184	3	Kruskal-Wallis Test	0.0572
	MOI 200	1.969 ± 1.220	3	Kruskal-Wallis Test	0.0459

3.1.9 PD-L1 protein expression in PHGK in response to heat-killed *F. nucleatum* ATCC 25586 infection

Compared to the other *F. nucleatum* strains, ATCC 25586 exhibited a distinct pattern of PD-L1 regulation in PHGK cells, characterized by an initial downregulation at early time points, followed by modest increases at later stages (Figure 14, Table 17). Unlike ATCC 10953, which triggered sporadic PD-L1 upregulation, ATCC 25586 demonstrated a more variable response, with only a few statistically significant changes.

At 4 hours (Figure 14.B.1), a notable decrease in PD-L1 expression was observed, particularly in the MOI 100 group (0.3283 ± 0.1012, p = 0.0084), marking a statistically significant reduction compared to the control. Other bacterial-treated groups (MOI 10, 50, and 200) also displayed reduced PD-L1 levels, though these changes did not reach statistical significance (P > 0.05). This suggests that ATCC 25586 may initially suppress PD-L1 expression in PHGK cells rather than inducing an early immune response. At 8 hours (Figure 14.B.2), the trend reversed, with MOI 10 and MOI 50 groups showing significant PD-L1 upregulation (p = 0.0366 and p = 0.0459, respectively). The remaining bacterial treatment groups exhibited moderate increases, but these were not statistically significant. This shift from early suppression to later induction implies that ATCC 25586 may have a delayed effect on PD-L1 regulation in PHGK cells. At 24 hours (Figure 14.B.3), PD-L1 expression remained elevated, particularly in the MOI 50 group (2.143 ± 0.9481, p = 0.2587), though statistical significance was not reached. The MOI 100 and MOI 200 groups showed variable responses, with no consistent pattern of regulation (P > 0.05). The sustained yet inconsistent PD-L1 levels suggest that ATCC 25586-induced PD-L1 upregulation may depend on bacterial dose and exposure duration. At 48 hours (Figure 14.B.4), PD-L1 expression remained moderately increased in the MOI 10, MOI 50, and MOI 200 groups, though none reached statistical significance (P > 0.05). Compared to earlier time points, the fluctuations in expression were less pronounced, indicating that ATCC 25586 does not trigger a strong long-term PD-L1 response in PHGK cells.

The results (Figure 14, Table 17) reveal that ATCC 25586 modulates PD-L1 expression in PHGK cells through a biphasic response—initial suppression followed by transient upregulation. The significant downregulation at 4 hours (MOI 100, p = 0.0084) contrasts with the increased expression at 8 hours (MOI 10 and MOI 50, P < 0.05), highlighting a potential strain-specific regulatory mechanism. However, at 24 and 48 hours, PD-L1 levels remained inconsistent, suggesting that ATCC 25586 does not exert a strong or sustained effect on PD-L1 expression in PHGK cells. These findings reinforce the strain-dependent nature of *F. nucleatum*'s influence on immune checkpoint regulation, with ATCC 25586 exhibiting a unique early suppression phase before inducing a moderate upregulation.

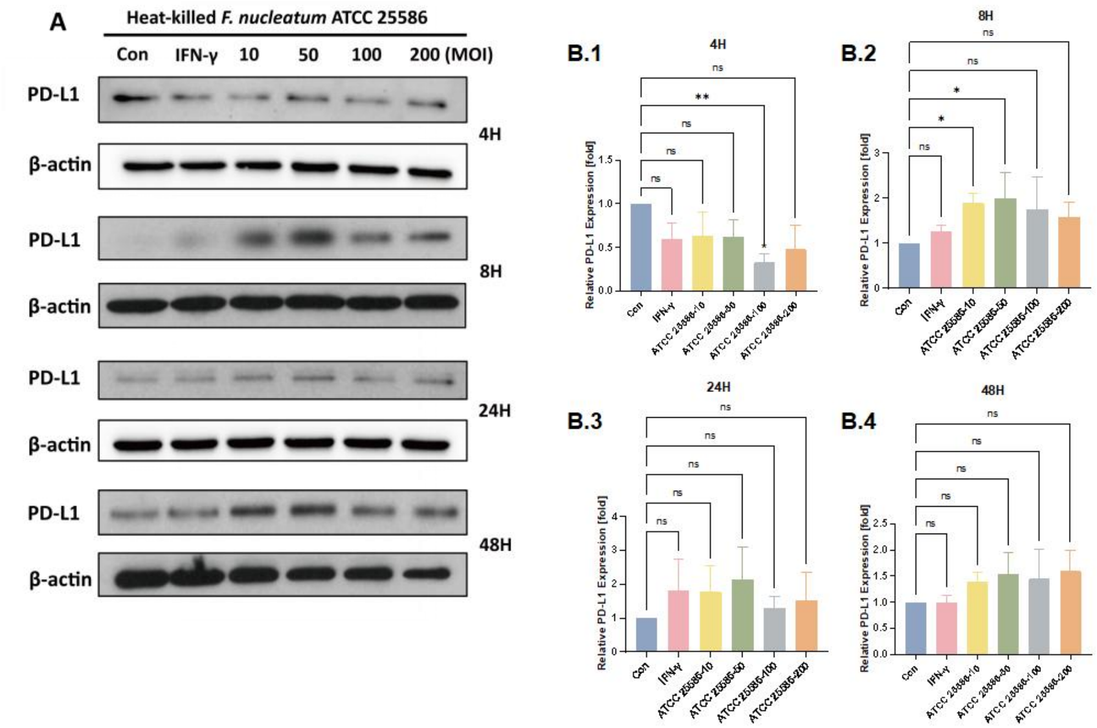

Figure 14. The protein expression of PD-L1 in response to heat-killed *F. nucleatum* ATCC 25586 infection in primary human gingival keratinocytes (PHGK) .

A. Western blot assays detecting PD-L1 protein expression in PHGK cells treated with heat-killed *F. nucleatum* ATCC 25586 (MOI=10, 50, 100, and 200), IFN-γ, and medium control. B. Quantitative analysis of the blots after 4-hour (B.1), 8-hour (B.2), 24-hour (B.3), and 48-hour (B.4).The expression of PD-L1 was normalized to ß-actin and the relative fold change was compared with the control group. The relative PD-L1 expression was presented as the mean ± standard deviation of at least three independent assays. * $p < 0.05$ (vs. con group).

Table 17. Statistical summary of PD-L1 protein expression in PHGK infected with heat-killed *F. nucleatum* ATCC 25586 at different MOIs and time points.

Time Point	Group	Mean ± SD	N (Sample Size)	Test Type	Adjusted P Value (vs Control)
4 hours	Control	1.000 ± 0.000	3	Kruskal-Wallis Test	N/A
	IFN- γ	0.5933 ± 0.1868	3	Kruskal-Wallis	0.4591

				Test	
	MOI 10	0.6325 ± 0.2797	3	Kruskal-Wallis Test	0.3899
	MOI 50	0.6192 ± 0.1940	3	Kruskal-Wallis Test	0.4591
	MOI 100	0.3283 ± 0.1012	3	Kruskal-Wallis Test	0.0084
	MOI 200	0.4819 ± 0.2672	3	Kruskal-Wallis Test	0.1927
8 hours	Control	1.000 ± 0.000	3	Kruskal-Wallis Test	N/A
	IFN- γ	1.272 ± 0.1241	3	Kruskal-Wallis Test	>0.9999
	MOI 10	1.900 ± 0.2019	3	Kruskal-Wallis Test	0.0366
	MOI 50	1.991 ± 0.5824	3	Kruskal-Wallis Test	0.0459
	MOI 100	1.761 ± 0.7175	3	Kruskal-Wallis Test	0.1595
	MOI 200	1.588 ± 0.3167	3	Kruskal-Wallis Test	0.2316
24 hours	Control	1.000 ± 0.000	3	ANOVA	N/A
	IFN- γ	1.815 ± 0.9311	3	ANOVA	0.5419
	MOI 10	1.767 ± 0.7679	3	ANOVA	0.5931
	MOI 50	2.143 ± 0.9481	3	ANOVA	0.2587
	MOI 100	1.294 ± 0.3577	3	ANOVA	0.9817
	MOI 200	1.505 ± 0.8584	3	ANOVA	0.8632
48 hours	Control	1.000 ± 0.000	3	Kruskal-Wallis Test	N/A
	IFN- γ	0.9892 ± 0.1454	3	Kruskal-Wallis Test	>0.9999
	MOI 10	1.393 ± 0.1790	3	Kruskal-Wallis Test	0.5066

MOI 50	1.538 ± 0.4106	3	Kruskal-Wallis Test	0.2464
MOI 100	1.453 ± 0.5608	3	Kruskal-Wallis Test	0.3838
MOI 200	1.601 ± 0.3934	3	Kruskal-Wallis Test	0.1726

3.2 mRNA expression of PD-L1 in cells stimulated with *F. nucleatum*

3.2.1 mRNA expression of PD-L1 in SCC-25 stimulated with heat-killed *F. nucleatum*

To evaluate the effects of different *F. nucleatum* strains on PD-L1 transcriptional regulation in SCC-25 cells, we assessed PD-L1 mRNA levels after stimulation with heat-killed *F. nucleatum* ATCC 49256, ATCC 10953, and ATCC 25586 over multiple time points (Figure 15, Tables 18 – 20). The results revealed strain-dependent variations, with no consistent upregulation of PD-L1 mRNA across all conditions.

PD-L1 mRNA expression in ATCC 49256-treated SCC-25 cells remained comparable to the control group across all time points (Figure 15A, Table 18). At 4 and 8 hours, PD-L1 expression levels did not show a statistically significant increase (P > 0.05). At 24 hours, MOI 10 displayed the highest relative expression (5.200 ± 8.400), suggesting a potential induction, though it did not reach significance. By 48 hours, PD-L1 expression stabilized across all conditions. These findings suggest that ATCC 49256 had a limited effect on PD-L1 mRNA transcription in SCC-25 cells.

Unlike ATCC 49256, ATCC 10953-treated SCC-25 cells exhibited a mild reduction in PD-L1 mRNA levels at early time points, though statistical significance was not observed (Figure 15B, Table 19). At 4 hours, PD-L1 expression in bacterial-treated groups was slightly lower than the control (P > 0.05). At 8 and 24 hours, expression returned to baseline, and by 48 hours, MOI 10 and MOI 50 exhibited a modest increase, though not statistically significant.

These findings suggest that ATCC 10953 does not strongly induce PD-L1 transcription in SCC-25 cells.

Among the three *F. nucleatum* strains, ATCC 25586 exhibited the most noticeable effect on PD-L1 mRNA expression, particularly at later time points (Figure 15C, Table 20). At 4 hours, IFN-γ stimulation led to a significant increase in PD-L1 expression (p = 0.0025), whereas bacterial-treated groups showed only mild changes. By 24 and 48 hours, MOI 10 and MOI 200 exhibited the highest PD-L1 expression levels, though they did not reach statistical significance. These results suggest that ATCC 25586 may exert a delayed regulatory effect on PD-L1 transcription.

The results (Figure 15, Tables 18 – 20) suggest that heat-killed *F. nucleatum* does not significantly upregulate PD-L1 mRNA expression in SCC-25 cells across multiple time points. While ATCC 25586 showed minor increases at later time points, neither ATCC 49256 nor

ATCC 10953 induced substantial PD-L1 transcriptional activation. These findings contrast with PD-L1 protein expression trends, implying the presence of post-transcriptional regulation mechanisms in response to *F. nucleatum* infection.

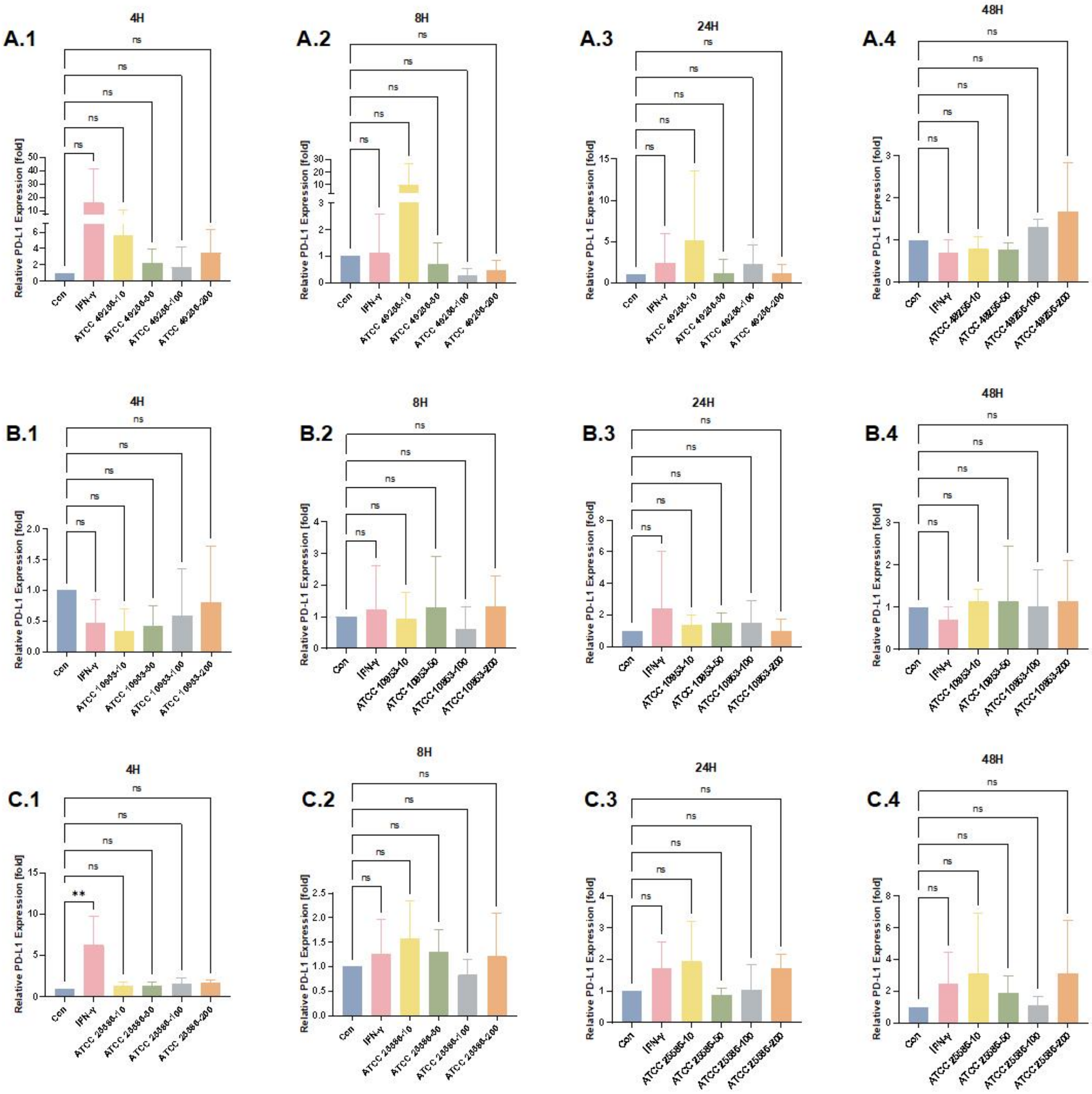

Figure 15. The mRNA expression of PD-L1 in response to heat-killed *F. nucleatum* ATCC 49256, ATCC 10953, and ATCC 25586 infection in SCC-25 cells.

PD-L1 mRNA levels were analyzed by RT-qPCR assay in cells after stimulated with heat-killed *F. nulceatum* ATCC 49256 (A), ATCC 10953 (B), and ATCC 25586 (C) at 4h, 8h, 24h, and 48h. The values were analyzed using the comparative CT (ΔΔCT) method. The amount of target ($2^{-\Delta\Delta CT}$) was obtained by normalizing an endogenous reference (β-actin) relative to non-infected cells. Results were presented as mean ± SD of at least three independent experiments. **$p < 0.01$ (vs. con group).

Table 18. Statistical summary of PD-L1 mRNA expression in response to heat-killed *F. nucleatum* ATCC 49256 infection in SCC-25.

Time Point	Group	Mean ± SD	N (Sample Size)	Test Type	P-value (vs control)
4 hours	Control	1.000 ± 0.000	3	Kruskal-Wallis Test	N/A
	IFN- γ	15.80 ± 25.88	3	Kruskal-Wallis Test	1.000
	MOI 10	5.550 ± 5.000	3	Kruskal-Wallis Test	0.727
	MOI 50	2.199 ± 1.689	3	Kruskal-Wallis Test	1.000
	MOI 100	1.699 ± 2.456	3	Kruskal-Wallis Test	1.000
	MOI 200	3.485 ± 2.799	3	Kruskal-Wallis Test	1.000
8 hours	Control	1.000 ± 0.000	3	Kruskal-Wallis Test	N/A
	IFN- γ	1.119 ± 1.458	3	Kruskal-Wallis Test	1.000
	MOI 10	9.887 ± 16.82	3	Kruskal-Wallis Test	1.000
	MOI 50	0.7107 ± 0.8000	3	Kruskal-Wallis Test	1.000
	MOI 100	0.3028 ± 0.2340	3	Kruskal-Wallis Test	0.6269
	MOI 200	0.4510 ± 0.3882	3	Kruskal-Wallis Test	0.7270
24 hours	Control	1.000 ± 0.000	3	Kruskal-Wallis Test	N/A
	IFN- γ	2.414 ± 3.615	3	Kruskal-Wallis Test	1.000
	MOI 10	5.200 ± 8.400	3	Kruskal-Wallis Test	1.000
	MOI 50	1.184 ± 1.700	3	Kruskal-Wallis Test	1.000
	MOI 100	2.251 ± 2.345	3	Kruskal-Wallis Test	0.6269
	MOI 200	1.218 ± 1.034	3	Kruskal-Wallis Test	0.7270
48 hours	Control	1.000 ± 0.000	3	Kruskal-Wallis Test	N/A

	IFN- γ	0.6962 ± 0.3062	3	Kruskal-Wallis Test	1.000
	MOI 10	0.7935 ± 0.2985	3	Kruskal-Wallis Test	1.000
	MOI 50	0.7891 ± 0.1409	3	Kruskal-Wallis Test	1.000
	MOI 100	1.305 ± 0.1844	3	Kruskal-Wallis Test	1.000
	MOI 200	1.668 ± 1.155	3	Kruskal-Wallis Test	1.000

Table 19. Statistical summary of PD-L1 mRNA expression in response to heat-killed *F. nucleatum* ATCC 10953 infection in SCC-25.

Time Point	Group	Mean ± SD	N (Sample Size)	Test Type	P-value (vs control)
4 hours	Control	1.000 ± 0.000	3	ANOVA	N/A
	IFN- γ	0.4625 ± 0.3887	3	ANOVA	0.6431
	MOI 10	0.3384 ± 0.3626	3	ANOVA	0.4680
	MOI 50	0.4261 ± 0.3245	3	ANOVA	0.5900
	MOI 100	0.5964 ± 0.7502	3	ANOVA	0.8303
	MOI 200	0.8091 ± 0.9157	3	ANOVA	0.9898
8 hours	Control	1.000 ± 0.000	3	ANOVA	N/A
	IFN- γ	1.212 ± 1.396	3	ANOVA	0.9992
	MOI 10	0.9405 ± 0.8348	3	ANOVA	1.0000
	MOI 50	1.304 ± 1.605	3	ANOVA	0.9957
	MOI 100	0.6067 ± 0.7187	3	ANOVA	0.9866
	MOI 200	1.312 ± 0.9700	3	ANOVA	0.9952
24 hours	Control	1.000 ± 0.000	3	Kruskal-Wallis Test	N/A
	IFN- γ	2.414 ± 3.615	3	Kruskal-Wallis Test	1.000

	MOI 10	1.361 ± 0.6331	3	Kruskal-Wallis Test	1.000
	MOI 50	1.488 ± 0.6214	3	Kruskal-Wallis Test	1.000
	MOI 100	1.506 ± 1.405	3	Kruskal-Wallis Test	1.000
	MOI 200	1.002 ± 0.7334	3	Kruskal-Wallis Test	1.000
48 hours	Control	1.000 ± 0.000	3	Kruskal-Wallis Test	1.000
	IFN- γ	0.6962 ± 0.3062	3	Kruskal-Wallis Test	1.000
	MOI 10	1.134 ± 0.3005	3	Kruskal-Wallis Test	1.000
	MOI 50	1.148 ± 1.287	3	Kruskal-Wallis Test	1.000
	MOI 100	1.008 ± 0.8775	3	Kruskal-Wallis Test	1.000
	MOI 200	1.134 ± 0.9668	3	Kruskal-Wallis Test	1.000

Table 20. Statistical summary of PD-L1 mRNA expression in response to heat-killed *F. nucleatum* ATCC 25586 infection in SCC-25.

Time Point	Group	Mean ± SD	N (Sample Size)	Test Type	P-value (vs control)
4 hours	Control	1.000 ± 0.000	3	ANOVA	N/A
	IFN- γ	6.359 ± 3.333	3	ANOVA	0.0025
	MOI 10	1.279 ± 0.4885	3	ANOVA	0.9993
	MOI 50	1.313 ± 0.4993	3	ANOVA	0.9988
	MOI 100	1.637 ± 0.6941	3	ANOVA	0.9714
	MOI 200	1.640 ± 0.3249	3	ANOVA	0.9708
8 hours	Control	1.000 ± 0.000	3	ANOVA	N/A
	IFN- γ	1.263 ± 0.6984	3	ANOVA	0.9731
	MOI 10	1.569 ± 0.7677	3	ANOVA	0.6676

	MOI 50	1.295 ± 0.4620	3	ANOVA	0.9573
	MOI 100	0.8451 ± 0.3004	3	ANOVA	0.9973
	MOI 200	1.216 ± 0.8670	3	ANOVA	0.9881
24 hours	Control	1.000 ± 0.000	3	ANOVA	N/A
	IFN- γ	1.712 ± 0.8347	3	ANOVA	0.6421
	MOI 10	1.964 ± 1.252	3	ANOVA	0.3851
	MOI 50	0.8914 ± 0.2130	3	ANOVA	0.9998
	MOI 100	1.032 ± 0.7899	3	ANOVA	1.0000
	MOI 200	1.716 ± 0.4486	3	ANOVA	0.6382
48 hours	Control	1.000 ± 0.000	3	ANOVA	N/A
	IFN- γ	2.441 ± 1.980	3	ANOVA	0.8954
	MOI 10	3.117 ± 3.823	3	ANOVA	0.6848
	MOI 50	1.890 ± 1.101	3	ANOVA	0.9834
	MOI 100	1.131 ± 0.5522	3	ANOVA	1.0000
	MOI 200	3.152 ± 3.301	3	ANOVA	0.6726

3.2.2 mRNA expression of PD-L1 in CL-11 stimulated with heat-killed *F. nucleatum*

To assess the transcriptional regulation of PD-L1 in CL-11 cells, we examined PD-L1 mRNA levels following stimulation with heat-killed *F. nucleatum* ATCC 49256, ATCC 10953, and ATCC 25586 over multiple time points (Figure 16, Tables 21 – 23). The results revealed strain-specific differences, with some conditions showing transient fluctuations in PD-L1 expression but no strong, consistent upregulation across all time points.

PD-L1 mRNA expression in ATCC 49256-treated CL-11 cells remained relatively unchanged compared to the control (Figure 16A, Table 21). At 4 and 8 hours, there were no statistically significant differences across all treatment groups, with MOI 10, 50, and 100 showing only minor variations ($P > 0.05$). At 24 hours, a slight downward trend was observed, with MOI 10 and MOI 50 groups displaying lower PD-L1 mRNA levels compared to control, though the differences were not significant. By 48 hours, MOI 50 exhibited the highest increase in expression (9.010 ± 11.03), but the variability was too high to reach statistical significance ($p = 0.2752$). These findings suggest that ATCC 49256 does not robustly regulate PD-L1 mRNA transcription in CL-11 cells.

Similar to ATCC 49256, ATCC 10953-treated CL-11 cells did not exhibit consistent PD-L1 mRNA upregulation (Figure 16B, Table 22). At 4 hours, MOI 100 displayed a moderate increase (3.111 ± 2.722), though this change was not significant ($p = 0.4184$). At 8 hours, a transient increase was observed in the IFN-γ group (5.772 ± 5.593, $p = 0.1187$), but no bacterial-treated groups exhibited statistically significant changes. At 24 hours, PD-L1 mRNA levels remained close to baseline, with no significant differences across groups. By 48 hours, MOI 200 exhibited a noticeable increase (13.86 ± 23.08), but due to the high variability, statistical significance was not reached. These findings indicate that ATCC 10953 does not strongly induce PD-L1 transcription in CL-11 cells.

Among the three *F. nucleatum* strains, ATCC 25586 demonstrated the most notable but inconsistent effects on PD-L1 mRNA expression in CL-11 cells (Figure 16C, Table 23). At 4 hours, MOI 50 showed the highest increase (87.92 ± 149.7), but the large standard deviation prevented significance ($P > 0.05$). At 8 hours, a significant PD-L1 mRNA upregulation was observed in the IFN-γ group ($p = 0.0014$), whereas bacterial-treated groups exhibited only mild changes. By 24 and 48 hours, PD-L1 expression returned to baseline, with no significant differences between bacterial-treated groups and control. These findings indicate that ATCC 25586 may transiently influence PD-L1 transcription in CL-11 cells, but its effects are not sustained over time.

The results (Figure 16, Tables 21 – 23) indicate that heat-killed *F. nucleatum* did not induce a consistent upregulation of PD-L1 mRNA expression in CL-11 cells. While ATCC 25586 showed a transient increase at 4 and 8 hours, the effect was not maintained at later time points.

Meanwhile, ATCC 49256 and ATCC 10953 exhibited only minor fluctuations without significant upregulation.

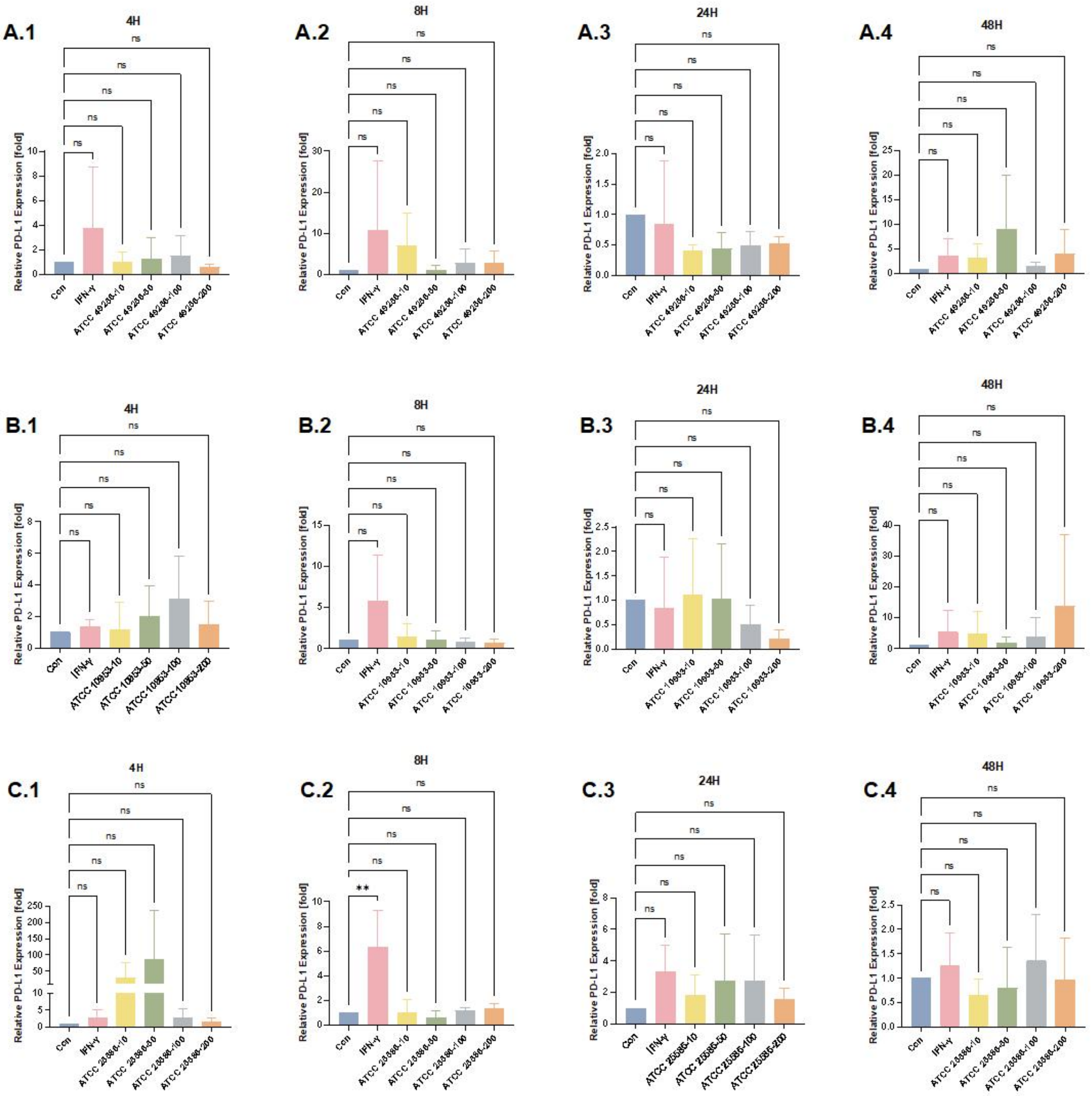

Figure 16. The mRNA expression of PD-L1 in response to heat-killed *F. nucleatum* ATCC 49256, ATCC 10953, and ATCC 25586 infection in CL-11.

PD-L1 mRNA levels were analyzed by qRT-PCR assay in cells after stimulated with heat-killed *F. nulceatum* ATCC 49256 (A), ATCC 10953 (B), and ATCC 25586 (C) at 4h, 8h, 24h, and 48h. The values were analyzed using the comparative CT (ΔΔCT) method. The amount of target ($2^{-\Delta\Delta CT}$) was obtained by normalizing an endogenous reference (β-actin) relative to non-infected cells. Results were presented as mean ± SD of at least three independent experiments. $^{**}p < 0.01$ (vs. con group).

Table 21. Statistical summary of PD-L1 mRNA expression in response to heat-killed *F. nucleatum* ATCC 49256 infection in CL-11.

Time Point	Group	Mean ± SD	N (Sample Size)	Test Type	P-value (vs control)
4 hours	Control	1.000 ± 0.000	3	Kruskal-Wallis Test	N/A
	IFN- γ	3.765 ± 4.960	3	Kruskal-Wallis Test	1.0000
	MOI 10	1.020 ± 0.8292	3	Kruskal-Wallis Test	1.0000
	MOI 50	1.269 ± 1.771	3	Kruskal-Wallis Test	1.0000
	MOI 100	1.509 ± 1.646	3	Kruskal-Wallis Test	1.0000
	MOI 200	0.6277 ± 0.2022	3	Kruskal-Wallis Test	1.0000
8 hours	Control	1.000 ± 0.000	3	Kruskal-Wallis Test	N/A
	IFN- γ	10.74 ± 16.80	3	Kruskal-Wallis Test	1.0000
	MOI 10	7.051 ± 7.889	3	Kruskal-Wallis Test	1.0000
	MOI 50	1.131 ± 0.9978	3	Kruskal-Wallis Test	1.0000
	MOI 100	2.863 ± 3.254	3	Kruskal-Wallis Test	1.0000
	MOI 200	2.730 ± 2.906	3	Kruskal-Wallis Test	1.0000
24 hours	Control	1.000 ± 0.000	3	ANOVA	N/A
	IFN- γ	0.8468 ± 1.028	3	ANOVA	0.9906
	MOI 10	0.4056 ± 0.1046	3	ANOVA	0.3864
	MOI 50	0.4442 ± 0.2560	3	ANOVA	0.4444
	MOI 100	0.4946 ± 0.2226	3	ANOVA	0.5270
	MOI 200	0.5322 ± 0.1119	3	ANOVA	0.5925
48 hours	Control	1.000 ± 0.000	3	ANOVA	N/A
	IFN- γ	3.662 ± 3.346	3	ANOVA	0.9531

	MOI 10	3.114 ± 2.973	3	ANOVA	0.9814
	MOI 50	9.010 ± 11.03	3	ANOVA	0.2752
	MOI 100	1.465 ± 0.9107	3	ANOVA	1.0000
	MOI 200	4.085 ± 4.782	3	ANOVA	0.9195

Table 22. Statistical summary of PD-L1 mRNA expression in response to heat-killed *F. nucleatum* ATCC 10953 infection in CL-11.

Time Point	Group	Mean ± SD	N (Sample Size)	Test Type	P-value (vs control)
4 hours	Control	1.000 ± 0.000	3	ANOVA	N/A
	IFN- γ	1.34 ± 0.4727	3	ANOVA	0.991
	MOI 10	1.169 ± 1.701	3	ANOVA	1.000
	MOI 50	1.996 ± 1.920	3	ANOVA	0.9107
	MOI 100	3.111 ± 2.722	3	ANOVA	0.4184
	MOI 200	1.514 ± 1.426	3	ANOVA	0.9938
8 hours	Control	1.000 ± 0.000	3	ANOVA	N/A
	IFN- γ	5.772 ± 5.593	3	ANOVA	0.1187
	MOI 10	1.438 ± 1.621	3	ANOVA	0.9995
	MOI 50	1.087 ± 1.118	3	ANOVA	1.0000
	MOI 100	0.7818 ± 0.5462	3	ANOVA	1.0000
	MOI 200	0.7036 ± 0.4126	3	ANOVA	1.0000
24 hours	Control	1.000 ± 0.000	3	Kruskal-Wallis Test	N/A
	IFN- γ	0.8468 ± 1.028	3	Kruskal-Wallis Test	1.0000
	MOI 10	1.112 ± 1.157	3	Kruskal-Wallis Test	1.0000

	MOI 50	1.023 ± 1.134	3	Kruskal-Wallis Test	1.0000
	MOI 100	0.5038 ± 0.3861	3	Kruskal-Wallis Test	0.4591
	MOI 200	0.2223 ± 0.1688	3	Kruskal-Wallis Test	0.1595
48 hours	Control	1.000 ± 0.000	3	Kruskal-Wallis Test	N/A
	IFN- γ	5.360 ± 7.127	3	Kruskal-Wallis Test	1.0000
	MOI 10	4.911 ± 7.134	3	Kruskal-Wallis Test	1.0000
	MOI 50	1.754 ± 2.044	3	Kruskal-Wallis Test	1.0000
	MOI 100	3.962 ± 6.236	3	Kruskal-Wallis Test	1.0000
	MOI 200	13.86 ± 23.08	3	Kruskal-Wallis Test	1.0000

Table 23. Statistical summary of PD-L1 mRNA expression in response to heat-killed *F. nucleatum* ATCC 25586 infection in CL-11.

Time Point	Group	Mean ± SD	N (Sample Size)	Test Type	P-value (vs control)
4 hours	Control	1.000 ± 0.000	3	Kruskal-Wallis Test	N/A
	IFN- γ	2.828 ± 2.192	3	Kruskal-Wallis Test	0.9634
	MOI 10	29.47 ± 48.13	3	Kruskal-Wallis Test	0.5378
	MOI 50	87.92 ± 149.7	3	Kruskal-Wallis Test	0.8389
	MOI 100	2.743 ± 2.728	3	Kruskal-Wallis Test	1.0000
	MOI 200	1.402 ± 1.195	3	Kruskal-Wallis Test	1.0000
8 hours	Control	1.000 ± 0.000	3	ANOVA	N/A
	IFN- γ	6.329 ± 2.949	3	ANOVA	0.0014
	MOI 10	1.055 ± 1.056	3	ANOVA	1.0000
	MOI 50	0.6332 ± 0.5728	3	ANOVA	0.9963

	MOI 100	1.209 ± 0.1660	3	ANOVA	0.9997
	MOI 200	1.324 ± 0.4182	3	ANOVA	0.9979
24 hours	Control	1.000 ± 0.000	3	ANOVA	N/A
	IFN- γ	3.309 ± 1.702	3	ANOVA	0.4851
	MOI 10	1.792 ± 1.304	3	ANOVA	0.9805
	MOI 50	2.728 ± 2.997	3	ANOVA	0.7188
	MOI 100	2.707 ± 2.939	3	ANOVA	0.7272
	MOI 200	1.556 ± 0.6942	3	ANOVA	0.9958
48 hours	Control	1.000 ± 0.000	3	ANOVA	N/A
	IFN- γ	1.252 ± 0.6751	3	ANOVA	0.9874
	MOI 10	0.6628 ± 0.3143	3	ANOVA	0.9584
	MOI 50	0.8059 ± 0.8223	3	ANOVA	0.9961
	MOI 100	1.357 ± 0.9370	3	ANOVA	0.9482
	MOI 200	0.9682 ± 0.8455	3	ANOVA	1.0000

3.2.3 mRNA expression of PD-L1 in PHGK stimulated with heat-killed *F. nucleatum*

To evaluate the transcriptional regulation of PD-L1 in PHGK cells, we assessed its mRNA expression following stimulation with heat-killed *F. nucleatum* ATCC 49256, ATCC 10953, and ATCC 25586 across different time points (Figure 17, Tables 24 – 26). Overall, PD-L1 mRNA levels remained largely stable, with only minor fluctuations observed in different treatment groups.

PD-L1 mRNA expression in PHGK cells treated with ATCC 49256 exhibited no substantial changes across all time points (Figure 17A, Table 24). While minor fluctuations were detected, such as a slight decrease at 4 hours and an increase at 8 hours, these variations were not statistically significant. By 24 and 48 hours, expression levels remained comparable to the control group, indicating that ATCC 49256 did not strongly regulate PD-L1 transcription in PHGK cells.

Similarly, treatment with ATCC 10953 did not lead to consistent or significant changes in PD-L1 mRNA expression in PHGK cells (Figure 17B, Table 25). Although some variability was noted, particularly at 24 hours where MOI 100 showed a moderate increase, no statistical significance was observed. Expression levels at 4, 8, and 48 hours remained relatively unchanged, suggesting that ATCC 10953 had no major impact on PD-L1 transcription in PHGK cells.

Among the three *F. nucleatum* strains, ATCC 25586 exhibited a slight but transient suppression of PD-L1 mRNA at early time points (Figure 17C, Table 26). At 4 hours, some groups showed a decrease in expression, particularly MOI 100, but this effect was not sustained. At 8 hours, PD-L1 mRNA levels remained largely stable across all treatment groups. By 24 and 48 hours, no significant differences were detected, indicating that any early suppressive effects of ATCC 25586 on PD-L1 transcription were not long-lasting.

Across all three *F. nucleatum* strains, PD-L1 mRNA expression in PHGK cells remained largely unchanged at all time points, with only minor and transient fluctuations observed (Figure 17, Tables 24 – 26). These results suggest that heat-killed *F. nucleatum* did not significantly modulate PD-L1 transcription in PHGK cells.

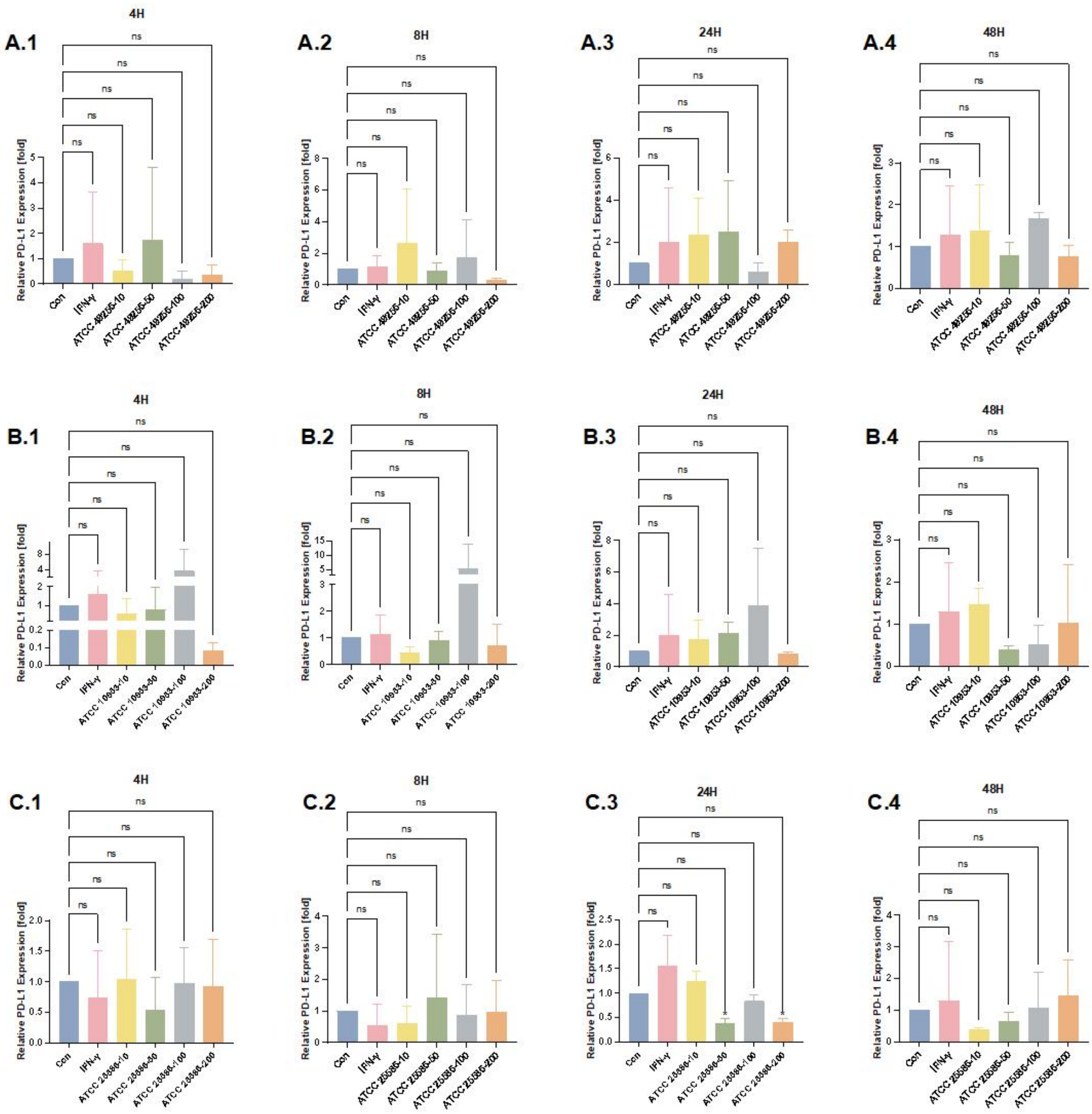

Figure 17. The mRNA expression of PD-L1 in response to heat-killed *F. nucleatum* ATCC 49256, ATCC 10953, and ATCC 25586 infection in primary human gingival keratinocytes (PHGK).

PD-L1 mRNA levels were analyzed by qRT-PCR assay in cells after stimulated with heat-killed *F. nulceatum* ATCC 49256 (A), ATCC 10953 (B), and ATCC 25586 (C) at 4h, 8h, 24h, and 48h. The values were analyzed using the comparative CT (ΔΔCT) method. The amount of target ($2^{-\Delta\Delta CT}$) was obtained by normalizing an endogenous reference (β-actin) relative to non-infected cells. Results were presented as mean ± SD of at least three independent experiments.

Table 24. Statistical summary of PD-L1 mRNA expression in response to heat-killed *F. nucleatum* ATCC 49256 infection in PHGK.

Time Point	Group	Mean ± SD	N (Sample Size)	Test Type	P-value (vs control)
4 hours	Control	1.000 ± 0.000	3	Kruskal-Wallis Test	N/A
	IFN- γ	1.599 ± 2.050	3	Kruskal-Wallis Test	1.0000
	MOI 10	0.5393 ± 0.3967	3	Kruskal-Wallis Test	1.0000
	MOI 50	1.725 ± 2.891	3	Kruskal-Wallis Test	0.6269
	MOI 100	0.2167 ± 0.2851	3	Kruskal-Wallis Test	0.0876
	MOI 200	0.3785 ± 0.3711	3	Kruskal-Wallis Test	0.6269
8 hours	Control	1.000 ± 0.000	3	ANOVA	N/A
	IFN- γ	1.140 ± 0.7299	3	ANOVA	1.0000
	MOI 10	2.670 ± 3.411	3	ANOVA	0.6621
	MOI 50	0.9125 ± 0.5018	3	ANOVA	1.0000
	MOI 100	1.742 ± 2.389	3	ANOVA	0.9763
	MOI 200	0.3191 ± 0.1312	3	ANOVA	0.9835
24 hours	Control	1.000 ± 0.000	3	Kruskal-Wallis Test	N/A
	IFN- γ	1.998 ± 2.567	3	Kruskal-Wallis Test	1.0000
	MOI 10	2.323 ± 1.772	3	Kruskal-Wallis Test	1.0000
	MOI 50	2.492 ± 2.442	3	Kruskal-Wallis Test	1.0000
	MOI 100	0.5964 ± 0.4211	3	Kruskal-Wallis Test	1.0000
	MOI 200	2.016 ± 0.5573	3	Kruskal-Wallis Test	1.0000
48 hours	Control	1.000 ± 0.000	3	ANOVA	N/A
	IFN- γ	1.292 ± 1.156	3	ANOVA	0.9749

	MOI 10	1.378 ± 1.103	3	ANOVA	0.9324
	MOI 50	0.7888 ± 0.3119	3	ANOVA	0.9938
	MOI 100	1.677 ± 0.1409	3	ANOVA	0.6286
	MOI 200	0.7715 ± 0.2519	3	ANOVA	0.9912

Table 25. Statistical summary of PD-L1 mRNA expression in response to heat-killed *F. nucleatum* ATCC 10953 infection in PHGK.

Time Point	Group	Mean ± SD	N (Sample Size)	Test Type	P-value (vs control)
4 hours	Control	1.000 ± 0.000	3	ANOVA	N/A
	IFN- γ	1.599 ± 2.050	3	ANOVA	0.9983
	MOI 10	0.5866 ± 0.7637	3	ANOVA	0.9997
	MOI 50	0.8172 ± 1.143	3	ANOVA	1.0000
	MOI 100	3.641 ± 5.706	3	ANOVA	0.5981
	MOI 200	0.08315 ± 0.04571	3	ANOVA	0.9883
8 hours	Control	1.000 ± 0.000	3	ANOVA	N/A
	IFN- γ	1.140 ± 0.7299	3	ANOVA	1.0000
	MOI 10	0.4426 ± 0.2343	3	ANOVA	0.9998
	MOI 50	0.9061 ± 0.3394	3	ANOVA	1.0000
	MOI 100	5.323 ± 8.656	3	ANOVA	0.4671
	MOI 200	0.7225 ± 0.7845	3	ANOVA	1.0000
24 hours	Control	1.000 ± 0.000	3	Kruskal-Wallis Test	N/A
	IFN- γ	1.998 ± 2.567	3	Kruskal-Wallis Test	1.0000
	MOI 10	1.760 ± 1.190	3	Kruskal-Wallis Test	1.0000

	MOI 50	2.116 ± 0.7335	3	Kruskal-Wallis Test	1.0000
	MOI 100	3.882 ± 3.631	3	Kruskal-Wallis Test	0.7270
	MOI 200	0.8312 ± 0.08902	3	Kruskal-Wallis Test	1.0000
48 hours	Control	1.000 ± 0.000	3	ANOVA	N/A
	IFN- γ	1.292 ± 1.156	3	ANOVA	0.9855
	MOI 10	1.471 ± 0.3649	3	ANOVA	0.9073
	MOI 50	0.3878 ± 0.08914	3	ANOVA	0.7904
	MOI 100	0.5051 ± 0.4566	3	ANOVA	0.8906
	MOI 200	1.030 ± 1.367	3	ANOVA	1.0000

Table 26. Statistical summaryof PD-L1 mRNA expression in response to heat-killed *F. nucleatum* ATCC 25586 infection in PHGK.

Time Point	Group	Mean ± SD	N (Sample Size)	Test Type	P-value (vs control)
4 hours	Control	1.000 ± 0.000	3	ANOVA	N/A
	IFN- γ	0.7363 ± 0.7690	3	ANOVA	0.9796
	MOI 10	1.039 ± 0.8271	3	ANOVA	1.0000
	MOI 50	0.5447 ± 0.5177	3	ANOVA	0.8492
	MOI 100	0.9733 ± 0.5822	3	ANOVA	1.0000
	MOI 200	0.9329 ± 0.7617	3	ANOVA	1.0000
8 hours	Control	1.000 ± 0.000	3	Kruskal-Wallis Test	N/A
	IFN- γ	0.5341 ± 0.6909	3	Kruskal-Wallis Test	1.0000
	MOI 10	0.6024 ± 0.5553	3	Kruskal-Wallis Test	1.0000
	MOI 50	1.436 ± 2.005	3	Kruskal-Wallis Test	1.0000

	MOI 100	0.8747 ± 0.9465	3	Kruskal-Wallis Test	1.0000
	MOI 200	0.9715 ± 1.008	3	Kruskal-Wallis Test	1.0000
24 hours	Control	1.000 ± 0.000	3	ANOVA	N/A
	IFN- γ	1.559 ± 0.6284	3	ANOVA	0.1077
	MOI 10	1.244 ± 0.2017	3	ANOVA	0.7306
	MOI 50	0.3917 ± 0.09720	3	ANOVA	0.0743
	MOI 100	0.8348 ± 0.1261	3	ANOVA	0.9170
	MOI 200	0.4036 ± 0.06992	3	ANOVA	0.0813
48 hours	Control	1.000 ± 0.000	3	Kruskal-Wallis Test	N/A
	IFN- γ	1.299 ± 1.859	3	Kruskal-Wallis Test	1.0000
	MOI 10	0.3814 ± 0.05464	3	Kruskal-Wallis Test	0.7270
	MOI 50	0.6369 ± 0.3052	3	Kruskal-Wallis Test	1.0000
	MOI 100	1.065 ± 1.143	3	Kruskal-Wallis Test	1.0000
	MOI 200	1.455 ± 1.137	3	Kruskal-Wallis Test	1.0000

3.3 Effects of heat-killed *F. nucleatum* on cell viability

3.3.1 Effects of heat-killed *F. nucleatum* ATCC 49256 on SCC-25 cell viability

The viability of SCC-25 cells in response to heat-killed *F. nucleatum* ATCC 49256 was assessed at 4, 8, 24, and 48 hours post-treatment using a CCK-8 assay (Figure 18, Table 27). A two-way ANOVA analysis revealed significant effects of treatment group ($p < 0.0001$, $\eta^2 = 0.0848$), time ($p < 0.0001$, $\eta^2 = 0.5470$), and their interaction ($p < 0.0001$, $\eta^2 = 0.3086$) (Table 28), suggesting that both bacterial concentration and incubation time influenced SCC-25 viability.

At 4 hours, a modest but statistically significant increase in cell viability was observed in the IFN-γ (1.070 $\pm$ 0.019, p = 0.0114), MOI 50 (1.057 $\pm$ 0.013, p = 0.0147), and MOI 200 (1.038 $\pm$ 0.014, p = 0.0343) groups compared to the control, whereas MOI 10 and MOI 100 showed no significant differences. At 8 hours, cell viability increased more prominently in the MOI 100 (1.393 $\pm$ 0.014, p = 0.0133) and MOI 200 (1.419 $\pm$ 0.010, p = 0.0133) groups, while the MOI 10 group displayed a non-significant upward trend (1.294 $\pm$ 0.104, p = 0.0532). IFN-γ and lower bacterial MOI conditions did not significantly alter cell viability. At 24 hours, no statistically significant differences were observed among the treatment groups ($p > 0.05$ for all conditions), with viability values remaining close to the control, indicating a transient effect of heat-killed *F. nucleatum* on SCC-25 viability at earlier time points. At 48 hours, a significant reduction in viability was observed in the MOI 50 (0.737 $\pm$ 0.021, p = 0.0101), MOI 100 (0.845 $\pm$ 0.036, p = 0.0317), and MOI 200 (0.773 $\pm$ 0.056, p = 0.0181) groups compared to the control, suggesting a time-dependent cytotoxic effect at higher bacterial concentrations. A downward trend was also noted for MOI 10 (0.713 $\pm$ 0.103, p = 0.0655) and IFN-γ (0.897 $\pm$ 0.026, p = 0.0993), though these changes did not reach statistical significance.

Overall, the results indicate that heat-killed *F. nucleatum* ATCC 49256 initially enhances SCC-25 viability at lower time points but induces cytotoxic effects at higher MOI levels following prolonged exposure. These findings highlight a biphasic response, with transient stimulation at early time points and reduced viability at 48 hours in a dose-dependent manner.

.

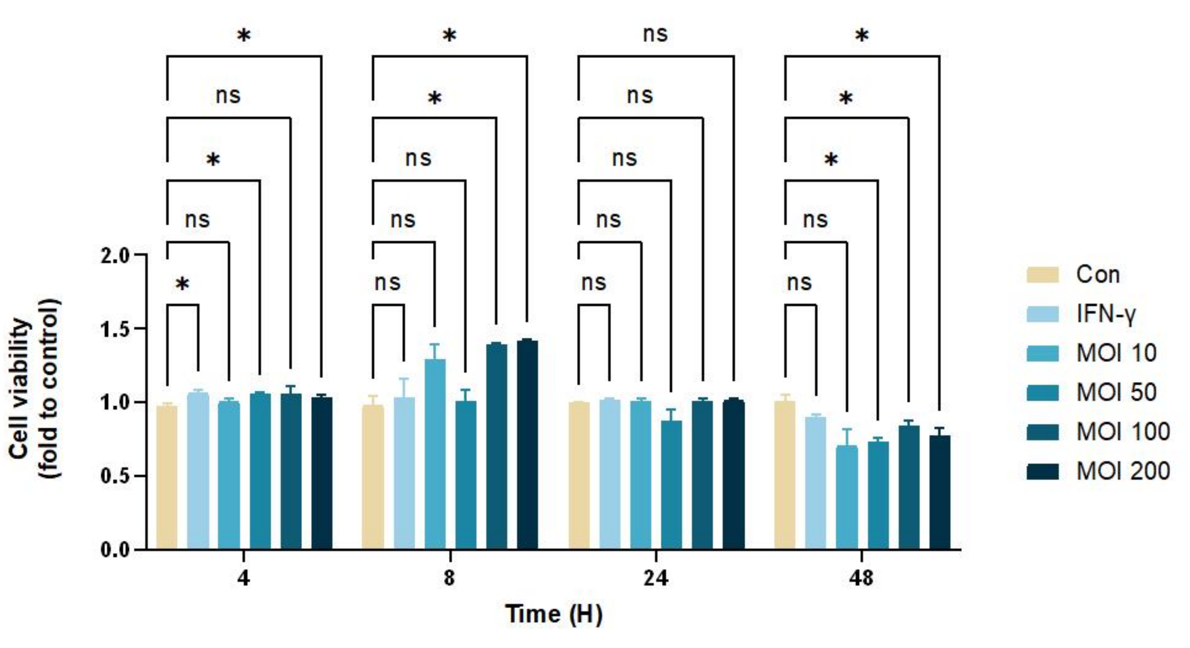

Figure 18. Effects of heat-killed *F. nucleatum* ATCC 49256 on the viability of SCC-25.

SCC-25 were treated with the control or with IFN-γ or with the heat-killed *F. nucleatum* ATCC 49256 with MOI 10, 50, 100, and 200. Cell viability was examined using cell counting kit-8 assay at 4h, 8h, 24h, and 48h. The results are expressed as the mean± SD of at least three independent experiments. *$p < 0.05$ (vs. Control group).

Table 27. Mean ± SD and post-hoc comparisons of SCC-25 viability in response to heat-killed *F. nucleatum* ATCC 49256 across time points

Time Point	Group	Mean±SD	N	Adjusted *P* Value
4 hours	Control	0.975±0.019	3	N/A
	IFN- γ	1.070±0.019	3	0.0114
	MOI 10	1.011±0.013	3	0.1626
	MOI 50	1.057±0.013	3	0.0147
	MOI 100	1.060±0.048	3	0.1946
	MOI 200	1.038±0.014	3	0.0343
8 hours	Control	0.986±0.060	3	N/A
	IFN- γ	1.031±0.130	3	0.9641

	MOI 10	1.294±0.104	3	0.0532
	MOI 50	1.012±0.071	3	0.9770
	MOI 100	1.393±0.014	3	0.0133
	MOI 200	1.419±0.010	3	0.0133
24 hours	Control	0.997±0.004	3	N/A
	IFN-γ	1.018±0.011	3	0.1885
	MOI 10	1.010±0.15	3	0.5931
	MOI 50	0.880±0.075	3	0.2591
	MOI 100	1.011±0.019	3	0.6387
	MOI 200	1.015±0.009	3	0.1621
48 hours	Control	1.006±0.046	3	N/A
	IFN-γ	0.897±0.026	3	0.0993
	MOI 10	0.713±0.103	3	0.0655
	MOI 50	0.737±0.021	3	0.0101
	MOI 100	0.845±0.036	3	0.0317
	MOI 200	0.773±0.056	3	0.0181

Table 28. Two-Way ANOVA results for SCC-25 viability in response to heat-killed *F. nucleatum* ATCC 49256

Source of Variation	F Value	P Value	Effect Size (η^2)
Time × Group	15.89	P<0.0001	0.3086
Time	140.8	P<0.0001	0.5470
Group	15.76	P<0.0001	0.0848

3.3.2 Effects of heat-killed *F. nucleatum* ATCC 10953 on SCC-25 cell viability

Figure 19 illustrates the effects of heat-killed *F. nucleatum* ATCC 10953 on the viability of SCC-25 cells over a time course of 4, 8, 24, and 48 hours. As summarized in Table 29, at 4 hours none of the treatment groups (IFN-γ, MOI 10, MOI 50, MOI 100, MOI 200) showed significant differences in viability compared to the control. At 8 hours, however, a significant decrease in viability was observed in the MOI 50 group (0.951 $\pm$ 0.014 vs. 1.063 $\pm$ 0.007; p = 0.0039), while the MOI 100 group exhibited a significant increase (1.097 $\pm$ 0.003; p = 0.0197) relative to the control. At 24 hours, only the MOI 50 group demonstrated a significant reduction in cell viability (0.760 $\pm$ 0.021 vs. 0.996 $\pm$ 0.010; p = 0.0013), whereas the other treatment groups did not differ significantly from the control. By 48 hours, significant decreases in viability were detected in the IFN-γ (0.807 $\pm$ 0.014; p = 0.0022), MOI 10 (0.888 $\pm$ 0.023; p = 0.0174), MOI 100 (0.918 $\pm$ 0.019; p = 0.0436), and MOI 200 (0.849 $\pm$ 0.044; p = 0.0461) groups compared to the control (0.988 $\pm$ 0.022), while the MOI 50 group did not reach statistical significance. Furthermore, the two-way ANOVA results (Table 30) revealed significant main effects of time (F = 218.4, p < 0.0001, η^2 = 0.4664) and treatment group (F = 16.93, p < 0.0001, η^2 = 0.1847), as well as a significant interaction between time and group (F = 27.82, p < 0.0001, η^2 = 0.2981). Collectively, early time points (4 and 8 hours) showed modest changes, with a significant viability reduction observed at 8 hours in the MOI 50 group and a slight stimulatory effect at MOI 100. However, prolonged exposure (48 hours) led to significant decreases in cell viability in several groups (IFN-γ, MOI 10, MOI 100, and MOI 200), indicating a shift toward cytotoxicity over time.

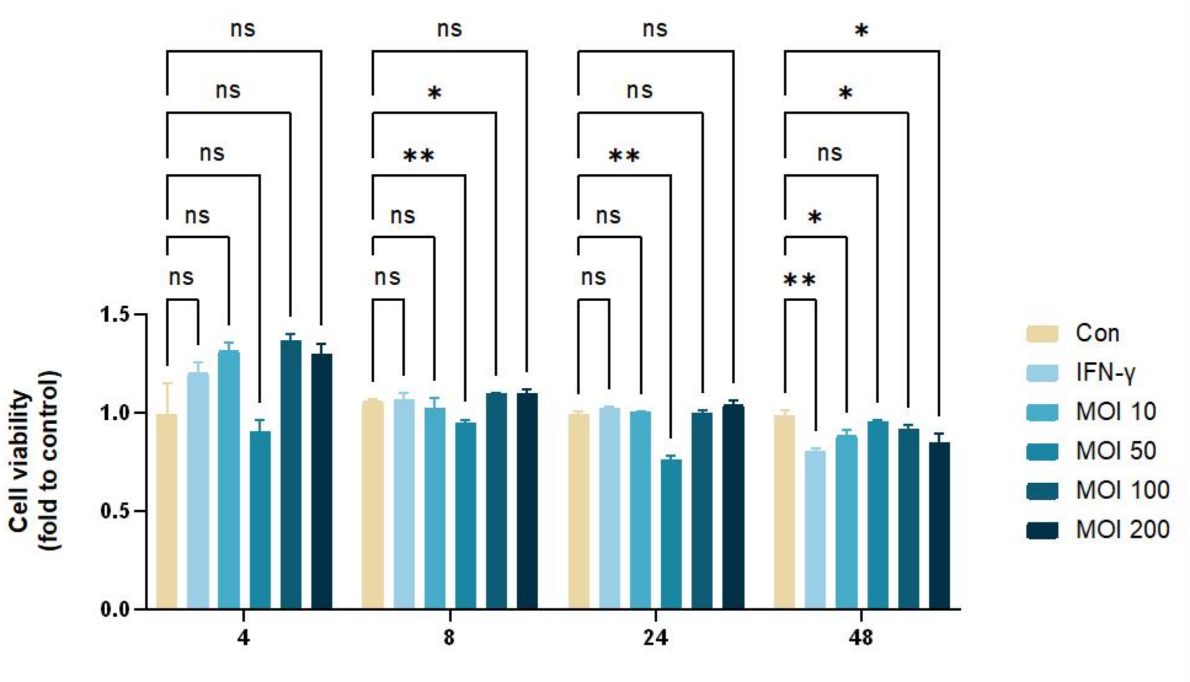

Figure 19. Effects of heat-killed *F. nucleatum* ATCC 10953 on the viability of SCC-25.

SCC-25 were treated with the control or with IFN-γ or with the heat-killed *F. nucleatum* ATCC 10953 with MOI 10, 50, 100, and 200. Cell viability was examined using cell counting kit-8 assay at 4h, 8h, 24h, and 48h. The results are expressed as the mean± SD of at least three independent experiments. $*p < 0.05$, $**p < 0.01$(vs. Control group).

Table 29. Mean ± SD and post-hoc comparisons of SCC-25 viability in response to heat-killed *F. nucleatum* ATCC 19053 across time points

Time Point	Group	Mean±SD	N	Adjusted P Value
4 hours	Control	0.994±0.157	3	N/A
	IFN- γ	1.205±0.050	3	0.3219
	MOI 10	1.320±0.037	3	0.1524
	MOI 50	0.908±0.056	3	0.8284
	MOI 100	1.369±0.031	3	0.1197
	MOI 200	1.301±0.053	3	0.1633
8 hours	Control	1.063±0.007	3	N/A

	IFN-γ	1.070±0.031	3	0.9887
	MOI 10	1.025±0.050	3	0.6600
	MOI 50	0.951±0.014	3	0.0039
	MOI 100	1.097±0.003	3	0.0197
	MOI 200	1.101±0.018	3	0.1367
24 hours	Control	0.996±0.010	3	N/A
	IFN-γ	1.025±0.005	3	0.0603
	MOI 10	1.004±0.002	3	0.6555
	MOI 50	0.760±0.021	3	0.0013
	MOI 100	0.998±0.013	3	0.9997
	MOI 200	1.043±0.017	3	0.0605
48 hours	Control	0.988±0.022	3	N/A
	IFN-γ	0.807±0.014	3	0.0022
	MOI 10	0.888±0.023	3	0.0174
	MOI 50	0.953±0.011	3	0.2391
	MOI 100	0.918±0.019	3	0.0436
	MOI 200	0.849±0.044	3	0.0461

Table 30. Two-Way ANOVA results for SCC-25 viability in response to heat-killed *F. nucleatum* ATCC 10953.

Source of Variation	F Value	P Value	Effect Size (η^2)
Time × Group	27.82	P<0.0001	0.2981
Time	218.4	P<0.0001	0.4664
Group	16.93	P<0.0001	0.1847

3.3.3 Effects of heat-killed *F. nucleatum* ATCC 25586 on SCC-25 cell viability

Figure 20 illustrates the effects of heat-killed *F. nucleatum* ATCC 25586 on the viability of SCC-25 cells over four time points (4, 8, 24, and 48 hours). As detailed in Table 31, at 4 hours the MOI 100 group exhibited a significant increase in viability (1.195 ± 0.038) compared to the control (0.989 ± 0.032, p = 0.0069), while the IFN-γ (0.754 ± 0.239, p = 0.4960), MOI 10 (0.835 ± 0.060, p = 0.0780), MOI 50 (1.080 ± 0.027, p = 0.0645), and MOI 200 (1.041 ± 0.021, p = 0.2451) groups did not differ significantly from the control. At 8 hours, both the IFN-γ (0.951 ± 0.021, p = 0.0273) and MOI 50 (0.911 ± 0.016, p = 0.0394) groups showed a significant reduction in viability relative to the control (1.029 ± 0.014), whereas the MOI 10, MOI 100, and MOI 200 groups did not exhibit significant differences. At 24 hours, no significant differences were observed among any treatment groups compared to the control (1.002 ± 0.028). By 48 hours, the MOI 50 (0.956 ± 0.074, p = 0.0125) and MOI 200 (0.881 ± 0.016, p = 0.0070) groups demonstrated a significant decrease in viability relative to the control (0.994 ± 0.007), while the IFN-γ, MOI 10, and MOI 100 groups remained statistically comparable to the control. Moreover, two-way ANOVA (Table 32) revealed significant main effects for both time (F = 11.05, p = 0.0021, η^2 = 0.1084) and treatment group (F = 5.769, p = 0.0061, η^2 = 0.1939), as well as a significant interaction between time and group (F = 10.18, $p < 0.0001$, η^2 = 0.4993). These results demonstrated a more pronounced early-phase response, with a significant viability enhancement at 4 hours in the MOI 100 group, while at 8 hours, both the IFN-γ and MOI 50 treatments induced a significant reduction in viability. By 48 hours, only the MOI 50 and MOI 200 groups showed significant declines.

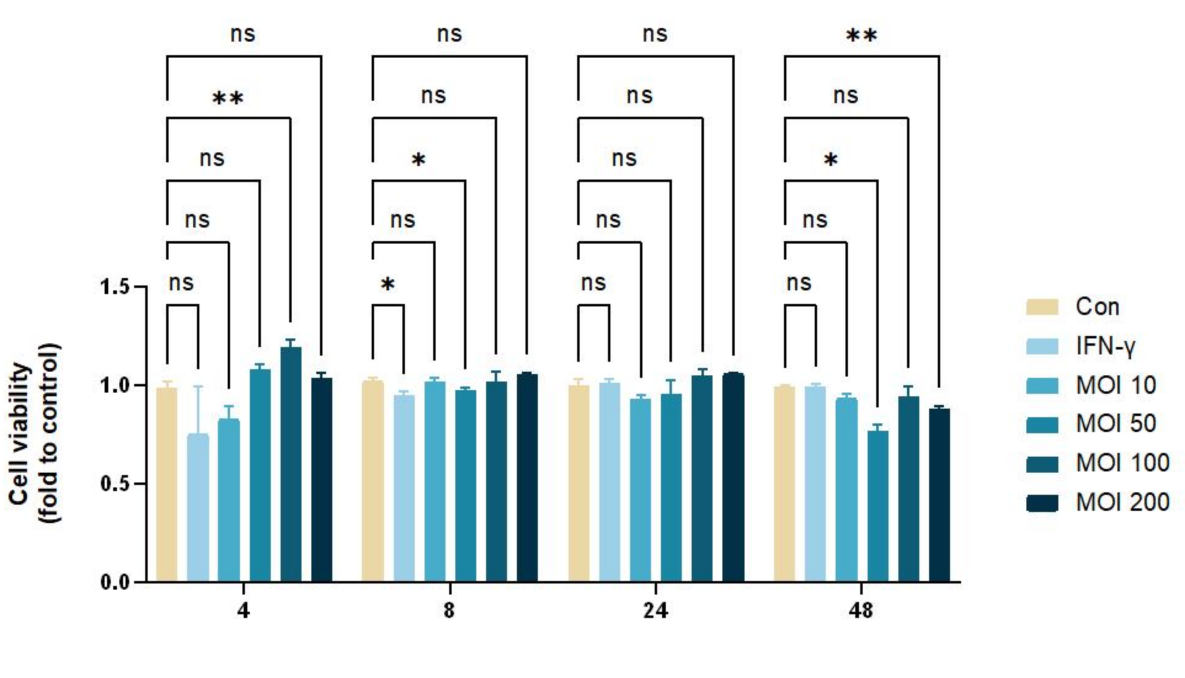

Figure 20. Effects of heat-killed *F. nucleatum* ATCC 25586 on the viability of SCC-25.

SCC-25 were treated with the control or with IFN-γ or with the heat-killed *F. nucleatum* ATCC 25586 with MOI 10, 50), 100, and 200. cell viability was examined using cell counting kit-8 assay at 4h, 8h, 24h, and 48h. The results are expressed as the mean± SD of at least three independent experiments. **p* < 0.05, ***p* < 0.01, ****p* < 0.001 (vs. Control group).

Table 31. Mean ± SD and post-hoc comparisons of SCC-25 viability in response to heat-killed *F. nucleatum* ATCC 25586 across time points.

Time Point	Group	Mean±SD	N	Adjusted *P* Value
4 hours	Control	0.989±0.032	3	N/A
	IFN- γ	0.754±0.239	3	0.4960
	MOI 10	0.835±0.060	3	0.0780
	MOI 50	1.080±0.027	3	0.0645
	MOI 100	1.195±0.038	3	0.0069
	MOI 200	1.041±0.021	3	0.2451

8 hours	Control	1.029±0.014	3	N/A
	IFN-γ	0.951±0.021	3	0.0273
	MOI 10	1.019±0.020	3	0.9170
	MOI 50	0.911±0.016	3	0.0394
	MOI 100	1.021±0.048	3	0.9971
	MOI 200	1.059±0.007	3	0.1093
24 hours	Control	1.002±0.028	3	N/A
	IFN-γ	1.011±0.019	3	0.9835
	MOI 10	0.932±0.021	3	0.0875
	MOI 50	0.956±0.074	3	0.7747
	MOI 100	1.052±0.030	3	0.2929
	MOI 200	1.064±0.001	3	0.1496
48 hours	Control	0.994±0.007	3	N/A
	IFN-γ	0.993±0.013	3	0.9993
	MOI 10	0.932±0.021	3	0.0882
	MOI 50	0.956±0.074	3	0.0125
	MOI 100	0.944±0.054	3	0.5301
	MOI 200	0.881±0.016	3	0.0070

Table 32. Two-Way ANOVA results for SCC-25 viability in response to heat-killed *F. nucleatum* ATCC 25586.

Source of Variation	F Value	P Value	Effect Size (η^2)
Time × Group	10.18	<0.0001	0.4993
Time	11.05	0.0021	0.1084
Group	5.769	0.0061	0.1939

3.3.4 Effects of heat-killed *F. nucleatum* ATCC 49256 on CL-11 cell viability

As shown in Figure 21, heat-killed *F. nucleatum* ATCC49256 affects the viability of CL-11 cells. The mean ± SD values and adjusted post-hoc p-values for CL-11 viability at 4, 8, 24, and 48 hours across various treatment groups—including the control, IFN-γ, and bacterial treatments at MOI 10, MOI 50, MOI 100, and MOI 200—are summarized in Table 33. The two-way ANOVA results evaluating the effects of time, treatment group, and their interaction on cell viability are presented in Table 34.

At 4 hours, the IFN-γ group (0.902 ± 0.033; $p = 0.0391$) and the MOI 200 group (0.930 ± 0.014; $p = 0.0397$) exhibited significant decreases in viability compared to the control (1.008 ± 0.024), whereas the MOI 10, MOI 50, and MOI 100 groups did not differ significantly. At 8 hours, IFN-γ continued to show a significant reduction in viability (0.813 ± 0.003 vs. 0.968 ± 0.023; $p = 0.0169$), with the MOI 200 group approaching significance ($p = 0.0505$). A more pronounced effect was observed at 24 hours, where the MOI 50 group demonstrated a marked decline in viability (0.549 ± 0.063; $p = 0.0107$) and the IFN-γ group also showed a significant decrease (0.889 ± 0.025; $p = 0.0190$) relative to the control (0.989 ± 0.018). By 48 hours, only the MOI 50 group maintained a significant reduction in viability (0.844 ± 0.017 vs. 1.010 ± 0.013; $p = 0.0009$), while the remaining treatment conditions were comparable to the control. The two-way ANOVA (Table 34) further substantiated these findings, revealing significant main effects of time ($F = 83.27$, $p < 0.0001$, $\eta^2 = 0.3121$) and treatment group ($F = 18.48$, $p < 0.0001$, $\eta^2 = 0.6751$), as well as a significant interaction between time and treatment group ($F = 44.77$, $p < 0.0001$, $\eta^2 = 0.8388$). These statistical outcomes confirm that the modulation of CL-11 cell viability by heat-killed *F. nucleatum* ATCC49256 is both time- and dose-dependent. These findings indicate that in CL-11 cells, heat-killed *F. nucleatum* ATCC49256 predominantly exerts an inhibitory effect on cell viability, with significant reductions observed under specific conditions, particularly following intermediate (24 hours) and prolonged (48 hours) exposure at certain bacterial concentrations.

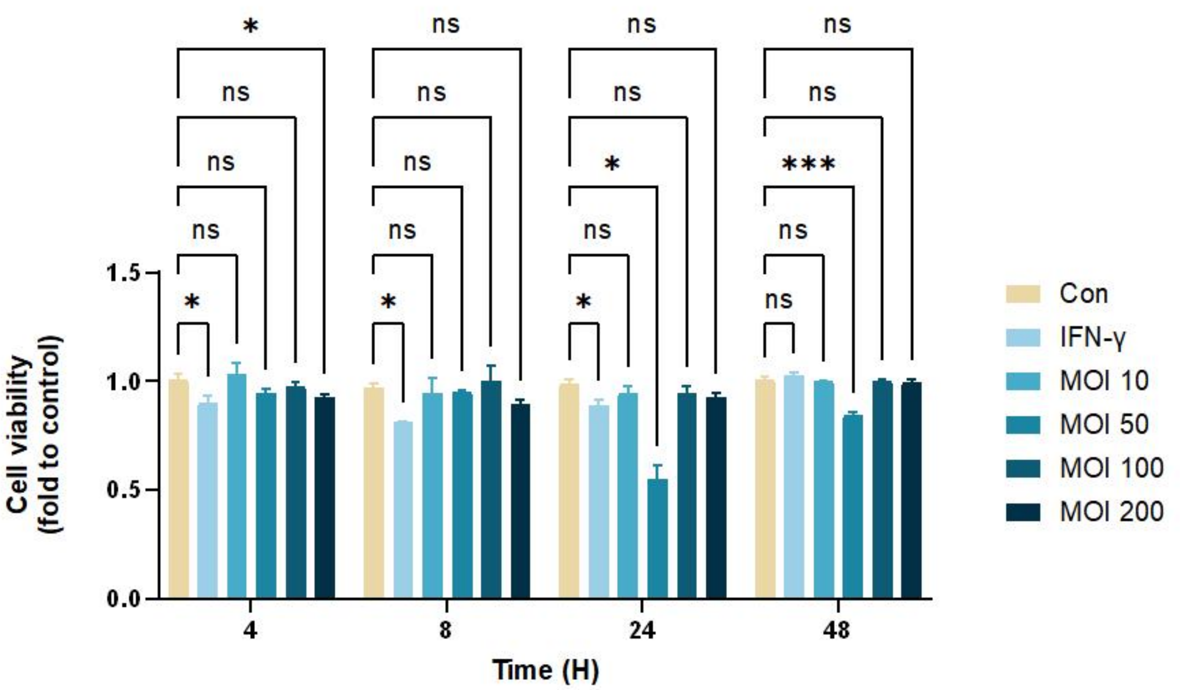

Figure 21. Effects of heat-killed *F. nucleatum* ATCC 49256 on the viability of CL-11.

CL-11 were treated with the control or with IFN-γ or with the heat-killed *F. nucleatum* ATCC 49256 with MOI 10, 50, 100, and 200. Cell viability was examined using cell counting kit-8 assay at 4h, 8h, 24h, and 48h. The results are expressed as the mean± SD of at least three independent experiments. *$p < 0.05$, **$p < 0.01$, ***$p < 0.001$ (vs. Control group).

Table 33. Mean ± SD and post-hoc comparisons of CL-11 viability in response to heat-killed *F. nucleatum* ATCC 49256 across time points

Time Point	Group	Mean±SD	N	Adjusted P Value
4 hours	Control	1.008±0.024	3	N/A

	IFN- γ	0.902±0.033	3	0.0391
	MOI 10	1.034±0.052	3	0.8787
	MOI 50	0.943±0.022	3	0.0754
	MOI 100	0.977±0.022	3	0.4324
	MOI 200	0.930±0.014	3	0.0397
8 hours	Control	0.968±0.023	3	N/A
	IFN- γ	0.813±0.003	3	0.0169
	MOI 10	0.943±0.075	3	0.9552
	MOI 50	0.955±0.003	3	0.7828
	MOI 100	1.001±0.072	3	0.8957
	MOI 200	0.898±0.015	3	0.0505
24 hours	Control	0.989±0.018	3	N/A
	IFN- γ	0.889±0.025	3	0.0190
	MOI 10	0.947±0.030	3	0.3164
	MOI 50	0.549±0.063	3	0.0107
	MOI 100	0.947±0.031	3	0.3250
	MOI 200	0.930±0.018	3	0.0501
48 hours	Control	1.010±0.013	3	N/A
	IFN- γ	1.024±0.015	3	0.6361
	MOI 10	0.999±0.002	3	0.6061
	MOI 50	0.844±0.017	3	0.0009
	MOI 100	1.004±0.007	3	0.9044

MOI 200	0.996±0.011	3	0.5520

Table 34. Two-Way ANOVA results for CL-11 viability in response to heat-killed *F. nucleatum* ATCC 49256.

Source of Variation	F Value	P Value	Effect Size (η^2)
Time × Group	44.77	<0.0001	0.8388
Time	83.27	<0.0001	0.3121
Group	18.48	<0.0001	0.6751

3.3.5 Effects of heat-killed *F. nucleatum* ATCC 10953 on CL-11 cell viability

Figure 22 depicts the effects of heat-killed *F. nucleatum* ATCC10953 on CL-11 cell viability. The mean ± SD values along with the adjusted post-hoc p-values for cell viability measured at 4, 8, 24, and 48 hours across various conditions—including the control, IFN-γ, and bacterial treatments at MOI 10, MOI 50, MOI 100, and MOI 200—are summarized in Table 35. Table 36 presents the two-way ANOVA analysis evaluating the main effects of time and treatment group, as well as their interaction.

At 4 hours, a significant decrease in viability was observed only in the MOI 50 group (0.657 ± 0.044; p = 0.0280) compared to the control (0.956 ± 0.079), whereas the IFN-γ, MOI 10, MOI 100, and MOI 200 groups did not exhibit significant changes. At 8 hours, both the MOI 50 (0.589 ± 0.010; p = 0.0025) and MOI 200 (0.460 ± 0.015; p = 0.0005) groups showed marked reductions in viability relative to the control (0.980 ± 0.079), while the IFN-γ and MOI 10 groups trended downward without reaching significance. By 24 hours, significant reductions were evident in the IFN-γ (0.858 ± 0.031; p = 0.0371), MOI 50 (0.844 ± 0.008; p = 0.0430), and MOI 100 (0.843 ± 0.042; p = 0.0475) groups compared with the control (0.972 ± 0.033), whereas the MOI 10 and MOI 200 groups remained statistically similar to the control. At 48 hours, a reversal was noted as the IFN-γ group

(1.075 ± 0.005; p = 0.0252) and the MOI 200 group (1.059 ± 0.006; p = 0.0380) exhibited significantly higher viability than the control (0.999 ± 0.016), with the MOI 10, MOI 50, and MOI 100 groups showing no significant differences. The two-way ANOVA (Table 36) further confirmed these observations by revealing significant main effects of time ($F = 119.7$, $p < 0.0001$, $\eta^2 = 0.4556$) and treatment group ($F = 9.494$, $p = 0.0007$, $\eta^2 = 0.2011$), as well as a significant interaction between time and treatment ($F = 12.97$, $p < 0.0001$, $\eta^2 = 0.2468$).

Collectively, these findings suggest that heat-killed *F. nucleatum* ATCC10953 exerts a complex, time-dependent influence on CL-11 cell viability. An early inhibitory effect is evident—particularly at 4 and 8 hours under higher bacterial doses—while by 48 hours, a stimulatory effect emerges in the IFN-γ and MOI 200 groups. This dynamic response underscores the crucial roles of both exposure duration and bacterial load in modulating CL-11 cell viability.

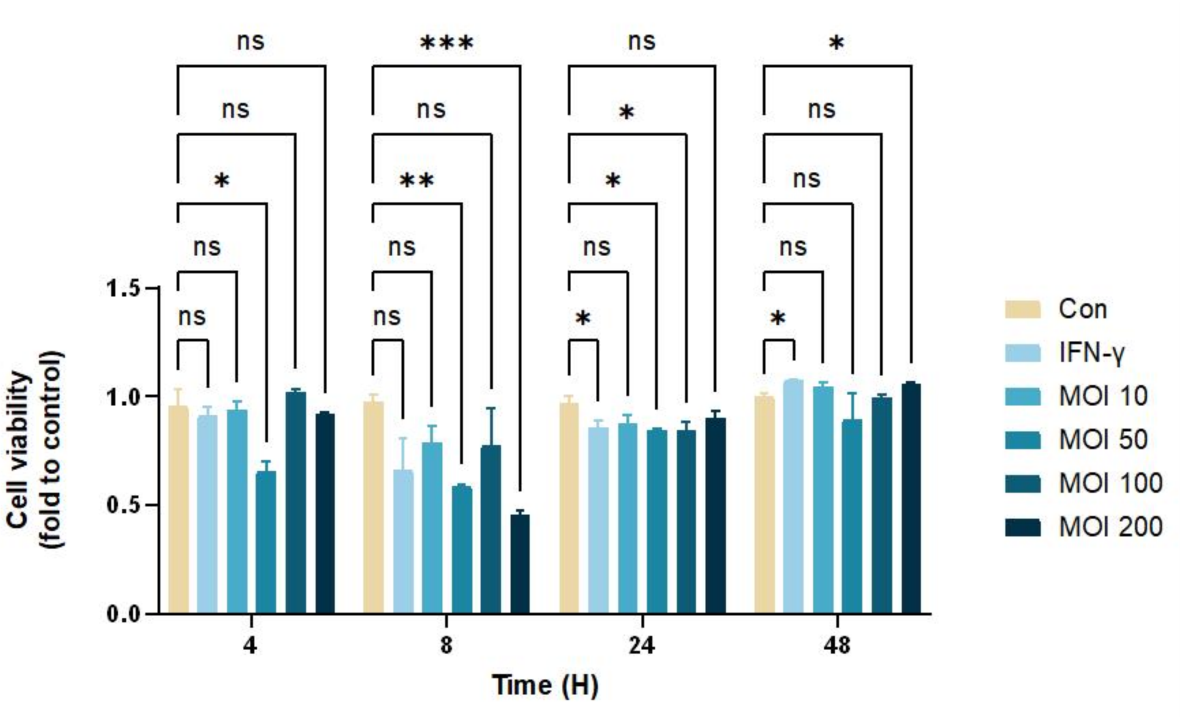

Figure 22. Effects of heat-killed *F. nucleatum* ATCC 10953 on the viability of CL-11.

CL-11 were treated with the control or with IFN-γ or with the heat-killed *F. nucleatum* ATCC 10953 with MOI 10, 50, 100, and 200. Cell viability was examined using cell counting kit-8 assay at 4h, 8h, 24h, and 48h. The results are expressed as the mean± SD of at least three independent experiments. *$p < 0.05$, **$p < 0.01$, ***$p < 0.001$ (vs. Control group).

Table 35. Mean ± SD and post-hoc comparisons of CL-11 viability in response to heat-killed *F. nucleatum* ATCC 10953 across time points.

Time Point	Group	Mean±SD	N	Adjusted P Value
4 hours	Control	0.956±0.079	3	N/A
	IFN-γ	0.916±0.038	3	0.8783
	MOI 10	0.940±0.037	3	0.9961
	MOI 50	0.657±0.044	3	0.0280
	MOI 100	1.022±0.015	3	0.5932
	MOI 200	0.923±0.003	3	0.9022
8 hours	Control	0.980±0.079	3	N/A
	IFN-γ	0.664±0.147	3	0.1450
	MOI 10	0.791±0.075	3	0.0916
	MOI 50	0.589±0.010	3	0.0025
	MOI 100	0.779±0.169	3	0.3893
	MOI 200	0.460±0.015	3	0.0005
24 hours	Control	0.972±0.033	3	N/A
	IFN-γ	0.858±0.031	3	0.0371
	MOI 10	0.878±0.039	3	0.1012
	MOI 50	0.844±0.008	3	0.0430

	MOI 100	0.843±0.042	3	0.0475
	MOI 200	0.904±0.030	3	0.1687
48 hours	Control	0.999±0.016	3	N/A
	IFN-γ	1.075±0.005	3	0.0252
	MOI 10	1.046±0.019	3	0.0961
	MOI 50	0.898±0.116	3	0.5641
	MOI 100	0.996±0.013	3	0.9977
	MOI 200	1.059±0.006	3	0.0380

Table 36. Two-Way ANOVA results for CL-11 viability in response to heat-killed *F. nucleatum* ATCC 10953.

Source of Variation	F Value	P Value	Effect Size (η^2)
Time × Group	12.97	<0.0001	0.2468
Time	119.7	<0.0001	0.4556
Group	9.494	0.0007	0.2011

3.3.6 Effects of heat-killed *F. nucleatum* ATCC 25586 on CL-11 cell viability

As illustrated in Figure 23, heat-killed *F. nucleatum* ATCC 25586 affected the viability of CL-11 cells in a time- and treatment-dependent manner. The mean ± SD values and adjusted post-hoc p-values for each experimental condition, including the control, IFN-γ, and bacterial treatments at MOI 10, MOI 50, MOI 100, and MOI 200 across the four time points (4, 8, 24, and 48 hours), are summarized in Table 37. The statistical outcomes from the two-way ANOVA, detailing the effects of time, treatment group, and their interaction on cell viability, are presented in Table 38.

At 4 hours, none of the treatment conditions led to a significant change in cell viability compared to the control (0.990 ± 0.081), with all p-values exceeding 0.05. However, by 8 hours, the MOI 50 group exhibited a marked reduction in viability (0.862 ± 0.025; $p < 0.0001$), whereas the MOI 100 and MOI 200 groups showed a trend toward increased viability, though neither reached statistical significance ($p = 0.0560$ for both). At 24 hours, no significant differences were observed among treatment conditions relative to the control (1.007 ± 0.038), despite a moderate decrease in viability in the MOI 10 (0.777 ± 0.104; $p = 0.1265$) and MOI 50 (0.862 ± 0.055; $p = 0.0723$) groups. By 48 hours, a significant decline was noted in the MOI 50 group (0.602 ± 0.069; $p = 0.0147$) compared to the control (0.974 ± 0.027), while the MOI 100 (1.161 ± 0.073; $p = 0.0923$) and MOI 200 (1.032 ± 0.042; $p = 0.3273$) groups showed non-significant upward trends. The two-way ANOVA (Table 38) confirmed that both time ($F = 21.90$, $p < 0.0001$, $\eta^2 = 0.0463$) and treatment group ($F = 10.46$, $p = 0.00005$, $\eta^2 = 0.4124$) exerted significant effects on CL-11 viability, with a notable interaction between these factors ($F = 39.86$, $p < 0.0001$, $\eta^2 = 0.4212$).

Together, these findings indicate that heat-killed *F. nucleatum* ATCC 25586 exerts a subtle but time-sensitive influence on CL-11 viability. While the effects were minimal at early time points, a significant reduction in cell viability emerged at 8 and 48 hours in the MOI 50 group. Meanwhile, higher bacterial doses (MOI 100 and MOI 200) showed a tendency toward increased viability at later time points. These observations highlight the complexity of bacterial-host interactions, where both cytotoxic and stimulatory responses can occur depending on exposure duration and bacterial load.

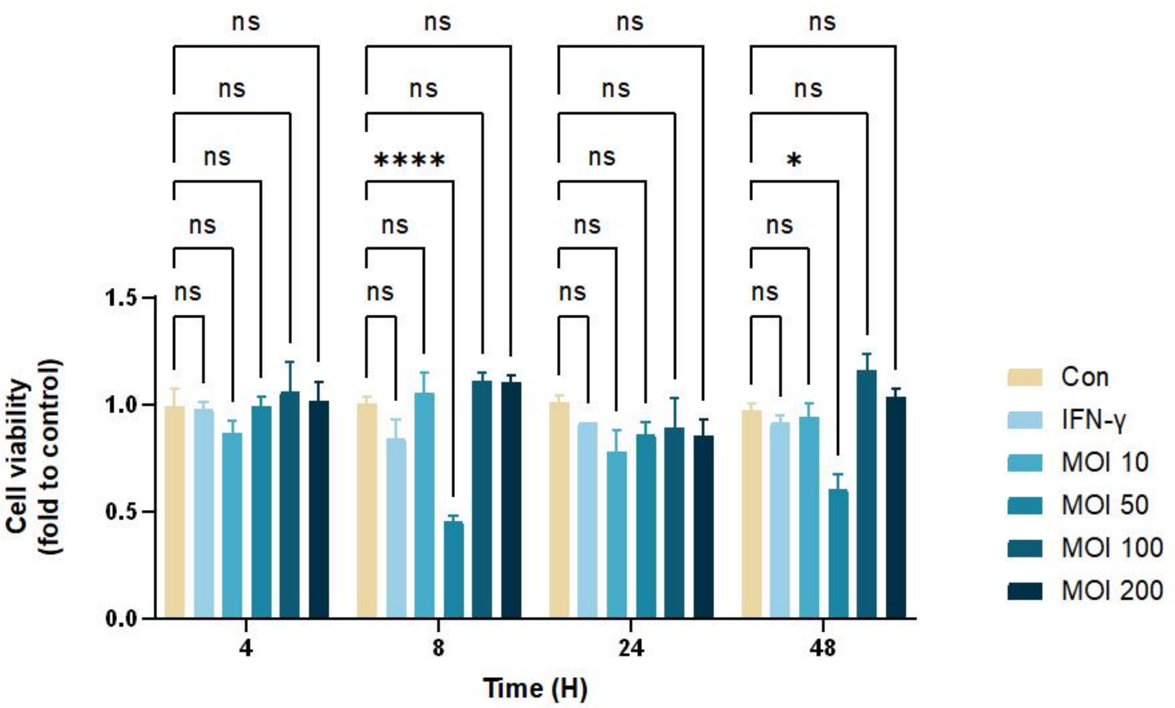

Figure 23. Effects of heat-killed *F. nucleatum* ATCC 25586 on the viability of CL-11.

CL-11 were treated with the control or with IFN-γ or with the heat-killed *F. nucleatum* ATCC 25586 with MOI 10, 50, 100, and 200. Cell viability was examined using cell counting kit-8 assay at 4h, 8h, 24h, and 48h. The results are expressed as the mean± SD of at least three independent experiments. *$p < 0.05$, ****$p < 0.0001$ (vs. Control group).

Table 37. Mean ± SD and post-hoc comparisons of CL-11 viability 0in response to heat-killed *F. nucleatum* ATCC 25586 across time points.

Time Point	Group	Mean±SD	N	Adjusted P Value
4 hours	Control	0.990±0.081	3	N/A
	IFN- γ	0.978±0.034	3	0.9984
	MOI 10	0.868±0.053	3	0.2780
	MOI 50	0.989±0.047	3	>0.9999

	MOI 100	1.062±0.136	3	0.8790
	MOI 200	1.019±0.088	3	0.9888
8 hours	Control	1.006±0.029	3	N/A
	IFN-γ	0.843±0.087	3	0.1787
	MOI 10	1.056±0.092	3	0.8240
	MOI 50	0.862±0.025	3	<0.0001
	MOI 100	1.110±0.036	3	0.0560
	MOI 200	1.104±0.033	3	0.0560
24 hours	Control	1.007±0.038	3	N/A
	IFN-γ	0.918±0.008	3	0.1217
	MOI 10	0.777±0.104	3	0.1265
	MOI 50	0.862±0.055	3	0.0723
	MOI 100	0.889±0.140	3	0.5939
	MOI 200	0.856±0.074	3	0.1398
48 hours	Control	0.974±0.027	3	N/A
	IFN-γ	0.914±0.036	3	0.2390
	MOI 10	0.941±0.063	3	0.8481
	MOI 50	0.602±0.069	3	0.0147
	MOI 100	1.161±0.073	3	0.0923
	MOI 200	1.032±0.042	3	0.3273

Table 38. Two-Way ANOVA results for CL-11 viability in response to heat-killed *F. nucleatum* ATCC 25586.

Source of Variation	F Value	P Value	Effect Size (η^2)
Time × Group	39.86	<0.0001	0.4212
Time	21.90	<0.0001	0.0463
Group	10.46	0.00005	0.4124

3.3.7 Effects of heat-killed *F. nucleatum* ATCC 49256 on PHGK cell viability

As presented in Figure 24, heat-killed *F. nucleatum* ATCC 49256 influenced the viability of primary human gingival keratinocytes (PHGK) in a time- and dose-dependent manner. The mean ± SD values and adjusted post-hoc p-values for each treatment condition across the four time points (4, 8, 24, and 48 hours), are summarized in Table 39. The statistical outcomes from the two-way ANOVA, detailing the significance of time, treatment group, and their interaction, are provided in Table 40.

At 4 hours, PHGK viability was significantly increased in the MOI 10 (2.474 ± 0.067; $p < 0.0001$), MOI 50 (1.916 ± 0.097; $p = 0.0025$), MOI 100 (2.186 ± 0.092; $p = 0.0009$), and MOI 200 (1.810 ± 0.168; $p = 0.0253$) groups relative to the control (1.001 ± 0.046), whereas IFN-γ treatment did not result in a significant change. By 8 hours, a marked decline was observed in the MOI 50 group (0.863 ± 0.029; $p = 0.0277$) compared to the control (0.979 ± 0.030), while the other groups did not exhibit significant differences. At 24 hours, the MOI 50 (0.560 ± 0.004; $p = 0.0035$) and MOI 200 (0.747 ± 0.022; $p = 0.0018$) groups demonstrated significant reductions in viability, whereas the MOI 100 group showed a downward trend that did not reach statistical significance (0.878 ± 0.043; $p = 0.0681$). By 48 hours, a substantial viability reduction was maintained in the MOI 50 group (0.652 ± 0.022; $p = 0.0003$), while the IFN-γ (1.060 ± 0.007; $p = 0.0201$) and MOI 200 (1.060 ± 0.015; $p = 0.0407$) groups exhibited a modest but significant increase in viability relative to the control (1.012 ± 0.012). The two-way ANOVA (Table 40) confirmed significant main effects of time (F = 895, $p < 0.0001$, $\eta^2 = 0.6349$) and treatment group (F = 17.57, $p < 0.0001$, $\eta^2 = 0.0800$), as well as a highly significant interaction between time and treatment condition (F = 74.89, $p < 0.0001$, $\eta^2 = 0.2656$), suggesting that bacterial concentration and exposure duration jointly influence PHGK viability.

Overall, these results indicate that heat-killed *F. nucleatum* ATCC 49256 initially exerts a strong stimulatory effect on PHGK viability, particularly at 4 hours, but prolonged exposure leads to a significant reduction in viability at specific bacterial concentrations, notably MOI 50 and MOI 200. The dynamic shift from early enhancement to later suppression highlights the complex, time-sensitive nature of PHGK responses to bacterial exposure.

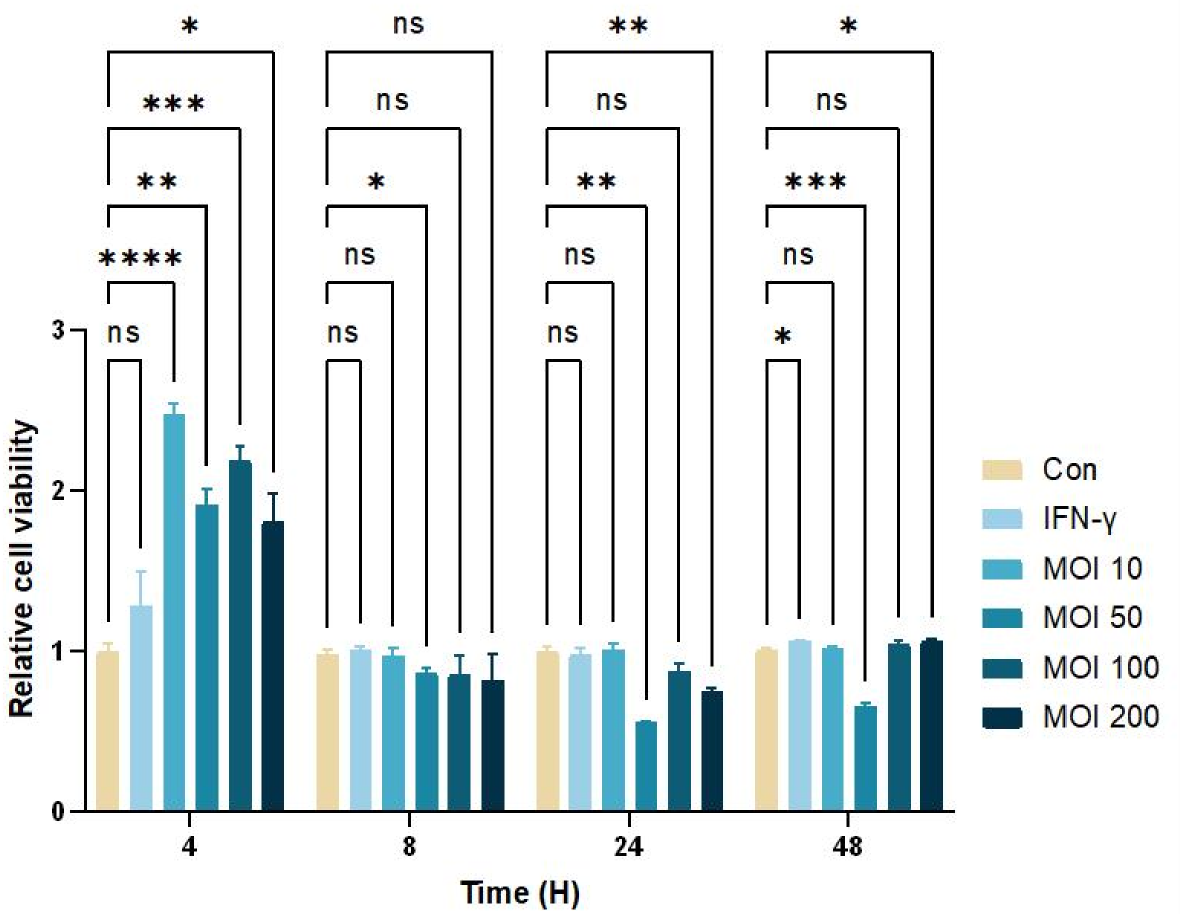

Figure 24. Effects of heat-killed *F. nucleatum* ATCC 49256 on the viability of primary human gingival keratinocytes (PHGK).

PHGK were treated with the control or with IFN-γ or with the heat-killed *F. nucleatum* ATCC 49256 with MOI 10, 50, 100 and 200. Cell viability was examined using cell counting kit-8 assay at 4h, 8h, 24, and 48h. The results are expressed as the mean± SD of at least three independent experiments. *$p < 0.05$, **$p < 0.01$, ***$p < 0.001$, ****$p < 0.0001$ (vs. Control group).

Table 39. Mean ± SD and post-hoc comparisons of PHGK viability in response to heat-killed *F. nucleatum* ATCC 49256 across time points.

Time Point	Group	Mean±SD	N	Adjusted P Value
4 hours	Control	1.001±0.046	3	N/A
	IFN- γ	1.280±0.219	3	0.3511
	MOI 10	2.474±0.067	3	<0.0001
	MOI 50	1.916±0.097	3	0.0025
	MOI 100	2.186±0.092	3	0.0009
	MOI 200	1.810±0.168	3	0.0253
8 hours	Control	0.979±0.030	3	N/A
	IFN- γ	1.011±0.020	3	0.4935
	MOI 10	0.966±0.054	3	0.9923
	MOI 50	0.863±0.029	3	0.0277
	MOI 100	0.858±0.117	3	0.4713
	MOI 200	0.814±0.165	3	0.4876
24 hours	Control	0.993±0.031	3	N/A
	IFN- γ	0.978±0.045	3	0.9792
	MOI 10	1.006±0.042	3	0.9857

	MOI 50	0.560±0.004	3	0.0035
	MOI 100	0.878±0.043	3	0.0681
	MOI 200	0.747±0.022	3	0.0018
48 hours	Control	1.012±0.012	3	N/A
	IFN-γ	1.060±0.007	3	0.0201
	MOI 10	1.019±0.009	3	0.8201
	MOI 50	0.652±0.022	3	0.0003
	MOI 100	1.043±0.027	3	0.4129
	MOI 200	1.060±0.015	3	0.0407

Table 40. Two-Way ANOVA results for PHGK viability in response to heat-killed *F. nucleatum* ATCC 49256.

Source of Variation	F Value	P Value	Effect Size (η^2)
Time × Group	74.89	<0.0001	0.2656
Time	895	<0.0001	0.6349
Group	17.57	<0.0001	0.0800

3.3.8 Effects of heat-killed *F. nucleatum* ATCC 10953 on PHGK cell viability

Figure 24 illustrates the effects of heat-killed *F. nucleatum* ATCC 49256 on the viability of primary human gingival keratinocytes (PHGK), demonstrating both time- and dose-dependent variations. A detailed summary of the mean ± SD values and adjusted post-hoc p-values for each experimental condition at different time points (4, 8, 24, and 48 hours) is presented in Table 39. The statistical significance of time, treatment group, and their interaction, as assessed by two-way ANOVA, is outlined in Table 40.

At 4 hours, the MOI 200 group exhibited a significant increase in viability (2.455 ± 0.124; p = 0.0032) relative to the control (0.959 ± 0.034), while other groups did not show statistically significant changes. By 8 hours, a decreasing trend was observed, with the MOI 200 group showing the lowest viability (0.627 ± 0.122; p = 0.0672), although it did not reach statistical significance. A more pronounced reduction became evident at 24 hours, where significant viability declines were recorded in the MOI 10 (p = 0.0223), MOI 50 (p = 0.0074), and MOI 100 (p = 0.0001) groups compared to the control (1.007 ± 0.010). The MOI 200 group also exhibited a downward trend (p = 0.0858), though it was not statistically significant. At 48 hours, the MOI 50 group showed a significant reduction in viability (0.746 ± 0.107; p = 0.0182), whereas the MOI 200 group displayed a slight increase in viability (1.010 ± 0.073; p = 0.0050). The statistical analysis (Table 42) revealed significant main effects of time (F = 300.8, p < 0.0001, η^2 = 0.4135) and treatment group (F = 8.379, p = 0.0013, η^2 = 0.0889), as well as a strong interaction between time and treatment (F = 66.29, p < 0.0001, η^2 = 0.4556), indicating that bacterial concentration and incubation duration jointly influenced PHGK viability.

Collectively, these findings suggest that heat-killed *F. nucleatum* ATCC 10953 elicits a biphasic response in PHGK, with an initial increase in viability at 4 hours, followed by a decline in multiple treatment groups at later time points. The reduction in viability is most pronounced at 24 hours, particularly in the MOI 50 and MOI 100 groups, whereas by 48 hours, the MOI 200 group exhibits a modest recovery. These results underscore the complex interplay between bacterial exposure and PHGK viability over time.

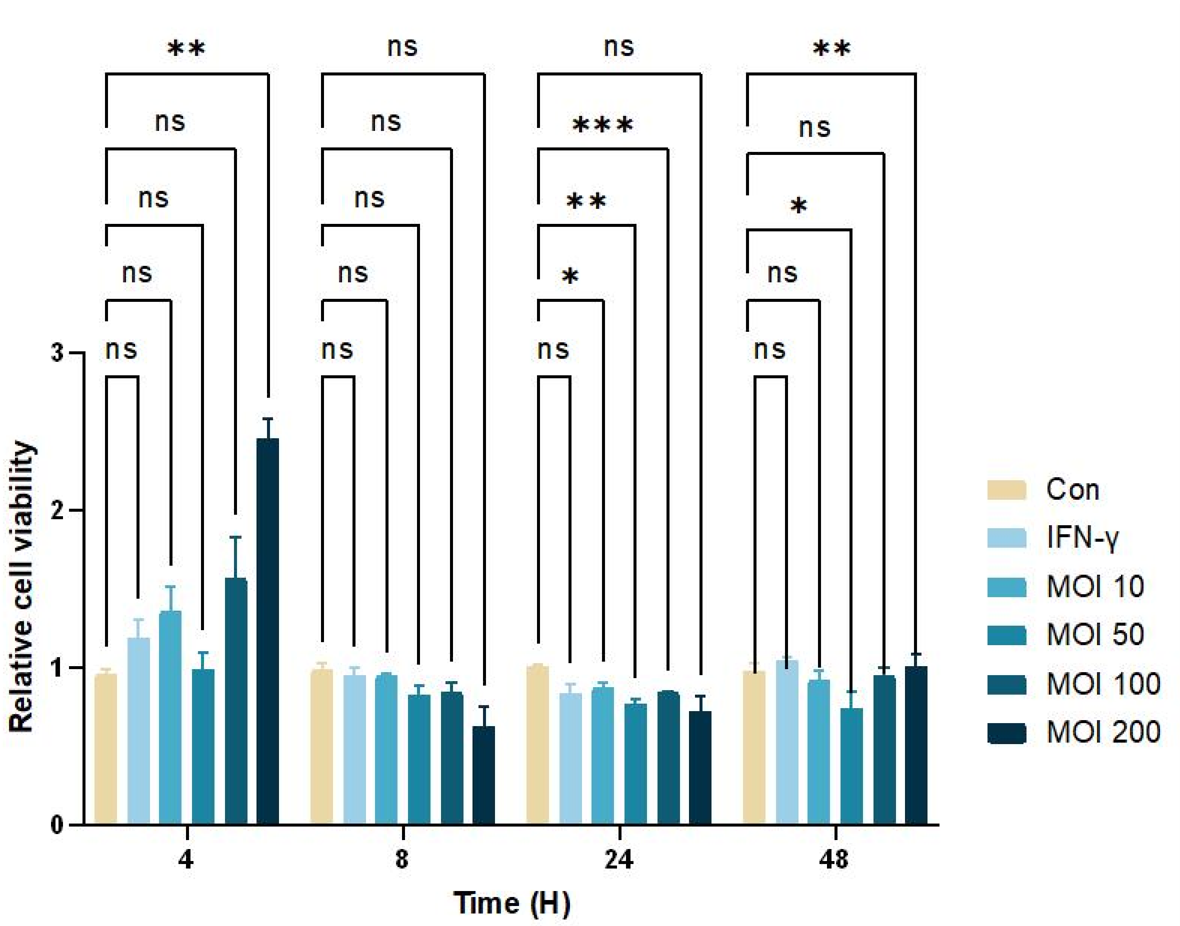

Figure 25. Effects of heat-killed *F. nucleatum* ATCC 10953 on the viability of primary human gingival keratinocytes (PHGK).

PHGK were treated with the control or with IFN-γ or with the heat-killed *F. nucleatum* ATCC 10953 with MOI 10, 50, 100, and 200. Cell viability was examined using cell counting kit-8 assay at 4h, 8h, 24, and 48h. The results are expressed as the mean± SD of at least three independent experiments. *$p < 0.05$, **$p < 0.01$, ***$p < 0.001$ (vs. Control group).

Table 41. Mean ± SD and post-hoc comparisons of PHGK viability in response to heat-killed *F. nucleatum* ATCC 10953 aross time points.

Time Point	Group	Mean±SD	N	Adjusted P Value
4 hours	Control	0.959±0.034	3	N/A
	IFN- γ	1.184±0.116	3	0.1691
	MOI 10	1.360±0.156	3	0.1033

	MOI 50	0.985±0.114	3	0.9910
	MOI 100	1.571±0.262	3	0.1302
	MOI 200	2.455±0.124	3	0.0032
8 hours	Control	0.986±0.044	3	N/A
	IFN- γ	0.955±0.014	3	0.8436
	MOI 10	0.951±0.007	3	0.6177
	MOI 50	0.770±0.030	3	0.0698
	MOI 100	0.848±0.052	3	0.0803
	MOI 200	0.627±0.122	3	0.0672
24 hours	Control	1.007±0.010	3	N/A
	IFN- γ	0.835±0.057	3	0.0776
	MOI 10	0.875±0.028	3	0.0223
	MOI 50	0.770±0.030	3	0.0074
	MOI 100	0.843±0.007	3	0.0001
	MOI 200	0.718±0.098	3	0.0858
48 hours	Control	0.980±0.051	3	N/A
	IFN- γ	1.044±0.022	3	0.5406
	MOI 10	0.923±0.060	3	1.0000
	MOI 50	0.746±0.107	3	0.0182
	MOI 100	0.946±0.051	3	0.6298
	MOI 200	1.010±0.073	3	0.0050

Table 42. Two-Way ANOVA results for PHGK viability in response to heat-killed *F. nucleatum* ATCC 10953

Source of Variation	F Value	P Value	Effect Size (η^2)
Time × Group	66.29	<0.0001	0.4556
Time	300.8	<0.0001	0.4135
Group	8.379	0.0013	0.0889

3.3.9 Effects of heat-killed *F. nucleatum* ATCC 25586 on PHGK cell viability

Figure 26 depicts the impact of heat-killed *F. nucleatum* ATCC 25586 on the viability of PHGK, revealing distinct responses across different time points and bacterial concentrations. The mean ± SD values and adjusted post-hoc p-values for each treatment condition are detailed in Table 43. The statistical significance of the effects of time, treatment group, and their interaction, as assessed by two-way ANOVA, is summarized in Table 44.

At 4 hours, none of the treatment groups showed statistically significant alterations in viability compared to the control (0.957 ± 0.048), although the IFN-γ (p = 0.0536) and MOI 200 (p = 0.0697) groups exhibited a trend toward increased viability. At 8 hours, the MOI 10 group displayed a moderate but non-significant increase in viability (1.162 ± 0.041; p = 0.0790), while the MOI 100 and MOI 200 groups exhibited a slight decrease relative to the control (0.997 ± 0.065), though these differences did not reach statistical significance. By 24 hours, cell viability remained largely unchanged across all treatment conditions, with none of the groups exhibiting significant deviations from the control (0.984 ± 0.032). At 48 hours, no statistically significant changes were observed, with all groups maintaining viability levels comparable to the control (1.000 ± 0.036). The two-way ANOVA results (Table 44) indicated a significant interaction between time and treatment group (F = 25.96, p < 0.0001, η^2 = 0.6305). However, neither time (F = 1.778, p = 0.1917, η^2 = 0.0086) nor treatment group alone (F = 2.334, p = 0.1064, η^2 = 0.1492) significantly influenced PHGK viability.

Taken together, these findings suggest that heat-killed *F. nucleatum* ATCC 25586 exerts minimal effects on PHGK viability under the tested conditions. While some treatment groups exhibited slight fluctuations in viability at earlier time points, none of these changes were statistically significant, and all groups showed comparable viability to the control by 48 hours. These results indicate that, unlike the other *F. nucleatum* strains, ATCC 25586 does not induce a strong stimulatory or cytotoxic response in PHGK cells over time.

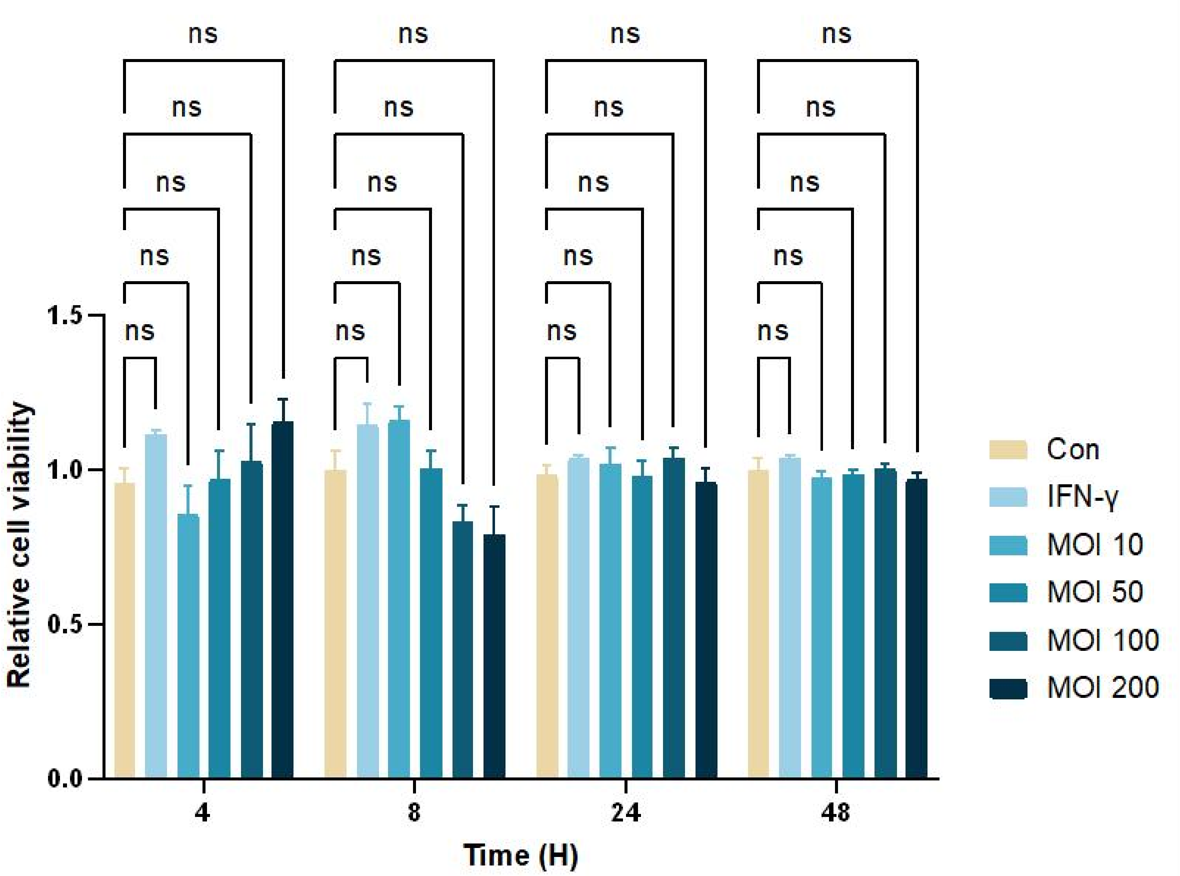

Figure 26. Effects of heat-killed *F. nucleatum* ATCC 25586 on the viability of primary human gingival keratinocytes (PHGK).

PHGK were treated with the control or with IFN-γ or with the heat-killed *F. nucleatum* ATCC 25586 with MOI 10, 50, 100, and 200. Cell viability was examined using cell counting kit-8 assay at 4h, 8h, 24, and 48h. The results are expressed as the mean± SD of at least three independent experiments.

Table 43. Mean ± SD and post-hoc comparisons of PHGK viability in response to heat-killed *F. nucleatum* ATCC 25586 across time points.

Time Point	Group	Mean±SD	N	Adjusted P Value
4 hours	Control	0.957±0.048	3	N/A
	IFN-γ	1.112±0.017	3	0.0536
	MOI 10	0.858±0.091	3	0.4642
	MOI 50	0.973±0.088	3	0.9976
	MOI 100	1.029±0.118	3	0.7864
	MOI 200	1.154±0.074	3	0.0697
8 hours	Control	0.997±0.065	3	N/A
	IFN-γ	1.145±0.069	3	0.1562
	MOI 10	1.162±0.041	3	0.0790
	MOI 50	1.002±0.061	3	>0.9999
	MOI 100	0.834±0.053	3	0.0876
	MOI 200	0.791±0.089	3	0.1058
24 hours	Control	0.984±0.032	3	N/A
	IFN-γ	1.035±0.011	3	0.2299
	MOI 10	1.019±0.054	3	0.7912
	MOI 50	0.979±0.048	3	0.9999
	MOI 100	1.039±0.031	3	0.2592
	MOI 200	0.959±0.047	3	0.8965
48 hours	Control	1.000±0.036	3	N/A

IFN-γ	1.038±0.010	3	0.5406
MOI 10	0.977±0.018	3	1.0000
MOI 50	0.983±0.017	3	1.0000
MOI 100	1.005±0.014	3	1.0000
MOI 200	0.970±0.020	3	1.0000

Table 44. Two-Way ANOVA results for PHGK viability in response to Heat-Killed *F. nucleatum* ATCC 25586.

Source of Variation	F Value	P Value	Effect Size (η^2)
Time × Group	25.96	<0.0001	0.6305
Time	1.778	0.1917	0.0086
Group	2.334	0.1064	0.1492

4. Discussion

F. nucleatum is a Gram-negative, anaerobic bacterium with a high degree of invasiveness. It also has been correlated with many diseases, such as periodontitis, angina, lung abscesses, chronic otitis, sinusitis, peritonsillar abscesses, cerebral abscesses, inflammatory bowel disease, ulcerative colitis, Crohn's disease, gynecological abscesses, neonatal sepsis, Lemierre's syndrome, and infective endocarditis[30; 170-173]. There is growing evidence indicating that *F. nucleatum* plays a role in the progression of an expanding array of tumor types, including CRC[174], pancreatic[175], gastric [176], esophageal[177], OSCC[178], and breast cancers[179].

Our findings revealed that heat-killed *F. nucleatum* differentially regulated PD-L1 expression in a strain- and cell type-dependent manner. While PD-L1 protein was upregulated in SCC-25 and CL-11 cells following stimulation, mRNA levels did not consistently reflect this increase. In contrast, PHGK cells exhibited a more modest response, with no significant PD-L1 upregulation at either the transcriptional or translational level. Additionally, heat-killed *F. nucleatum* exhibited strain-dependent effects on cell viability, with certain strains exerting a more pronounced influence on proliferation. The observed discrepancies between mRNA and protein expression suggest post-transcriptional regulatory mechanisms, warranting further investigation.

This study investigated the expression of PD-L1 after infection with different strains of heat-killed *F. nucelatum* and the influence on cell proliferation on different cancer cell lines and PHGK. Also the hypothesis was tested that different heat-killed *F. nucleatum* strains regulate PD-L1 expression in variable ways. Understanding the differences in pathogenicity of individual *F. nucleatum* subspecies may reveal new pathogenic factors and provide potential therapeutic targets for prevention and treatment of *F. nucleatum*-mediated infections and diseases.

4.1 Heat-killed *F. nucleatum* induces PD-L1 expression in SCC-25

Our study revealed that heat-killed *F. nucleatum* strains differentially regulated PD-L1 expression in SCC-25 cells in a strain- and time-dependent manner. ATCC 49256 and ATCC 10953 induced significant PD-L1 upregulation, while ATCC 25586 exhibited only a transient increase at early time points. Notably, ATCC 49256 triggered an early and dose-dependent PD-L1 increase at 4 hours, which peaked at 24 hours before returning to baseline by 48 hours. In contrast, ATCC 10953 exhibited a more gradual but sustained PD-L1 upregulation, peaking at 24 hours and persisting at 48 hours. The weaker and short-lived response of ATCC 25586 suggests that its immunomodulatory effects may differ from the other with two strains.

OSCC is a prevalent sub-type of HNSCC, with a poor 5-year survival rate remains suboptimal owing to the high incidence of metastasis or recurrence[187]. *Fusobacterium* species are regarded as one of the main components of the oral micro-biome in OSCC[188], and *F. nucleatum* has been detected in the invasive margins of OSCC tissues[187]. The contribution of *F. nucleatum* to the pathogenesis of OSCC is increasingly being acknowledged, but its role in immune evasion remains unclear. Several reports have shown that the PD-L1 expression on OSCC[189; 190], with early reports demonstrated that 66% of freshly isolated HNSCC samples exhibited PD-L1 expression[191]. Concomitant with significant alterations in the tumor micro-environment, the up-regulation of PD-L1 during OSCC carcinogenesis is notable. Several reports have shown that PD-L1 is also induced at various level in cultured SCCHN cell lines SCC-4, SCC-19, SCC-15, SCC-25, SCC-99, and Cal-27, and its inducing is up-regulated in response to the pro-inflammatory cytokines, IFN-γ, TNF-α, HBD3, IL-1α and IL-1ß[116; 192-194]. Previous studies demonstrated that PD-L1 expression was induced by *P. gingivalis* in SCC-25, especially the total membrane, outer and inner membrane of *P. gingivalis*[109; 110]. Moreover, internalized PDG of *P. gingivalis* can also trigger PD-L1 expression in a MyD88-independent and receptor-interacting serine/threonine-protein kinase 2 (RIP2)-dependent fashion[195]. However, the influence of *F. nucleatum* on PD-L1 expression in OSCC remains largely unexplored. Our results provide the first evidence that heat-killed *F. nucleatum* strains significantly upregulate PD-L1 expression in SCC-25 cells, with strain- and time-dependent variations. Notably, ATCC 49256 and ATCC 10953 triggered a sustained PD-L1 increase, whereas ATCC 25586 induced only transient upregulation at early time points. This suggests that different *F. nucleatum* strains may exert distinct immunomodulatory effects on OSCC cells. Given that PD-L1 is a crucial factor in immune evasion, our findings indicate that *F. nucleatum* may contribute to OSCC progression by enhancing immune checkpoint expression.

A previous study found the ability of *F. nucleatum* to induce epithelial-mesenchymal transition (EMT)-associated features in OSCC cells[196]. Inflammatory mediators such as cytokines and growth factors can activate various downstream signaling cascades involved in EMT, including JAK/STAT, MEK/ERK, PI3K/Akt, and mTOR. The signaling molecules associated with EMT also overlap with those involved in the extrinsic induction of PD-L1[116]. These findings suggest that *F. nucleatum* may influence PD-L1 expression through multiple immune regulatory pathways, highlighting the need for further mechanistic studies.

Notably, mRNA levels of PD-L1 did not show significant upregulation despite increased protein expression, highlighting the role of post-transcriptional mechanisms. Presumably, there are at least three reasons that may account for the poor correlations commonly observed in the literature between mRNA levels and protein levels, and these reasons are likely not mutually exclusive[197]. There are many intricate and diverse post-transcriptional mechanisms in converting mRNA into protein. They still are not well-characterized enough to estimate protein concentrations based on mRNA levels accurately. Furthermore, the *in vivo* half-lives of proteins may vary considerably. Lastly, significant levels of error and noise exist in both mRNA and protein experiments, which can impede our ability to obtain a precise understanding[197-199]. However, it's important to consider potential factors that may have influenced these findings, such as variations in bacterial purity and concentration. While the experiments were conducted with whole bacteria, variations in the purity of bacterial suspensions could have inadvertently impacted the number of bacteria introduced into the assays, potentially contributing to the observed discrepancies in the results. While acknowledging these potential confounding factors, it's essential to emphasize the robustness of the experimental design and the reproducibility of the results. Despite the complexities involved, the consistent trends observed in PD-L1 protein expression across different experimental conditions suggest a meaningful biological response to bacterial stimulation. Therefore, while acknowledging the limitations, the findings provide valuable insights into the interaction between bacteria and host immune response.

Collectively, these findings indicate that heat-killed *F. nucleatum* strains can modulate PD-L1 expression in OSCC cells in a strain-dependent manner, with ATCC 10953 and ATCC 25586 exhibiting stronger effects than ATCC 49256. Given the role of PD-L1 in immune evasion and tumor progression, further studies are warranted to elucidate the precise molecular mechanisms by which *F. nucleatum* regulates PD-L1 expression and its implications for OSCC pathogenesis.

4.2 Heat-killed *F. nucleatum* induces PD-L1 expression in CL-11

In CL-11 cells, heat-killed *F. nucleatum* strains exhibited differential effects on PD-L1 protein expression, with ATCC 10953 inducing the most robust and sustained upregulation, followed by ATCC 49256, which elicited a weaker but delayed response, and ATCC 25586, which had the least consistent effect. PD-L1 mRNA expression, however, did not consistently reflect these protein-level changes, suggesting the involvement of post-transcriptional regulatory mechanisms. WB analysis revealed that ATCC 10953 induced significant PD-L1 upregulation at 24 and 48 hours, with MOI 50, 100, and 200 all showing statistically significant increases at 24 hours ($P < 0.05$), and MOI 100 and 200 maintaining significance at 48 hours. This suggests that prolonged exposure to heat-killed *F. nucleatum* ATCC 10953 is necessary to drive a sustained PD-L1 response in CRC cells. In contrast, ATCC 49256 elicited a weaker but delayed response, with only the MOI 200 group at 48 hours showing a statistically significant increase ($p = 0.0290$). This delayed effect suggests that ATCC 49256 may require a longer exposure time to exert its immunomodulatory effects. Meanwhile, ATCC 25586 induced inconsistent changes, with only the MOI 50 group at 48 hours exhibiting significant upregulation.

The role of *F. nucleatum* in CRC progression has been widely studied, with multiple reports indicating that *F. nucleatum* is enriched in the gut mucosal and fecal samples of CRC patients compared to healthy individuals[200-204]. There are three main components of *F. nucleatum* to mediate CRC oncogenic properties: Fap2, FadA, and LPS. The binding of Fap2 to Gal-GalNAc and FadA to E-cadherin enhances the pro-inflammatory state. LPS activate MyD88 and NF-κB signaling pathways by interaction with TLR. In addition, interplay of LPS with TIGIT receptors of NK and T cells leads to suppression of antitumor immunity. Ultimately, these events damage DNA, promote cell proliferation, and lead to CRC tumorigenesis[202]. The ability of ATCC 10953 to induce stronger and more sustained PD-L1 upregulation suggests that strain-specific factors, such as differences in adhesion molecules, metabolic byproducts, or immune-modulatory surface proteins, may contribute to its immunosuppressive properties.

Various reports indicate that the correlation between PD-L1 and prognosis varies across different types of tumors[205]. Furthermore, there are increasing evidences shown that microbiome can impact the effectiveness of anti-PD-1/PD-L1 treatments[206][207], our findings suggest that F. nucleatum, particularly ATCC 10953, may play a role in modulating PD-L1 expression in CRC, potentially influencing therapeutic outcomes. Interestingly, prior studies have shown that *P. gingivalis* upregulates PD-L1 in CRC cells through NOD1/NOD2-dependent pathways[111]. However, the role of *F. nucleatum* in PD-L1 regulation in CRC remains unclear. Our study indicates that different strains of *F. nucleatum* may have unique immunomodulatory effects, warranting further investigation into their specific bacterial components and molecular interactions.

4.3 Heat-killed *F. nucleatum* induces PD-L1 expression in PHGK

In PHGK cells, the response to heat-killed *F. nucleatum* varied depending on the strain. ATCC 10953 significantly upregulated PD-L1 protein expression at later time points, whereas ATCC 25586 led to a reduction in PD-L1 levels. In contrast, ATCC 49256 did not induce any significant changes in PD-L1 expression at any time point. Similar to SCC-25 and CL-11, PD-L1 mRNA expression remained largely unchanged, further suggesting that heat-killed *F. nucleatum*-mediated regulation of PD-L1 occurs primarily at the post-transcriptional level.

The regulation of PD-L1 in non-malignant epithelial cells, such as PHGK, is less well understood compared to its role in cancer. Previous studies have shown that bacterial stimulation can induce PD-L1 expression in normal epithelial cells, particularly in response to inflammatory cytokines[108; 116; 208]. However, our results indicate that heat-killed *F. nucleatum* strains exhibit distinct effects on PD-L1 expression in PHGK cells, with ATCC 10953 being the only strain that elicited a detectable upregulation. This suggests that normal gingival keratinocytes may possess strain-specific regulatory mechanisms that control immune checkpoint expression, potentially to maintain immune homeostasis and prevent excessive immune activation.

Interestingly, ATCC 25586 stimulation led to a reduction in PD-L1 protein levels, a phenomenon that may be attributed to proteolytic cleavage by matrix metalloproteinases (MMPs). Gursoy et al. (2008) reported that *F. nucleatum* ATCC 25586 increased MMP-9 and MMP-13 secretion in HaCaT epithelial cells[209]. Dezutter-Dambuyant et al. (2015) found that proteolytic cleavage of PD-L1 and PD-L2 occurring through the release of MMPs[210]. Based on the above study, a plausible explanation for the observed decrease in PD-L1 protein expression, resulting from the stimulation of PHGK cells with heat-killed *F. nucleatum* ATCC 25586 in this experiment, could be attributed to the proteolytic cleavage of PD-L1 by the matrix metalloproteinases (MMPs) released from the cells.

Overall, the differential responses observed in PHGK cells compared to SCC-25 and CL-11 highlight the complexity of *F. nucleatum*-mediated immune modulation. ATCC 10953 was capable of inducing PD-L1 in normal keratinocytes, whereas ATCC 25586 led to a reduction, and ATCC 49256 had no apparent effect. Future studies should aim to dissect the molecular mechanisms underlying these strain-specific effects and determine whether distinct bacterial components selectively induce or suppress PD-L1 in normal versus malignant cells.

4.4 Strain-Specific Differences in *F. nucleatum*-Mediated Immune Modulation

A key finding of this study is the strain-dependent regulation of PD-L1 expression across different cell types. *F. nucleatum* is classified into five subspecies (*ssp. nucleatum, ssp. polymorphum, ssp. fusiforme, ssp. vincentii, and ssp. animalis*), each exhibiting distinct virulence properties[211; 212]. *F. nucleatum* - *ssp. nucleatum* ATCC 25586, *ssp. polymorphum* ATCC 10953, and *ssp. vincentii* ATCC 49256 are linked to periodontal disease and also identified in CRC samples[213; 214]. Even within the same subspecies, individual strains can vary significantly in their ability to evade immune detection, induce cytokine responses, and modulate host signaling pathways. Kurgan et al. (2017) found that neutrophils are more efficient in their capacity for phagocytic elimination of *F. nucleatum* ATCC 10953 compared with ATCC 25586 and ATCC 49256[165]. They also reported that *F. nucleatum* ATCC 25586 and ATCC 10953 have a distinct role in modulating immune response, efficiently preventing neutrophil-induced oxidative killing[165]. These factors may suggest differences in virulence properties of different *F. nucleatum* strains. Studies reported that there are variations in biofilm forming ability and the growth capacity of different *F. nucleatum* strains within the biofilm, which can impact the growth of the surrounding species and even alter biofilm structure[215; 216].

4.5 Heat-killed *F. nucleatum* influences cell viability

This study investigated the effects of heat-killed *F. nucleatum* strains (ATCC 49256, ATCC 10953, and ATCC 25586) on the viability of SCC-25, CL-11, and PHGK cells across different time points. The results revealed distinct strain- and cell-type-specific responses, demonstrating both stimulatory and cytotoxic effects that varied depending on bacterial concentration and exposure duration

Each heat-killed *F. nucleatum* strain exhibited a unique pattern of influence on cell viability. ATCC 49256 generally displayed a biphasic response, characterized by an initial increase in viability at earlier time points followed by a decrease at prolonged exposure, particularly at higher MOI levels. This effect was most pronounced in SCC-25 and CL-11 cells, where ATCC 49256 significantly reduced viability at 24 and 48 hours, suggesting that while early interactions may trigger temporary pro-survival mechanisms, prolonged bacterial exposure induces cytotoxicity. ATCC 10953, in contrast, demonstrated a more complex response with an early-stage viability decrease in CL-11 cells and sustained reductions at later time points in SCC-25 and PHGK. Interestingly, the viability of PHGK cells exhibited a notable increase at 4 hours with ATCC 10953 at high MOI but transitioned into a suppressive effect at 24 hours, highlighting a dynamic, dose-dependent cellular response. Among the three strains, ATCC 25586 exerted the least significant effect on cell viability, with no major deviations from the control condition across cell lines, suggesting a relatively weaker interaction with these epithelial and carcinoma cells.

Distinct responses were observed across SCC-25, CL-11, and PHGK cells, emphasizing the role of cellular context in bacterial-host interactions. In SCC-25, heat-killed *F. nucleatum* stains exhibited both early-stage viability increases (notably with ATCC 49256 and ATCC 10953) and significant viability reductions at later time points, particularly at MOI 50 and above. These findings suggest that heat-killed *F. nucleatum* may transiently enhance carcinoma cell survival, potentially through inflammatory or metabolic pathways, before inducing cytotoxic effects upon prolonged exposure. CL-11, a colon cancer cell line, displayed a similar trend, with heat-killed *F. nucleatum* ATCC 49256 and ATCC 10953 reducing viability more markedly over time. However, CL-11 cells appeared more sensitive to ATCC 10953, experiencing a significant viability decline as early as 4 hours, suggesting potential differences in receptor-mediated bacterial recognition and host immune response pathways between oral and colorectal epithelial-derived carcinoma cells. In contrast, PHGK cells exhibited a more variable response. Both ATCC 49256 and ATCC 10953 initially increased viability at 4 hours, particularly at higher MOI levels, before reducing viability at later time points. This pattern suggests that *F. nucleatum* may transiently promote gingival keratinocyte survival or metabolic activity before exerting cytotoxic effects, potentially through inflammation-related signaling cascades.

The effects of *F. nucleatum* on different cell types remain controversial, with both stimulatory and inhibitory effects reported in the literature. Kang et al. (2019) and Gao et al. (2020) reported that *F. nucleatum* inhibits human gingival fibroblasts and osteoblasts proliferation and promotes cell apoptosis[217; 218]. Furthermore, *F. nucleatum* can also impair the proliferation of human umbilical vein endothelial cells and endothelial cells[219; 220]. Interestingly, the impact of *F. nucleatum* on cancer cells remains controversial. Yu et al. (2017) found that *F. nucleatum* showed no effect on the colorectal cancer cell lines HCT116 and HT29[221]. This outcome is in contrast to that of Yang et al. (2017) who found that *F. nucleatum* significantly promotes cell growth of HCT116 and LoVo cells after 48 h of treatment[95]. A possible explanation for this discrepancy might be the disparity in the experimental conditions, particularly the bacterial load used. Yu et al. (2017) used *F. nucleatum* at MOI 100 while Yang et al. (2017) used *F. nucleatum* at MOI 1000 to stimulate HCT116 cells. This suggests that *F. nucleatum*-induced cancer cell proliferation may be dose-dependent, with higher bacterial burdens potentially activating pro-survival signaling pathways. The present study further supports the notion that *F. nucleatum* exerts differential effects depending on the host cell type and bacterial load, with significant cytotoxicity observed in CL-11 and SCC-25 cells, while PHGK cells exhibit a more transient, biphasic response.

The modulation of cancer cell proliferation by *F. nucleatum* may also be linked to its influence on PD-L1 expression. Song et al. (2013) reported that the proliferation of pancreatic tumor cells is promoted in PD-L1 over-expressing cell lines. The researchers conducted functional studies on pancreatic cell lines that were genetically modified to exhibit either high or low levels of PD-L1 expression. Their findings revealed that pancreatic ductal adenocarcinoma cells with over-expressed PD-L1 via plasmid transfection exhibited increased cell proliferation[186]. Similarly, Ghebeh et al. (2007) observed a significant linear correlation between PD-L1 expression and Ki-67, a key proliferation marker, in breast cancer tissues[222]. However, the findings of the current study do not support the previous research. This difference may be attributed to the diversity of cell types under investigation. According to existing reports, *F. nucleatum* has been found to inhibit the proliferation of osteoblasts by stimulating the expression of caspase-8 and inflammatory cytokines such as TNF-α, IL-6, and Rank1[218]. Furthermore, infection with *F. nucleatum* has been observed to influence the expression of several genes associated with the suppression of cell growth and inflammatory reactions. The bacterium also activates various inflammatory signaling pathways, including NF-κB, Ku70/p53, TLR, and TNF signaling pathways[95; 188; 218; 223]. Given that cell proliferation is governed by distinct molecular mechanisms in normal epithelial cells compared to cancer cells, the observed differences in SCC-25, CL-11, and PHGK responses may stem from differential pathway activation in response to heat-killed *F. nucleatum* exposure. Further investigations will be required to delineate these mechanistic differences and clarify how bacterial interactions influence PD-L1 expression and cell viability in different cellular contexts.

4.6 Limitation and future work

4.6.1 Heat-killed *F. nucleatum*

Ji et al. (2009) conducted a comparative analysis to elucidate the regulatory mechanisms underlying the induction of HBD-2 and HBD-3 expression by live *F. nucleatum* and heat-killed *F. nucleatum*[39]. They surprisingly found that heat-killed bacteria specifically induced HBD-3 expression while failing to induce HBD-2 expression, suggesting distinct regulatory mechanisms for HBD-2 and HBD-3. Furthermore, the activation of NF-κB and MAPKs was observed in response to heat-killed *F. nucleatum*, although JNK activation was comparatively lower than that induced by live bacteria. This could be the reason that heat-killed *F.*

nucleatum failed to induce HBD-2. Additionally, heat-killed *F. nucleatum*'s ability to activate TLR2 was slightly reduced, and its capacity to invade epithelial cells was significantly impaired[39]. Multiple reports have demonstrated the critical dependence of PD-L1 upregulation in immune cells and various cancer cell types on TLR or IFN-γ-mediated signaling pathways[116]. Given the diminished capacity of heat-killed *F. nucleatum* to activate TLR2, it is plausible that it may impact PD-L1 expression. However, it is important to note that this study only utilized heat-killed *F. nucleatum*, and it is conceivable that viable *F. nucleatum* may exert a more substantial influence on PD-L1 expression. While our study provides valuable insights into the potential effects of bacterial stimulation on PD-L1 expression, further research utilizing viable *F. nucleatum* is warranted to fully elucidate the extent of its impact. Future studies incorporating viable bacteria could provide a more comprehensive understanding of the dynamic interactions between live bacterial cells and host immune responses, potentially offering insights into novel therapeutic strategies targeting PD-L1 expression in the context of bacterial infections.

4.6.2 Lack of immune cells

Another possible limitation to consider is the lack of immune cells in this study. However, this deliberate choice aimed to highlight that autocrine and paracrine signaling from tissue cells alone can sufficiently influence tumor growth and immune evasion. Although this work is restricted to heat-killed *F. nucleatum*, we demonstrated the PD-L1 expression and cell viability are influenced differentially by various subspecies of heat-killed *F. nucleatum*, including *ssp. nucleatum*, *ssp. polymorphum*, and *ssp. vincentii*. Although *F. nucleatum* may not directly transform normal cells into cancer cells, it may indirectly contribute to tumor progression through paracrine crosstalk. While the interaction between PD-1-expressing immune cells and cancer cells has been extensively studied, the specific role of *F. nucleatum* in modulating this interaction remains unclear. Future experiments will investigate the role of *F. nucleatum* in modulating PD-1/PD-L1 interactions using co-culture models that incorporate T cells, B cells, and NK cells to better mimic the tumor microenvironment. Additionally, *in vivo* studies using murine models will be conducted to examine whether *F. nucleatum*-induced PD-L1 upregulation influences the efficacy of anti-PD-1 immunotherapy.

4.6.3 A link between PD-L1 induction and malignant conversion

EMT` plays a crucial role in the conversion of normal epithelial cells into tumor cells and facilitates metastasis[116; 224]. Through this mechanism, epithelial cells undergo a transition, acquiring both mesenchymal and epithelial phenotypes to facilitate cell migration and proliferation. It is widely recognized that during EMT, epithelial cells exhibit enhanced survival capabilities in adverse environmental conditions, enabling tumor cells to evade immune destruction. EMT triggers various signaling cascades, including Akt/mTOR, NF-kB, and MAPK, which are activated by growth factor receptors. Notably, various signaling molecules associated with the EMT also coincide with those implicated in the exogenous induction of PD-L1. Hence, differences between specific events triggered by exogenous stimuli and inherent cellular changes are challenging. Hirai et al. (2016) have found a close relationship between PD-L1 expression and EMT[152]. Currently, the link between PD-L1, *F. nucleatum*, and EMT processes in OSCC and CRC is unclear. Nonetheless, further investigation is necessary to explore the involvement of *F. nucleatum* in tumor immune evasion, particularly in relation to the interactions between EMT and PD-L1.

4.6.4 Future work

This study provides new insights into the strain-specific effects of heat-killed *F. nucleatum* on PD-L1 expression and cell viability in different cell lines. However, several questions remain unanswered and warrant further investigation.

First, while this study demonstrated post-transcriptional regulation of PD-L1 in SCC-25 and CL-11 cells, the precise mechanisms underlying this regulation remain unclear. Proteomic and transcriptomic analyses could help identify key regulatory factors involved in this process. Second, this study revealed complex, strain-specific, and cell-type-dependent effects of *F. nucleatum* on cell viability. SCC-25 and CL-11 cells exhibited an initial transient increase in viability followed by a significant reduction at later time points, suggesting a biphasic response. In contrast, PHGK cells demonstrated early viability enhancement, particularly at higher MOI levels, followed by a return to baseline or slight viability suppression. The molecular mechanisms underlying these differential responses remain unclear. Further investigations should examine whether *F. nucleatum*-induced changes in cell viability are linked to bacterial modulation of apoptosis, autophagy, or inflammatory signaling pathways such as NF-κB, TLR, and TNF. Third, although this study utilized heat-killed *F. nucleatum*, the role of viable bacteria in cell viability regulation remains to be determined. Live *F. nucleatum* is known to invade epithelial and cancer cells and directly interact with host signaling pathways. Investigating whether viable *F. nucleatum* induces similar biphasic viability effects or triggers distinct cytotoxic mechanisms could provide further insight into bacterial-host interactions. Additionally, understanding how *F. nucleatum* affects cancer cell proliferation and survival in a live infection model will be crucial for determining its potential role in tumor progression. Fourth, the specific bacterial components responsible for modulating both PD-L1 expression and cell viability remain unidentified. Previous studies have implicated bacterial adhesins (e.g., Fap2, FadA), LPS, and metabolic byproducts in immune evasion and pro-inflammatory signaling. Future research employing bacterial fractionation could help determine which components drive *F. nucleatum*-mediated changes in cell viability and PD-L1 expression. Fifth, while this study focused on *in vitro* models using SCC-25, CL-11, and PHGK cells, *in vivo* validation is necessary to determine whether these effects are consistent in a physiological setting. Animal models could be employed to assess whether *F. nucleatum* colonization in the tumor microenvironment affects PD-L1 expression and cell survival, leading to tumor immune evasion.

Addressing these future directions will help elucidate the full impact of *F. nucleatum* on tumor progression and immune modulation, potentially leading to new therapeutic approaches targeting bacteria-driven immune evasion and cancer cell survival mechanisms.

5. Summary

This study investigated the impact of heat-killed *Fusobacterium nucleatum* (*F. nucleatum*) strains on PD-L1 expression and cell viability in three distinct cell types: SCC-25 (oral squamous cell carcinoma), CL-11 (colorectal cancer), and primary human gingival keratinocytes (PHGK). Our results demonstrated that heat-killed *F. nucleatum* strains modulate PD-L1 expression in a strain- and cell type-dependent manner, with notable differences in protein and mRNA expression. Additionally, the effects of bacterial exposure on cell viability varied over time, further emphasizing the complexity of *F. nucleatum*-host interactions.

In SCC-25 cells, all three *F. nucleatum* strains (ATCC 49256, ATCC10953, and ATCC 25586) significantly upregulated PD-L1 protein expression, particularly at 24 hours. However, mRNA expression did not consistently correlate with these changes, suggesting that PD-L1 regulation may involve post-transcriptional mechanisms. Cl-11 cells exhibited a similar trend, with ATCC 10953 inducing the most pronounced PD-L1 upregulation, followed by ATCC 49256 and ATCC 25586 at later time points. In contrast, PHGK cells exhibited a more limited response to bacterial stimulation, ATCC 49256 did not significantly alter PD-L1 expression, while ATCC 10953 and ATCC 25586 induced modest upregulation at later time points.

The effects of heat-killed *F. nucleatum* on cell viability were also highly dynamic and strain-dependent. In SCC-25 cells, bacterial exposure initially promoted viability at early time points, but prolonged exposure (48 hours) resulted in a dose-dependent decrease, particularly at higher multiplicity of infection (MOI). This biphasic response was most pronounced in ATCC 49256 and ATCC 10953, whereas ATCC 25586 exhibited a weaker effect. In CL-11 cells, *F. nucleatum* predominatly exerted an inhibitory effect on viability, with significant reductions observed in specific treatment groups, particularly at 24 and 48 hours. However, some conditions, notably higher bacterial doses, showed signs of viability recovery at later time points, particularly for ATCC10953. In PHGK cells, viability responses varied depending on the strain and exposure duration. ATCC 49256 and ATCC 10953 initially enhanced viability at 4 hours but induced significant reductions at 24 and 48 hours, whereas ATCC 25586 had minimal effects on PHGK viability.

Overall, these findings highlight the strain-specific and time- dependent effects of heat-killed *F. nucleatum* on immune modulation and cellular responses. The differential induction of PD-L1 suggests that distinct bacterial components may contribute to immune evasion, while the observed viability changes indicate that heat-killed *F. nucleatum* interactions with host cells are complex and dynamic. Further research is needed to elucidate the molecular mechanisms underlying these responses and to determine the potential implications for progression and therapeutic interventions.

Zusammenfassung

Diese Studie untersuchte die Auswirkungen von hitzeinaktivierten *Fusobacterium nucleatum* (*F. nucleatum*)-Stämmen auf die PD-L1-Expression und die Zellviabilität in drei verschiedenen Zelltypen: SCC-25 (orales Plattenepithelkarzinom), CL-11 (kolorektales Karzinom) und primäre humane gingivale Keratinozyten (PHGK). Unsere Ergebnisse zeigen, dass *F. nucleatum*-Stämme die PD-L1-Expression stamm- und zelltypspezifisch modulieren, wobei deutliche Unterschiede zwischen Protein- und mRNA-Expression bestehen. Darüber hinaus variierten die Auswirkungen der bakteriellen Exposition auf die Zellviabilität über die Zeit, was die Komplexität der *F. nucleatum*-Wirt-Interaktionen weiter unterstreicht.

In SCC-25-Zellen führten alle drei *F. nucleatum*-Stämme (ATCC 49256, ATCC 10953 und ATCC 25586) zu einer signifikanten Hochregulation der PD-L1-Proteinexpression, insbesondere nach 24 Stunden. Die mRNA-Expression zeigte jedoch keine durchgängig korrelierenden Veränderungen, was darauf hindeutet, dass die PD-L1-Regulation möglicherweise durch post-transkriptionelle Mechanismen gesteuert wird. In CL-11-Zellen zeigte sich ein ähnlicher Trend, wobei ATCC 10953 die stärkste PD-L1-Induktion nach 24 und 48 Stunden aufwies, gefolgt von ATCC 49256 und ATCC 25586. Im Gegensatz dazu reagierten PHGK-Zellen nur begrenzt auf die bakterielle Stimulation. ATCC 49256 veränderte die PD-L1-Expression nicht signifikant, während ATCC 10953 und ATCC 25586 zu einer moderaten Hochregulation zu späteren Zeitpunkten führten.

Auch die Auswirkungen von *F. nucleatum* auf die Zellviabilität waren hochdynamisch und stammabhängig. In SCC-25-Zellen förderte die bakterielle Exposition zunächst die Zellviabilität zu frühen Zeitpunkten, während eine längere Exposition (48 Stunden) zu einer dosisabhängigen Abnahme führte, insbesondere bei höheren Multiplicities of Infection (MOI). Diese biphasische Reaktion war bei ATCC 49256 und ATCC 10953 am deutlichsten ausgeprägt, während ATCC 25586 einen schwächeren Effekt zeigte. In CL-11-Zellen wirkte *F. nucleatum* überwiegend inhibierend auf die Viabilität, mit signifikanten Reduktionen in bestimmten Behandlungsgruppen, insbesondere nach 24 und 48 Stunden. Bei einigen Bedingungen, insbesondere bei höheren bakteriellen Dosen, zeigte sich jedoch zu späteren Zeitpunkten eine Erholung der Zellviabilität, insbesondere für ATCC 10953. In PHGK-Zellen variierten die Viabilitätsreaktionen je nach Stamm und Expositionsdauer. ATCC 49256 und

ATCC 10953 erhöhten die Viabilität zunächst nach 4 Stunden, führten jedoch nach 24 und 48 Stunden zu signifikanten Reduktionen, während ATCC 25586 nur minimale Auswirkungen auf die PHGK-Viabilität hatte.

Insgesamt unterstreichen diese Ergebnisse die stammabhängigen und zeitabhängigen Effekte von *F. nucleatum* auf die Immunmodulation und zelluläre Reaktionen. Die differenzielle Induktion von PD-L1 legt nahe, dass spezifische bakterielle Komponenten zur Immunevasion beitragen könnten, während die beobachteten Viabilitätsveränderungen darauf hinweisen, dass die Interaktionen zwischen *F. nucleatum* und Wirtszellen komplex und dynamisch sind. Weitere Untersuchungen sind erforderlich, um die zugrundeliegenden molekularen Mechanismen dieser Reaktionen aufzuklären und die möglichen Implikationen für die Tumorprogression und therapeutische Interventionen zu bestimmen.

6. References

[1] Han Y W. Fusobacterium nucleatum: a commensal-turned pathogen[J]. Current Opinion in Microbiology, 2015, 23: 141-147.
[2] Yang N Y, Zhang Q, Li J L, et al. Progression of periodontal inflammation in adolescents is associated with increased number of Porphyromonas gingivalis, Prevotella intermedia, Tannerella forsythensis, and Fusobacterium nucleatum[J]. Int J Paediatr Dent, 2014, 24(3): 226-33.
[3] Alon-Maimon T, Mandelboim O, Bachrach G. Fusobacterium nucleatum and cancer[J]. Periodontol 2000, 2022, 89(1): 166-180.
[4] Mcilvanna E, Linden G J, Craig S G, et al. Fusobacterium nucleatum and oral cancer: a critical review[J]. BMC Cancer, 2021, 21(1): 1212.
[5] Brennan C A, Garrett W S. Fusobacterium nucleatum - symbiont, opportunist and oncobacterium[J]. Nat Rev Microbiol, 2019, 17(3): 156-166.
[6] Kolenbrander P E, Palmer R J, Jr., Periasamy S, et al. Oral multispecies biofilm development and the key role of cell-cell distance[J]. Nat Rev Microbiol, 2010, 8(7): 471-80.
[7] Rizzato C, Torres J, Kasamatsu E, et al. Potential Role of Biofilm Formation in the Development of Digestive Tract Cancer With Special Reference to Helicobacter pylori Infection[J]. Front Microbiol, 2019, 10: 846.
[8] Groeger S E, Meyle J. Epithelial barrier and oral bacterial infection[J]. Periodontol 2000, 2015, 69(1): 46-67.
[9] Edwards A M, Grossman T J, Rudney J D. Fusobacterium nucleatum transports noninvasive Streptococcus cristatus into human epithelial cells[J]. Infect Immun, 2006, 74(1): 654-62.
[10] Guo L, Shokeen B, He X, et al. Streptococcus mutans SpaP binds to RadD of Fusobacterium nucleatum ssp. polymorphum[J]. Mol Oral Microbiol, 2017, 32(5): 355-364.
[11] Kaplan C W, Lux R, Haake S K, et al. The Fusobacterium nucleatum outer membrane protein RadD is an arginine-inhibitable adhesin required for inter-species adherence and the structured architecture of multispecies biofilm[J]. Mol Microbiol, 2009, 71(1): 35-47.
[12] Zhao T, Wang X, Fu L, et al. Fusobacterium nucleatum: a new player in regulation of cancer development and therapeutic response[J]. Cancer Drug Resist, 2022, 5(2): 436-450.
[13] Lima B P, Shi W, Lux R. Identification and characterization of a novel Fusobacterium nucleatum adhesin involved in physical interaction and biofilm formation with Streptococcus gordonii[J]. Microbiologyopen, 2017, 6(3).
[14] Han Y. in Oral Microbial Communities: Genomic Inquiry and Interspecies Communication[J], 2011.
[15] Rubinstein M R, Wang X, Liu W, et al. Fusobacterium nucleatum promotes colorectal carcinogenesis by modulating E-cadherin/beta-catenin signaling via its FadA adhesin[J]. Cell Host Microbe, 2013, 14(2): 195-206.
[16] Chattopadhyay I, Verma M, Panda M. Role of Oral Microbiome Signatures in Diagnosis and Prognosis of Oral Cancer[J]. Technol Cancer Res Treat, 2019, 18: 1533033819867354.
[17] Ma C T, Luo H S, Gao F, et al. Fusobacterium nucleatum promotes the progression of colorectal cancer by interacting with E-cadherin[J]. Oncol Lett, 2018, 16(2): 2606-2612.
[18] Silva B S, Castro C A, Von Zeidler S L, et al. Altered beta-catenin expression in oral mucosal dysplasia: a comparative study[J]. J Appl Oral Sci, 2015, 23(5): 472-8.
[19] Fardini Y, Wang X, Témoin S, et al. Fusobacterium nucleatum adhesin FadA binds vascular endothelial cadherin and alters endothelial integrity[J]. Mol Microbiol, 2011, 82(6): 1468-80.
[20] Kaplan A, Kaplan C W, He X, et al. Characterization of aid1, a novel gene involved in Fusobacterium nucleatum interspecies interactions[J]. Microb Ecol, 2014, 68(2): 379-87.
[21] Abed J, Emgård J E, Zamir G, et al. Fap2 Mediates Fusobacterium nucleatum Colorectal Adenocarcinoma Enrichment by Binding to Tumor-Expressed Gal-GalNAc[J]. Cell Host Microbe, 2016, 20(2): 215-25.

[22] Gur C, Ibrahim Y, Isaacson B, et al. Binding of the Fap2 protein of Fusobacterium nucleatum to human inhibitory receptor TIGIT protects tumors from immune cell attack[J]. Immunity, 2015, 42(2): 344-355.
[23] Martin-Gallausiaux C, Malabirade A, Habier J, et al. Fusobacterium nucleatum Extracellular Vesicles Modulate Gut Epithelial Cell Innate Immunity via FomA and TLR2[J]. Front Immunol, 2020, 11: 583644.
[24] Toussi D N, Liu X, Massari P. The FomA porin from Fusobacterium nucleatum is a Toll-like receptor 2 agonist with immune adjuvant activity[J]. Clin Vaccine Immunol, 2012, 19(7): 1093-101.
[25] Nakagaki H, Sekine S, Terao Y, et al. Fusobacterium nucleatum envelope protein FomA is immunogenic and binds to the salivary statherin-derived peptide[J]. Infect Immun, 2010, 78(3): 1185-92.
[26] Park S R, Kim D J, Han S H, et al. Diverse Toll-like receptors mediate cytokine production by Fusobacterium nucleatum and Aggregatibacter actinomycetemcomitans in macrophages[J]. Infect Immun, 2014, 82(5): 1914-20.
[27] Chaushu S, Wilensky A, Gur C, et al. Direct recognition of Fusobacterium nucleatum by the NK cell natural cytotoxicity receptor NKp46 aggravates periodontal disease[J]. PLoS Pathog, 2012, 8(3): e1002601.
[28] Bui F Q, Johnson L, Roberts J, et al. Fusobacterium nucleatum infection of gingival epithelial cells leads to NLRP3 inflammasome-dependent secretion of IL-1beta and the danger signals ASC and HMGB1[J]. Cell Microbiol, 2016, 18(7): 970-81.
[29] Binder Gallimidi A, Fischman S, Revach B, et al. Periodontal pathogens Porphyromonas gingivalis and Fusobacterium nucleatum promote tumor progression in an oral-specific chemical carcinogenesis model[J]. Oncotarget, 2015, 6(26): 22613-23.
[30] Gholizadeh P, Eslami H, Kafil H S. Carcinogenesis mechanisms of Fusobacterium nucleatum[J]. Biomed Pharmacother, 2017, 89: 918-925.
[31] Peyyala R, Kirakodu S S, Novak K F, et al. Oral microbial biofilm stimulation of epithelial cell responses[J]. Cytokine, 2012, 58(1): 65-72.
[32] Dickinson B C, Moffatt C E, Hagerty D, et al. Interaction of oral bacteria with gingival epithelial cell multilayers[J]. Mol Oral Microbiol, 2011, 26(3): 210-20.
[33] Zhang G, Chen R, Rudney J D. Streptococcus cristatus modulates the Fusobacterium nucleatum-induced epithelial interleukin-8 response through the nuclear factor-kappa B pathway[J]. J Periodontal Res, 2011, 46(5): 558-67.
[34] Krisanaprakornkit S, Kimball J R, Weinberg A, et al. Inducible expression of human beta-defensin 2 by Fusobacterium nucleatum in oral epithelial cells: multiple signaling pathways and role of commensal bacteria in innate immunity and the epithelial barrier[J]. Infect Immun, 2000, 68(5): 2907-15.
[35] Gholizadeh P, Eslami H, Yousefi M, et al. Role of oral microbiome on oral cancers, a review[J]. Biomed Pharmacother, 2016, 84: 552-558.
[36] Lee S J, Choi B K. Involvement of NLRP10 in IL-1alpha induction of oral epithelial cells by periodontal pathogens[J]. Innate Immun, 2017, 23(7): 569-577.
[37] Gupta S, Ghosh S K, Scott M E, et al. Fusobacterium nucleatum-associated beta-defensin inducer (FAD-I): identification, isolation, and functional evaluation[J]. J Biol Chem, 2010, 285(47): 36523-31.
[38] Ji S, Shin J E, Kim Y C, et al. Intracellular degradation of Fusobacterium nucleatum in human gingival epithelial cells[J]. Mol Cells, 2010, 30(6): 519-26.
[39] Ji S, Shin J E, Kim Y S, et al. Toll-like receptor 2 and NALP2 mediate induction of human beta-defensins by fusobacterium nucleatum in gingival epithelial cells[J]. Infect Immun, 2009, 77(3): 1044-52.
[40] Bhattacharyya S, Ghosh S K, Shokeen B, et al. FAD-I, a Fusobacterium nucleatum Cell Wall-Associated Diacylated Lipoprotein That Mediates Human Beta Defensin 2 Induction through Toll-Like Receptor-1/2 (TLR-1/2) and TLR-2/6[J]. Infect Immun, 2016, 84(5): 1446-1456.
[41] Ji S, Kim Y, Min B M, et al. Innate immune responses of gingival epithelial cells to nonperiodontopathic and periodontopathic bacteria[J]. J Periodontal Res, 2007, 42(6): 503-10.

[42] Hung S C, Huang P R, Almeida-Da-Silva C L C, et al. NLRX1 modulates differentially NLRP3 inflammasome activation and NF-kappaB signaling during Fusobacterium nucleatum infection[J]. Microbes Infect, 2018, 20(9-10): 615-625.
[43] De Andrade K Q, Almeida-Da-Silva C L C, Coutinho-Silva R. Immunological Pathways Triggered by Porphyromonas gingivalis and Fusobacterium nucleatum: Therapeutic Possibilities?[J]. Mediators Inflamm, 2019, 2019: 7241312.
[44] Sims G P, Rowe D C, Rietdijk S T, et al. HMGB1 and RAGE in inflammation and cancer[J]. Annu Rev Immunol, 2010, 28: 367-88.
[45] Seoane J M, Varela-Centelles P I, Ramirez J R, et al. Heat shock proteins (HSP70 and HSP27) as markers of epithelial dysplasia in oral leukoplakia[J]. Am J Dermatopathol, 2006, 28(5): 417-22.
[46] Uitto V J, Baillie D, Wu Q, et al. Fusobacterium nucleatum Increases Collagenase 3 Production and Migration of Epithelial Cells[J]. Infection and Immunity, 2005, 73(2): 1171-1179.
[47] Mahtout H, Chandad F, Rojo J M, et al. Fusobacterium nucleatum binding to complement regulatory protein CD46 modulates the expression and secretion of cytokines and matrix metalloproteinases by oral epithelial cells[J]. J Periodontol, 2011, 82(2): 311-9.
[48] Jewett A, Hume W R, Le H, et al. Induction of apoptotic cell death in peripheral blood mononuclear and polymorphonuclear cells by an oral bacterium, Fusobacterium nucleatum[J]. Infect Immun, 2000, 68(4): 1893-8.
[49] Kaplan C W, Lux R, Huynh T, et al. Fusobacterium nucleatum apoptosis-inducing outer membrane protein[J]. J Dent Res, 2005, 84(8): 700-4.
[50] Kostic A D, Chun E, Robertson L, et al. Fusobacterium nucleatum potentiates intestinal tumorigenesis and modulates the tumor-immune microenvironment[J]. Cell Host Microbe, 2013, 14(2): 207-15.
[51] Li R, Hu Y, Hou S. An Exploration of Oral-Gut Pathogens Mediating Immune Escape of Pancreatic Cancer via miR-21/PTEN Axis[J]. Front Microbiol, 2022, 13: 928846.
[52] Vidotto T, Melo C M, Castelli E, et al. Emerging role of PTEN loss in evasion of the immune response to tumours[J]. Br J Cancer, 2020, 122(12): 1732-1743.
[53] Li Y, Guo H, Wang X, et al. Coinfection with Fusobacterium nucleatum can enhance the attachment and invasion of Porphyromonas gingivalis or Aggregatibacter actinomycetemcomitans to human gingival epithelial cells[J]. Arch Oral Biol, 2015, 60(9): 1387-93.
[54] Bartold P M, Gully N J, Zilm P S, et al. Identification of components in Fusobacterium nucleatum chemostat-culture supernatants that are potent inhibitors of human gingival fibroblast proliferation[J]. J Periodontal Res, 1991, 26(4): 314-22.
[55] Bachrach G, Rosen G, Bellalou M, et al. Identification of a Fusobacterium nucleatum 65 kDa serine protease[J]. Oral Microbiol Immunol, 2004, 19(3): 155-9.
[56] Liu J, Hsieh C L, Gelincik O, et al. Proteomic characterization of outer membrane vesicles from gut mucosa-derived fusobacterium nucleatum[J]. J Proteomics, 2019, 195: 125-137.
[57] Engevik M A, Danhof H A, Ruan W, et al. Fusobacterium nucleatum Secretes Outer Membrane Vesicles and Promotes Intestinal Inflammation[J]. mBio, 2021, 12(2).
[58] Han Y W. Fusobacterium nucleatum: a commensal-turned pathogen[J]. Curr Opin Microbiol, 2015, 23: 141-7.
[59] Xu B, Han Y W. Oral bacteria, oral health, and adverse pregnancy outcomes[J]. Periodontol 2000, 2022, 89(1): 181-189.
[60] Han Y W, Fardini Y, Chen C, et al. Term stillbirth caused by oral Fusobacterium nucleatum[J]. Obstet Gynecol, 2010, 115(2 Pt 2): 442-445.
[61] Wang X, Buhimschi C S, Temoin S, et al. Comparative microbial analysis of paired amniotic fluid and cord blood from pregnancies complicated by preterm birth and early-onset neonatal sepsis[J]. PLoS One, 2013, 8(2): e56131.
[62] Han Y W, Redline R W, Li M, et al. Fusobacterium nucleatum induces premature and term stillbirths in pregnant mice: implication of oral bacteria in preterm birth[J]. Infect Immun, 2004, 72(4): 2272-9.

[63] Garcia-So J, Zhang X, Yang X, et al. Omega-3 fatty acids suppress Fusobacterium nucleatum-induced placental inflammation originating from maternal endothelial cells[J]. JCI Insight, 2019, 4(3).
[64] Carrion J, Scisci E, Miles B, et al. Microbial carriage state of peripheral blood dendritic cells (DCs) in chronic periodontitis influences DC differentiation, atherogenic potential[J]. J Immunol, 2012, 189(6): 3178-87.
[65] Lee H R, Jun H K, Kim H D, et al. Fusobacterium nucleatum GroEL induces risk factors of atherosclerosis in human microvascular endothelial cells and ApoE(-/-) mice[J]. Mol Oral Microbiol, 2012, 27(2): 109-23.
[66] Zhao X, Liu Z, Shu D, et al. Association of Periodontitis with Rheumatoid Arthritis and the Effect of Non-Surgical Periodontal Treatment on Disease Activity in Patients with Rheumatoid Arthritis[J]. Med Sci Monit, 2018, 24: 5802-5810.
[67] Ebbers M, Lübcke P M, Volzke J, et al. Interplay between P. gingivalis, *F. nucleatum* and A. actinomycetemcomitans in murine alveolar bone loss, arthritis onset and progression[J]. Sci Rep, 2018, 8(1): 15129.
[68] Hong M, Li Z, Liu H, et al. Fusobacterium nucleatum aggravates rheumatoid arthritis through FadA-containing outer membrane vesicles[J]. Cell Host Microbe, 2023, 31(5): 798-810.e7.
[69] Lakner L. The problem of oral infection and its relation to systemic diseases[J]. Edinb Med J, 1945, 52(10): 366-72.
[70] Strauss J, Kaplan G G, Beck P L, et al. Invasive potential of gut mucosa-derived Fusobacterium nucleatum positively correlates with IBD status of the host[J]. Inflamm Bowel Dis, 2011, 17(9): 1971-8.
[71] Ozmeric N, Bissada N, Da Silva A P B. The Association between Inflammatory Bowel Disease and Periodontal Conditions: Is There a Common Bacterial Etiology?[J]. J Int Acad Periodontol, 2018, 20(2): 40-51.
[72] Williams M D, Kerber C A, Tergin H F. Unusual presentation of Lemierre's syndrome due to Fusobacterium nucleatum[J]. J Clin Microbiol, 2003, 41(7): 3445-8.
[73] Swidsinski A, Dörffel Y, Loening-Baucke V, et al. Acute appendicitis is characterised by local invasion with Fusobacterium nucleatum/necrophorum[J]. Gut, 2011, 60(1): 34-40.
[74] Ohyama H, Nakasho K, Yamanegi K, et al. An unusual autopsy case of pyogenic liver abscess caused by periodontal bacteria[J]. Jpn J Infect Dis, 2009, 62(5): 381-3.
[75] Greten Fr, Si. G. Inflammation and Cancer: Triggers, Mechanisms, and Consequences.[J]. Immunity, 2019, 51(1): 27-41.
[76] Grivennikov Si, Greten Fr, M K. Immunity, inflammation, and cancer.[J]. Cell, 2010, 140(6): 883-99.
[77] A M, P A, A S, et al. Cancer-related inflammation[J]. Nature, 2008, 454(7203): 436-44.
[78] Muller T, Braun M, Dietrich D, et al. PD-L1: a novel prognostic biomarker in head and neck squamous cell carcinoma[J]. Oncotarget, 2017, 8(32): 52889-52900.
[79] Lindemann A, Takahashi H, Patel A A, et al. Targeting the DNA Damage Response in OSCC with TP53 Mutations[J]. J Dent Res, 2018, 97(6): 635-644.
[80] Bray F, Ferlay J, Soerjomataram I, et al. Global cancer statistics 2018: GLOBOCAN estimates of incidence and mortality worldwide for 36 cancers in 185 countries[J]. CA Cancer J Clin, 2018, 68(6): 394-424.
[81] Nagy K N, Sonkodi I, Szöke I, et al. The microflora associated with human oral carcinomas[J]. Oral Oncol, 1998, 34(4): 304-8.
[82] Zhang W L, Wang S S, Wang H F, et al. Who is who in oral cancer?[J]. Exp Cell Res, 2019, 384(2): 111634.
[83] Chang C, Geng F, Shi X, et al. The prevalence rate of periodontal pathogens and its association with oral squamous cell carcinoma[J]. Appl Microbiol Biotechnol, 2019, 103(3): 1393-1404.
[84] Schmidt B L, Kuczynski J, Bhattacharya A, et al. Changes in abundance of oral microbiota associated with oral cancer[J]. PLoS One, 2014, 9(6): e98741.
[85] Al-Hebshi N N, Nasher A T, Maryoud M Y, et al. Inflammatory bacteriome featuring Fusobacterium nucleatum and Pseudomonas aeruginosa identified in association with oral squamous cell carcinoma[J]. Scientific reports, 2017, 7(1): 1834-1834.

[86] Perera M, Al-Hebshi N N, Perera I, et al. Inflammatory Bacteriome and Oral Squamous Cell Carcinoma[J]. J Dent Res, 2018, 97(6): 725-732.
[87] Harrandah A M, Chukkapalli S S, Bhattacharyya I, et al. Fusobacteria modulate oral carcinogenesis and promote cancer progression[J]. J Oral Microbiol, 2020, 13(1): 1849493.
[88] Arnold M, Sierra M S, Laversanne M, et al. Global patterns and trends in colorectal cancer incidence and mortality[J]. Gut, 2017, 66(4): 683-691.
[89] Villéger R, Lopès A, Veziant J, et al. Microbial markers in colorectal cancer detection and/or prognosis[J]. World J Gastroenterol, 2018, 24(22): 2327-2347.
[90] Kostic A D, Gevers D, Pedamallu C S, et al. Genomic analysis identifies association of Fusobacterium with colorectal carcinoma[J]. Genome Res, 2012, 22(2): 292-8.
[91] Mima K, Nishihara R, Qian Z R, et al. Fusobacterium nucleatum in colorectal carcinoma tissue and patient prognosis[J]. Gut, 2016, 65(12): 1973-1980.
[92] Yu T, Guo F, Yu Y, et al. Fusobacterium nucleatum Promotes Chemoresistance to Colorectal Cancer by Modulating Autophagy[J]. Cell, 2017, 170(3): 548-563 e16.
[93] Komiya Y, Shimomura Y, Higurashi T, et al. Patients with colorectal cancer have identical strains of Fusobacterium nucleatum in their colorectal cancer and oral cavity[J]. Gut, 2019, 68(7): 1335-1337.
[94] Rubinstein M R, Wang X, Liu W, et al. Fusobacterium nucleatum promotes colorectal carcinogenesis by modulating E-cadherin/β-catenin signaling via its FadA adhesin[J]. Cell Host Microbe, 2013, 14(2): 195-206.
[95] Yang Y, Weng W, Peng J, et al. Fusobacterium nucleatum Increases Proliferation of Colorectal Cancer Cells and Tumor Development in Mice by Activating Toll-Like Receptor 4 Signaling to Nuclear Factor-κB, and Up-regulating Expression of MicroRNA-21[J]. Gastroenterology, 2017, 152(4): 851-866.e24.
[96] Dong J, Li Y, Xiao H, et al. Oral microbiota affects the efficacy and prognosis of radiotherapy for colorectal cancer in mouse models[J]. Cell Rep, 2021, 37(4): 109886.
[97] Ishida Y, Agata Y, Shibahara K, et al. Induced expression of PD-1, a novel member of the immunoglobulin gene superfamily, upon programmed cell death[J]. Embo j, 1992, 11(11): 3887-95.
[98] Dong H, Zhu G, Tamada K, et al. B7-H1, a third member of the B7 family, co-stimulates T-cell proliferation and interleukin-10 secretion[J]. Nat Med, 1999, 5(12): 1365-9.
[99] Salama A D, Chitnis T, Imitola J, et al. Critical role of the programmed death-1 (PD-1) pathway in regulation of experimental autoimmune encephalomyelitis[J]. J Exp Med, 2003, 198(1): 71–78.
[100] Dong H, Zhu G, Tamada K, et al. B7-H1 determines accumulation and deletion of intrahepatic CD8(+) T lymphocytes[J]. Immunity, 2004, 20(3): 327-336.
[101] Rodig N, Ryan T, Allen J A, et al. Endothelial expression of PD-L1 and PD-L2 down-regulates CD8+ T cell activation and cytolysis[J]. Eur J Immunol, 2003, 33(11): 3117-26.
[102] Youngnak-Piboonratanakit P, Tsushima F, Otsuki N, et al. The expression of B7–H1 on keratinocytes in chronic inflammatory mucocutaneous disease and its regulatory role[J]. Immunol Lett, 2004, 94(3): 215-22.
[103] Liang S C, Latchman Y E, Buhlmann J E, et al. Regulation of PD-1, PD-L1, and PD-L2 expression during normal and autoimmune responses[J]. Eur J Immunol, 2003, 33(10): 2706–2716.
[104] Ritprajak P, Azuma M. Intrinsic and Extrinsic Control of Expression of the Immunoregulatory Molecule PD-L1 in Epithelial Cells and Squamous Cell Carcinoma[J]. Oral Oncol, 2015, 51(3): 221–228.
[105] Lenouvel D, González-Moles M, Talbaoui A, et al. An update of knowledge on PD-L1 in head and neck cancers: Physiologic, prognostic and therapeutic perspectives[J]. Oral Dis, 2020, 26(3): 511-526.
[106] Greenwald R J, Freeman G J, Sharpe A H. The B7 family revisited[J]. Annu Rev Immunol, 2005, 23: 515-48.
[107] Quezada S A, Peggs K S. Exploiting CTLA-4, PD-1 and PD-L1 to reactivate the host immune response against cancer[J]. Br J Cancer, 2013, 108(8): 1560-5.
[108] Cao Y, Zhang L, Kamimura Y, et al. B7–H1 overexpression regulates epithelial-mesenchymal transition and accelerates carcinogenesis in skin[J]. Cancer Res, 2011, 71(4): 1235–1243.

[109] Groeger S, Jarzina F, Mamat U, et al. Induction of B7-H1 receptor by bacterial cells fractions of Porphyromonas gingivalis on human oral epithelial cells: B7-H1 induction by Porphyromonas gingivalis fractions[J]. Immunobiology, 2017, 222(2): 137-147.
[110] Groeger S, Domann E, Gonzales J R, et al. B7-H1 and B7-DC receptors of oral squamous carcinoma cells are upregulated by Porphyromonas gingivalis[J]. Immunobiology, 2011, 216(12): 1302-10.
[111] Adel-Khattab D, Groeger S, Domann E, et al. Porphyromonas gingivalis induced up-regulation of PD-L1 in colon carcinoma cells[J]. Mol Oral Microbiol, 2021, 36(3): 172-181.
[112] Groeger S, Wu F, Wagenlehner F, et al. PD-L1 Up-Regulation in Prostate Cancer Cells by Porphyromonas gingivalis[J]. Front Cell Infect Microbiol, 2022, 12: 935806.
[113] Groeger S, Howaldt H P, Raifer H, et al. Oral Squamous Carcinoma Cells Express B7-H1 and B7-DC Receptors in Vivo[J]. Pathol Oncol Res, 2017, 23(1): 99-110.
[114] Yoshida S, Nagatsuka H, Nakano K, et al. Significance of PD-L1 Expression in Tongue Cancer Development[J]. Int J Med Sci, 2018, 15(14): 1723-1730.
[115] Chen J, Jiang C C, Jin L, et al. Regulation of PD-L1: a novel role of pro-survival signalling in cancer[J]. Ann Oncol, 2016, 27(3): 409-16.
[116] Ritprajak P, Azuma M. Intrinsic and extrinsic control of expression of the immunoregulatory molecule PD-L1 in epithelial cells and squamous cell carcinoma[J]. Oral Oncol, 2015, 51(3): 221-8.
[117] Yuan J, Dong X, Yap J, et al. The MAPK and AMPK signalings: interplay and implication in targeted cancer therapy[J]. J Hematol Oncol, 2020, 13(1): 113.
[118] Stutvoet T S, Kol A, De Vries E G, et al. MAPK pathway activity plays a key role in PD-L1 expression of lung adenocarcinoma cells[J]. J Pathol, 2019, 249(1): 52-64.
[119] Zhang Y, Velez-Delgado A, Mathew E, et al. Myeloid cells are required for PD-1/PD-L1 checkpoint activation and the establishment of an immunosuppressive environment in pancreatic cancer[J]. Gut, 2017, 66(1): 124-136.
[120] Parsa A T, Waldron J S, Panner A, et al. Loss of tumor suppressor PTEN function increases B7-H1 expression and immunoresistance in glioma[J]. Nat Med, 2007, 13(1): 84-8.
[121] Zhu J, Chen L, Zou L, et al. MiR-20b, -21, and -130b inhibit PTEN expression resulting in B7-H1 over-expression in advanced colorectal cancer[J]. Hum Immunol, 2014, 75(4): 348-53.
[122] Mittendorf E A, Philips A V, Meric-Bernstam F, et al. PD-L1 expression in triple-negative breast cancer[J]. Cancer Immunol Res, 2014, 2(4): 361-70.
[123] Kim Y B, Ahn J M, Bae W J, et al. Functional loss of ARID1A is tightly associated with high PD-L1 expression in gastric cancer[J]. Int J Cancer, 2019, 145(4): 916-926.
[124] Garcia-Diaz A, Shin D S, Moreno B H, et al. Interferon Receptor Signaling Pathways Regulating PD-L1 and PD-L2 Expression[J]. Cell Rep, 2017, 19(6): 1189-1201.
[125] Palicelli A, Croci S, Bisagni A, et al. What Do We Have to Know about PD-L1 Expression in Prostate Cancer? A Systematic Literature Review. Part 3: PD-L1, Intracellular Signaling Pathways and Tumor Microenvironment[J]. Int J Mol Sci, 2021, 22(22).
[126] Ikeda S, Okamoto T, Okano S, et al. PD-L1 Is Upregulated by Simultaneous Amplification of the PD-L1 and JAK2 Genes in Non-Small Cell Lung Cancer[J]. J Thorac Oncol, 2016, 11(1): 62-71.
[127] Akbay E A, Koyama S, Carretero J, et al. Activation of the PD-1 pathway contributes to immune escape in EGFR-driven lung tumors[J]. Cancer Discov, 2013, 3(12): 1355-63.
[128] Lee S K, Seo S H, Kim B S, et al. IFN-gamma regulates the expression of B7-H1 in dermal fibroblast cells[J]. J Dermatol Sci, 2005, 40(2): 95-103.
[129] Abiko K, Matsumura N, Hamanishi J, et al. IFN-γ from lymphocytes induces PD-L1 expression and promotes progression of ovarian cancer[J]. Br J Cancer, 2015, 112(9): 1501-9.
[130] Yi M, Niu M, Xu L, et al. Regulation of PD-L1 expression in the tumor microenvironment[J]. J Hematol Oncol, 2021, 14(1): 10.
[131] Wang X, Yang L, Huang F, et al. Inflammatory cytokines IL-17 and TNF-α up-regulate PD-L1 expression in human prostate and colon cancer cells[J]. Immunol Lett, 2017, 184: 7-14.

[132] Jiang C, Yuan F, Wang J, et al. Oral squamous cell carcinoma suppressed antitumor immunity through induction of PD-L1 expression on tumor-associated macrophages[J]. Immunobiology, 2017, 222(4): 651-657.
[133] Barsoum I B, Smallwood C A, Siemens D R, et al. A mechanism of hypoxia-mediated escape from adaptive immunity in cancer cells[J]. Cancer Res, 2014, 74(3): 665-74.
[134] Franzen A, Vogt T J, Müller T, et al. PD-L1 (CD274) and PD-L2 (PDCD1LG2) promoter methylation is associated with HPV infection and transcriptional repression in head and neck squamous cell carcinomas[J]. Oncotarget, 2018, 9(1): 641-650.
[135] Amini M, Hejazi M, Ghorban K, et al. Identification of functional methylated CpG loci in PD-L1 promoter as the novel epigenetic biomarkers for primary gastric cancer[J]. Gene, 2021, 772: 145376.
[136] Micevic G, Thakral D, Mcgeary M, et al. PD-L1 methylation regulates PD-L1 expression and is associated with melanoma survival[J]. Pigment Cell Melanoma Res, 2019, 32(3): 435-440.
[137] Zhao Z, Shilatifard A. Epigenetic modifications of histones in cancer[J]. Genome Biol, 2019, 20(1): 245.
[138] Woods D M, Sodré A L, Villagra A, et al. HDAC Inhibition Upregulates PD-1 Ligands in Melanoma and Augments Immunotherapy with PD-1 Blockade[J]. Cancer Immunol Res, 2015, 3(12): 1375-85.
[139] Wang H, Fu C, Du J, et al. Enhanced histone H3 acetylation of the PD-L1 promoter via the COP1/c-Jun/HDAC3 axis is required for PD-L1 expression in drug-resistant cancer cells[J]. J Exp Clin Cancer Res, 2020, 39(1): 29.
[140] Darvin P, Sasidharan Nair V, Elkord E. PD-L1 Expression in Human Breast Cancer Stem Cells Is Epigenetically Regulated through Posttranslational Histone Modifications[J]. J Oncol, 2019, 2019: 3958908.
[141] Gong A Y, Zhou R, Hu G, et al. MicroRNA-513 regulates B7-H1 translation and is involved in IFN-gamma-induced B7-H1 expression in cholangiocytes[J]. J Immunol, 2009, 182(3): 1325-33.
[142] Wang X, Li J, Dong K, et al. Tumor suppressor miR-34a targets PD-L1 and functions as a potential immunotherapeutic target in acute myeloid leukemia[J]. Cell Signal, 2015, 27(3): 443-52.
[143] Yee D, Shah K M, Coles M C, et al. MicroRNA-155 induction via TNF-α and IFN-γ suppresses expression of programmed death ligand-1 (PD-L1) in human primary cells[J]. J Biol Chem, 2017, 292(50): 20683-20693.
[144] Xie W B, Liang L H, Wu K G, et al. MiR-140 Expression Regulates Cell Proliferation and Targets PD-L1 in NSCLC[J]. Cell Physiol Biochem, 2018, 46(2): 654-663.
[145] Cioffi M, Trabulo S M, Vallespinos M, et al. The miR-25-93-106b cluster regulates tumor metastasis and immune evasion via modulation of CXCL12 and PD-L1[J]. Oncotarget, 2017, 8(13): 21609-21625.
[146] Fan Z, Wu C, Chen M, et al. The generation of PD-L1 and PD-L2 in cancer cells: From nuclear chromatin reorganization to extracellular presentation[J]. Acta Pharm Sin B, 2022, 12(3): 1041-1053.
[147] Lin Y M, Sung W W, Hsieh M J, et al. High PD-L1 Expression Correlates with Metastasis and Poor Prognosis in Oral Squamous Cell Carcinoma[J]. PLoS One, 2015, 10(11): e0142656.
[148] Lenouvel D, González-Moles M, Ruiz-Ávila I, et al. Prognostic and clinicopathological significance of PD-L1 overexpression in oral squamous cell carcinoma: A systematic review and comprehensive meta-analysis[J]. Oral Oncol, 2020, 106: 104722.
[149] Strome S E, Dong H, Tamura H, et al. B7–H1 blockade augments adoptive T-cell immunotherapy for squamous cell carcinoma[J]. Cancer Res, 2003, 63(19): 6501–6505.
[150] Malaspina T S, Gasparoto T H, Costa M R, et al. Enhanced programmed death 1 (PD-1) and PD-1 ligand (PD-L1) expression in patients with actinic cheilitis and oral squamous cell carcinoma[J]. Cancer Immunol Immunother, 2011, 60(7): 965-74.
[151] Kouketsu A, Sato I, Oikawa M, et al. Expression of immunoregulatory molecules PD-L1 and PD-1 in oral cancer and precancerous lesions: A cohort study of Japanese patients[J]. J Craniomaxillofac Surg, 2019, 47(1): 33-40.
[152] Hirai M, Kitahara H, Kobayashi Y, et al. Regulation of PD-L1 expression in a high-grade invasive human oral squamous cell carcinoma microenvironment[J]. Int J Oncol, 2017, 50(1): 41-48.

[153] Troeltzsch M, Woodlock T, Pianka A, et al. Is There Evidence for the Presence and Relevance of the PD-1/PD-L1 Pathway in Oral Squamous Cell Carcinoma? Hints From an Immunohistochemical Study[J]. J Oral Maxillofac Surg, 2017, 75(5): 969-977.
[154] Wang S, Yuan B, Wang Y, et al. Clinicopathological and prognostic significance of PD-L1 expression in colorectal cancer: a meta-analysis[J]. Int J Colorectal Dis, 2021, 36(1): 117-130.
[155] Tang M, Zheng Z, Shang J, et al. Risk Analysis of Positive PD-L1 Expression and Clinicopathological Features and Survival Prognosis in Patients with Colorectal Cancer: Systematic Review and Meta-Analysis[J]. J Healthc Eng, 2022, 2022: 8212486.
[156] Shen Z, Gu L, Mao D, et al. Clinicopathological and prognostic significance of PD-L1 expression in colorectal cancer: a systematic review and meta-analysis[J]. World J Surg Oncol, 2019, 17(1): 4.
[157] Masugi Y, Nishihara R, Yang J, et al. Tumor PDCD1LG2 (PD-L2) expression and the lymphocytic reaction to colorectal cancer[J]. Gut, 2017, 66(8): 1463–1473.
[158] Park H E, Kim J H, Cho N-Y, et al. Intratumoral Fusobacterium nucleatum abundance correlates with macrophage infiltration and CDKN2A methylation in microsatellite-unstable colorectal carcinoma[J]. Virchows Arch, 2017, 471(13): 329–336.
[159] Kanehisa M, Araki M, Goto S, et al. KEGG for linking genomes to life and the environment[J]. Nucleic Acids Res., 2008, 36(Database issue): D480-4.
[160] Von Mering C, Jensen L J, Snel B, et al. STRING: known and predicted protein-protein associations, integrated and transferred across organisms[J]. Nucleic Acids Res., 2005, 33(Database issue): D433-7.
[161] Chung M, Zhao N, Meier R, et al. Comparisons of oral, intestinal, and pancreatic bacterial microbiomes in patients with pancreatic cancer and other gastrointestinal diseases[J]. J Oral Microbiol, 2021, 13(1): 1887680.
[162] Ramos R T, Sodré C S, De Sousa Rodrigues P, et al. High-throughput nucleotide sequencing for bacteriome studies in oral squamous cell carcinoma: a systematic review[J]. Oral Maxillofac Surg, 2020, 24(4): 387-401.
[163] Gao Y, Bi D, Xie R, et al. Fusobacterium nucleatum enhances the efficacy of PD-L1 blockade in colorectal cancer[J]. Signal Transduct Target Ther, 2021, 6(1): 398.
[164] Gao Y, Zou T, Xu P, et al. Fusobacterium nucleatum stimulates cell proliferation and promotes PD-L1 expression via IFIT1-related signal in colorectal cancer[J]. Neoplasia, 2023, 35: 100850.
[165] Kurgan S, Kansal S, Nguyen D, et al. Strain-Specific Impact of Fusobacterium nucleatum on Neutrophil Function[J]. J Periodontol, 2017, 88(4): 380-389.
[166] Milward M R, Chapple I L, Wright H J, et al. Differential activation of NF-kappaB and gene expression in oral epithelial cells by periodontal pathogens[J]. Clin Exp Immunol, 2007, 148(2): 307-24.
[167] Abdulkareem A A, Shelton R M, Landini G, et al. Potential role of periodontal pathogens in compromising epithelial barrier function by inducing epithelial-mesenchymal transition[J]. J Periodontal Res, 2018, 53(4): 565-574.
[168] Fan P, Zhang Y, Ding S, et al. Integrating RNA-seq and scRNA-seq to explore the mechanism of macrophage ferroptosis associated with COPD[J]. Front Pharmacol, 2023, 14: 1139137.
[169] Zhao M Y, Liu P, Sun C, et al. Propofol Augments Paclitaxel-Induced Cervical Cancer Cell Ferroptosis In Vitro[J]. Front Pharmacol, 2022, 13: 816432.
[170] Kostic A D, Xavier R J, Gevers D. The microbiome in inflammatory bowel disease: current status and the future ahead[J]. Gastroenterology, 2014, 146(6): 1489-99.
[171] Han X Y, Weinberg J S, Prabhu S S, et al. Fusobacterial brain abscess: a review of five cases and an analysis of possible pathogenesis[J]. J Neurosurg, 2003, 99(4): 693-700.
[172] Brook I. Fusobacterial infections in children[J]. J Infect, 1994, 28(2): 155-65.
[173] Groeger S, Zhou Y, Ruf S, et al. Pathogenic Mechanisms of Fusobacterium nucleatum on Oral Epithelial Cells[J]. Front Oral Health, 2022, 3: 831607.
[174] Narikiyo M, Tanabe C, Yamada Y, et al. Frequent and preferential infection of Treponema denticola, Streptococcus mitis, and Streptococcus anginosus in esophageal cancers[J]. Cancer Sci, 2004, 95(7): 569-74.

[175] Del Castillo E, Meier R, Chung M, et al. The Microbiomes of Pancreatic and Duodenum Tissue Overlap and Are Highly Subject Specific but Differ between Pancreatic Cancer and Noncancer Subjects[J]. Cancer Epidemiol Biomarkers Prev, 2019, 28(2): 370-383.
[176] Chen X H, Wang A, Chu A N, et al. Mucosa-Associated Microbiota in Gastric Cancer Tissues Compared With Non-cancer Tissues[J]. Front Microbiol, 2019, 10: 1261.
[177] Yamamura K, Baba Y, Nakagawa S, et al. Human Microbiome Fusobacterium Nucleatum in Esophageal Cancer Tissue Is Associated with Prognosis[J]. Clin Cancer Res, 2016, 22(22): 5574-5581.
[178] Zhang Z, Yang J, Feng Q, et al. Compositional and Functional Analysis of the Microbiome in Tissue and Saliva of Oral Squamous Cell Carcinoma[J]. Front Microbiol, 2019, 10: 1439.
[179] Parhi L, Alon-Maimon T, Sol A, et al. Breast cancer colonization by Fusobacterium nucleatum accelerates tumor growth and metastatic progression[J]. Nat Commun, 2020, 11(1): 3259.
[180] Salmaninejad A, Valilou S F, Shabgah A G, et al. PD-1/PD-L1 pathway: Basic biology and role in cancer immunotherapy[J]. J Cell Physiol, 2019, 234(10): 16824-16837.
[181] Ji M, Liu Y, Li Q, et al. PD-1/PD-L1 pathway in non-small-cell lung cancer and its relation with EGFR mutation[J]. J Transl Med, 2015, 13: 5.
[182] Cha J H, Chan L C, Li C W, et al. Mechanisms Controlling PD-L1 Expression in Cancer[J]. Mol Cell, 2019, 76(3): 359-370.
[183] Thompson R H, Gillett M D, Cheville J C, et al. Costimulatory B7-H1 in renal cell carcinoma patients: Indicator of tumor aggressiveness and potential therapeutic target[J]. Proc Natl Acad Sci U S A, 2004, 101(49): 17174-9.
[184] Ohaegbulam K C, Assal A, Lazar-Molnar E, et al. Human cancer immunotherapy with antibodies to the PD-1 and PD-L1 pathway[J]. Trends Mol Med, 2015, 21(1): 24-33.
[185] Choi B B R, Choi J H, Kim U K, et al. Gold nanoparticles conjugated with programmed death-ligand 1 antibodies induce apoptosis of SCC-25 oral squamous cell carcinoma cells via programmed death-ligand 1/signal transducer and transcription 3 pathway[J]. Arch Oral Biol, 2021, 125: 105085.
[186] Song X, Liu J, Lu Y, et al. Overexpression of B7-H1 correlates with malignant cell proliferation in pancreatic cancer[J]. Oncol Rep, 2014, 31(3): 1191-8.
[187] Sun J, Tang Q, Yu S, et al. F. nucleatum facilitates oral squamous cell carcinoma progression via GLUT1-driven lactate production[J]. EBioMedicine, 2023, 88: 104444.
[188] Geng F, Zhang Y, Lu Z, et al. Fusobacterium nucleatum Caused DNA Damage and Promoted Cell Proliferation by the Ku70/p53 Pathway in Oral Cancer Cells[J]. DNA Cell Biol, 2020, 39(1): 144-151.
[189] Girolami I, Pantanowitz L, Munari E, et al. Prevalence of PD-L1 expression in head and neck squamous precancerous lesions: a systematic review and meta-analysis[J]. Head Neck, 2020, 42(10): 3018-3030.
[190] Xu S B, Wang M Y, Shi X Z, et al. Influence of PD-1/PD-L1 on immune microenvironment in oral leukoplakia and oral squamous cell carcinoma[J]. Oral Dis, 2022.
[191] Strome S E, Dong H, Tamura H, et al. B7-H1 blockade augments adoptive T-cell immunotherapy for squamous cell carcinoma[J]. Cancer Res, 2003, 63(19): 6501-5.
[192] Wang W, Tan J. Co-inhibition of BET proteins and PD-L1 as a potential therapy for OSCC through synergistic inhibition of FOXM1 and PD-L1 expressions[J]. J Oral Pathol Med, 2019, 48(9): 817-825.
[193] Bates A M, Lanzel E A, Qian F, et al. Cell genomics and immunosuppressive biomarker expression influence PD-L1 immunotherapy treatment responses in HNSCC-a computational study[J]. Oral Surg Oral Med Oral Pathol Oral Radiol, 2017, 124(2): 157-164.
[194] Gomez Hernandez M P, Bates A M, Starman E E, et al. HBD3 Induces PD-L1 Expression on Head and Neck Squamous Cell Carcinoma Cell Lines[J]. Antibiotics (Basel), 2019, 8(4).
[195] Groeger S, Denter F, Lochnit G, et al. Porphyromonas gingivalis Cell Wall Components Induce Programmed Death Ligand 1 (PD-L1) Expression on Human Oral Carcinoma Cells by a Receptor-Interacting Protein Kinase 2 (RIP2)-Dependent Mechanism[J]. Infect Immun, 2020, 88(5).
[196] Zhang S, Li C, Liu J, et al. Fusobacterium nucleatum promotes epithelial-mesenchymal transiton through regulation of the lncRNA MIR4435-2HG/miR-296-5p/Akt2/SNAI1 signaling pathway[J]. Febs j, 2020, 287(18): 4032-4047.

[197] Greenbaum D, Colangelo C, Williams K, et al. Comparing protein abundance and mRNA expression levels on a genomic scale[J]. Genome Biol, 2003, 4(9): 117.
[198] Baldi P, Long A D. A Bayesian framework for the analysis of microarray expression data: regularized t -test and statistical inferences of gene changes[J]. Bioinformatics, 2001, 17(6): 509-19.
[199] Szallasi Z. Genetic network analysis in light of massively parallel biological data acquisition[J]. Biocomputing'99, 1999: 5-16.
[200] Nakatsu G, Li X, Zhou H, et al. Gut mucosal microbiome across stages of colorectal carcinogenesis[J]. Nat Commun, 2015, 6: 8727.
[201] Flemer B, Lynch D B, Brown J M, et al. Tumour-associated and non-tumour-associated microbiota in colorectal cancer[J]. Gut, 2017, 66(4): 633-643.
[202] Flemer B, Warren R D, Barrett M P, et al. The oral microbiota in colorectal cancer is distinctive and predictive[J]. Gut, 2018, 67(8): 1454-1463.
[203] Wu N, Yang X, Zhang R, et al. Dysbiosis signature of fecal microbiota in colorectal cancer patients[J]. Microb Ecol, 2013, 66(2): 462-70.
[204] Chen W, Liu F, Ling Z, et al. Human intestinal lumen and mucosa-associated microbiota in patients with colorectal cancer[J]. PLoS One, 2012, 7(6): e39743.
[205] Li Y, Liang L, Dai W, et al. Prognostic impact of programed cell death-1 (PD-1) and PD-ligand 1 (PD-L1) expression in cancer cells and tumor infiltrating lymphocytes in colorectal cancer[J]. Mol Cancer, 2016, 15(1): 55.
[206] Guglielmi G. How gut microbes are joining the fight against cancer[J]. Nature, 2018, 557(7706): 482-484.
[207] Vétizou M, Pitt J M, Daillère R, et al. Anticancer immunotherapy by CTLA-4 blockade relies on the gut microbiota[J]. Science, 2015, 350(6264): 1079-84.
[208] Youngnak-Piboonratanakit P, Tsushima F, Otsuki N, et al. The expression of B7-H1 on keratinocytes in chronic inflammatory mucocutaneous disease and its regulatory role[J]. Immunol Lett, 2004, 94(3): 215-22.
[209] Gursoy U K, Könönen E, Uitto V J. Stimulation of epithelial cell matrix metalloproteinase (MMP-2, -9, -13) and interleukin-8 secretion by fusobacteria[J]. Oral Microbiol Immunol, 2008, 23(5): 432-4.
[210] Dezutter-Dambuyant C, Durand I, Alberti L, et al. A novel regulation of PD-1 ligands on mesenchymal stromal cells through MMP-mediated proteolytic cleavage[J]. Oncoimmunology, 2016, 5(3): e1091146.
[211] Dzink J L, Sheenan M T, Socransky S S. Proposal of three subspecies of Fusobacterium nucleatum Knorr 1922: Fusobacterium nucleatum subsp. nucleatum subsp. nov., comb. nov.; Fusobacterium nucleatum subsp. polymorphum subsp. nov., nom. rev., comb. nov.; and Fusobacterium nucleatum subsp. vincentii subsp. nov., nom. rev., comb. nov[J]. Int J Syst Bacteriol, 1990, 40(1): 74-8.
[212] Gharbia S E, Shah H N. Fusobacterium nucleatum subsp. fusiforme subsp. nov. and Fusobacterium nucleatum subsp. animalis subsp. nov. as additional subspecies within Fusobacterium nucleatum[J]. Int J Syst Bacteriol, 1992, 42(2): 296-8.
[213] Gharbia S E, Shah H N, Lawson P A, et al. Distribution and frequency of Fusobacterium nucleatum subspecies in the human oral cavity[J]. Oral Microbiol Immunol, 1990, 5(6): 324-7.
[214] Senthakumaran T, Moen A E F, Tannæs T M, et al. Microbial dynamics with CRC progression: a study of the mucosal microbiota at multiple sites in cancers, adenomatous polyps, and healthy controls[J]. Eur J Clin Microbiol Infect Dis, 2023, 42(3): 305-322.
[215] Thurnheer T, Karygianni L, Flury M, et al. Fusobacterium Species and Subspecies Differentially Affect the Composition and Architecture of Supra- and Subgingival Biofilms Models[J]. Front Microbiol, 2019, 10: 1716.
[216] Muchova M, Balacco D L, Grant M M, et al. Fusobacterium nucleatum Subspecies Differ in Biofilm Forming Ability in vitro[J]. Front Oral Health, 2022, 3: 853618.
[217] Kang W, Jia Z, Tang D, et al. Fusobacterium nucleatum Facilitates Apoptosis, ROS Generation, and Inflammatory Cytokine Production by Activating AKT/MAPK and NF-kappaB Signaling Pathways in Human Gingival Fibroblasts[J]. Oxid Med Cell Longev, 2019, 2019: 1681972.

[218] Gao H, Sun T, Yang F, et al. The Pathogenic Effects of Fusobacterium nucleatum on the Proliferation, Osteogenic Differentiation, and Transcriptome of Osteoblasts[J]. Front Cell Dev Biol, 2020, 8: 807.
[219] Wang Q, Zhao L, Xu C, et al. Fusobacterium nucleatum stimulates monocyte adhesion to and transmigration through endothelial cells[J]. Arch Oral Biol, 2019, 100: 86-92.
[220] Mendes R T, Nguyen D, Stephens D, et al. Endothelial Cell Response to Fusobacterium nucleatum[J]. Infect Immun, 2016, 84(7): 2141-2148.
[221] Yu T, Guo F, Yu Y, et al. Fusobacterium nucleatum Promotes Chemoresistance to Colorectal Cancer by Modulating Autophagy[J]. Cell, 2017, 170(3): 548-563.e16.
[222] Ghebeh H, Tulbah A, Mohammed S, et al. Expression of B7-H1 in breast cancer patients is strongly associated with high proliferative Ki-67-expressing tumor cells[J]. Int J Cancer, 2007, 121(4): 751-8.
[223] Zhang G, Rudney J D. Streptococcus cristatus attenuates Fusobacterium nucleatum-induced cytokine expression by influencing pathways converging on nuclear factor-κB[J]. Mol Oral Microbiol, 2011, 26(2): 150-63.
[224] Cui B, Chen J, Luo M, et al. PKD3 promotes metastasis and growth of oral squamous cell carcinoma through positive feedback regulation with PD-L1 and activation of ERK-STAT1/3-EMT signalling[J]. Int J Oral Sci, 2021, 13(1): 8.

Appendix

Table S1. Normality Test Results for PD-L1 Protein Expression in Response to Heat-Killed *F. nucleatum* ATCC 49625 Infection in SCC-25 Cells

Time Point	Group	Shapiro-Wilk P-value	Normality Conclusion
4 hours	Control	N/A*	Not Applicable
	IFN-γ	0.2636	Normal
	MOI 10	0.9668	Normal
	MOI 50	0.1194	Normal
	MOI 100	0.1272	Normal
	MOI 200	0.8765	Normal
8 hours	Control	N/A*	Not Applicable
	IFN-γ	0.1321	Normal
	MOI 10	0.6670	Normal
	MOI 50	0.6426	Normal
	MOI 100	0.4928	Normal
	MOI 200	0.2814	Normal
24 hours	Control	N/A*	Not Applicable
	IFN-γ	0.5585	Normal
	MOI 10	0.1126	Normal
	MOI 50	0.7889	Normal
	MOI 100	0.7394	Normal

	MOI 200	0.7554	Normal
48 hours	Control	N/A*	Not Applicable
	IFN-γ	0.1574	Normal
	MOI 10	0.7017	Normal
	MOI 50	0.8199	Normal
	MOI 100	0.8230	Normal
	MOI 200	0.5878	Normal

* The control group was normalized (Mean = 1, SD = 0), making it ineligible for Shapiro-Wilk normality testing due to the absence of variability. Thus, P-values for the control group were not calculated.

Table S2: Homogeneity of Variance and Statistical Analysis Results for PD-L1 Protein Expression in Response to Heat-Killed *F. nucleatum* ATCC 49625 Infection in SCC-25 Cells

Time point	Homogeneity of Variance Test F-value	Homogeneity of Variance Test P-value	Test Type	F / H-value	P-value	Effect Size (η^2)
4 hours	0.4498	0.8056	ANOVA (raw data)	4.856	0.012	0.669
8 hours	0.6384	0.6751	ANOVA (raw data)	2.749	0.070	0.533
24 hours	1.538	0.2380	ANOVA (raw data)	8.553	0.001	0.781
48 hours	1.253	0.3449	ANOVA (raw data)	0.470	0.792	0.163

Table S3. Normality Test Results for PD-L1 Protein Expression in Response to Heat-Killed *F. nucleatum* ATCC 10953 Infection in SCC-25 Cells

Time Point	Group	Shapiro-Wilk P-value	Normality Conclusion
4 hours	Control	N/A*	Not Applicable
	IFN-γ	0.8661	Normal
	MOI 10	0.2209	Normal
	MOI 50	0.8175	Normal
	MOI 100	0.8833	Normal
	MOI 200	0.7610	Normal
8 hours	Control	N/A*	Not Applicable
	IFN-γ	0.5345	Normal
	MOI 10	0.1257	Normal
	MOI 50	0.2081	Normal
	MOI 100	0.0284	Non-normal
	MOI 200	0.0396	Non-normal
24 hours	Control	N/A*	Not Applicable
	IFN-γ	0.5847	Normal
	MOI 10	0.8109	Normal
	MOI 50	0.3984	Normal
	MOI 100	0.9963	Normal
	MOI 200	0.0045	Normal
48 hours	Control	N/A*	Not Applicable

IFN- γ	0.5444	Normal
MOI 10	0.0198	Non-normal
MOI 50	0.3381	Normal
MOI 100	0.2885	Normal
MOI 200	0.5250	Normal

* The control group was normalized (Mean = 1, SD = 0), making it ineligible for Shapiro-Wilk normality testing due to the absence of variability. Thus, P-values for the control group were not calculated.

Table S4: Homogeneity of Variance and Statistical Analysis Results for PD-L1 Protein Expression in Response to Heat-Killed *F. nucleatum* ATCC 10953 Infection in SCC-25 Cells

Time point	Homogeneity of Variance Test F-value	Homogeneity of Variance Test P-value	Test Type	F / H-value	P-value	Effect Size (η^2)
4 hours	1.077	0.4206	ANOVA	2.899	0.0607	0.5472
8 hours	N/A	N/A	Kruskal-Wallis Test	8.427	0.1342	0.4957
24 hours	N/A	N/A	Kruskal-Wallis Test	9.836	0.0800	0.5786
48 hours	N/A	N/A	Kruskal-Wallis Test	7.957	0.1586	0.4681

Table S5. Normality and Homogeneity of Variance Test Results for PD-L1 Protein Expression in Response to Heat-Killed *F. nucleatum* ATCC 25586 Infection in SCC-25 Cells

Time Point	Group	Shapiro-Wilk P-value	Normality Conclusion
4 hours	Control	N/A*	Not Applicable
	IFN- γ	0.1125	Normal
	MOI 10	0.8404	Normal
	MOI 50	0.9411	Normal
	MOI 100	0.7732	Normal
	MOI 200	0.7760	Normal
8 hours	Control	N/A*	Not Applicable
	IFN- γ	0.2272	Normal
	MOI 10	0.0195	Non-normal
	MOI 50	0.0604	Normal
	MOI 100	0.0192	Non-normal
	MOI 200	0.3140	Normal
24 hours	Control	N/A*	Not Applicable
	IFN- γ	0.9572	Normal
	MOI 10	0.1709	Normal
	MOI 50	0.2211	Normal
	MOI 100	0.3849	Normal
	MOI 200	0.4529	Normal
48 hours	Control	N/A*	Not Applicable

	IFN-γ	0.7967	Normal
	MOI 10	0.6894	Normal
	MOI 50	0.4699	Normal
	MOI 100	0.3580	Normal
	MOI 200	0.6737	Normal

* The control group was normalized (Mean = 1, SD = 0), making it ineligible for Shapiro-Wilk normality testing due to the absence of variability. Thus, P-values for the control group were not calculated.

Table S6. Homogeneity of Variance and Statistical Analysis Results for Protein Expression of PD-L1 in Response to Heat-Killed *F. nucleatum* ATCC 25586 Infection in SCC-25 Cells

Time point	Homogeneity of Variance Test F-value	Homogeneity of Variance Test P-value	Test Type	F / H-value	P-value	Effect Size (η^2)
4 hours	0.7437	0.6057	ANOVA	6.041	0.0051	0.7051
8 hours	N/A	N/A	Kruskal-Wallis Test	7.323	0.1977	0.4308
24 hours	1.303	0.3257	ANOVA	0.4426	0.8106	0.1557
48 hours	1.663	0.2178	ANOVA	0.8888	0.5182	0.2702

Table S7. Normality and Homogeneity of Variance Test Results for PD-L1 Protein Expression in Response to Heat-Killed *F. nucleatum* ATCC 49256 Infection in CL-11 Cells

Time Point	Group	Shapiro-Wilk P-value	Normality Conclusion
4 hours	Control	N/A*	Not Applicable

	IFN- γ	0.9323	Normal
	MOI 10	0.8556	Normal
	MOI 50	0.1387	Normal
	MOI 100	0.7090	Normal
	MOI 200	0.4566	Normal
8 hours	Control	N/A*	Not Applicable
	IFN- γ	0.6696	Normal
	MOI 10	0.9858	Normal
	MOI 50	0.2677	Normal
	MOI 100	0.8712	Normal
	MOI 200	0.4222	Normal
24 hours	Control	N/A*	Not Applicable
	IFN- γ	0.1237	Normal
	MOI 10	0.2761	Normal
	MOI 50	0.4525	Normal
	MOI 100	0.3742	Normal
	MOI 200	0.2998	Normal
48 hours	Control	N/A*	Not Applicable
	IFN- γ	0.7655	Normal
	MOI 10	0.8163	Normal
	MOI 50	0.4294	Normal
	MOI 100	0.7179	Normal
	MOI 200	0.0154	Non-normal

* The control group was normalized (Mean = 1, SD = 0), making it ineligible for Shapiro-Wilk normality testing due to the absence of variability. Thus, P-values for the control group were not calculated.

Table S8. Homogeneity of Variance and Statistical Analysis Results for Protein Expression of PD-L1 in Response to Heat-Killed *F. nucleatum* ATCC 49256 Infection in CL-11 Cells

Time point	Homogeneity of Variance Test F-value	Homogeneity of Variance Test P-value	Test Type	F / H-value	P-value	Effect Size (η^2)
4 hours	0.5504	0.7356	ANOVA	1.391	0.2952	0.367
8 hours	1.305	0.3251	ANOVA	0.987	0.4647	0.292
24 hours	0.4617	0.7974	ANOVA	1.470	0.2699	0.380
48 hours	N/A	N/A	Kruskal-Wallis Test	12.37	0.030	0.728

Table S9. Normality and Homogeneity of Variance Test Results for PD-L1 Protein Expression in Response to Heat-Killed *F. nucleatum* ATCC 10953 Infection in CL-11 Cells

Time Point	Group	Shapiro-Wilk P-value	Normality Conclusion
4 hours	Control	N/A*	Not Applicable
	IFN- γ	0.8899	Normal
	MOI 10	0.2112	Normal
	MOI 50	0.9069	Normal
	MOI 100	0.8028	Normal
	MOI 200	0.9080	Normal

8 hours	Control	N/A*	Not Applicable
	IFN- γ	0.2062	Normal
	MOI 10	0.1017	Normal
	MOI 50	0.2615	Normal
	MOI 100	0.1547	Normal
	MOI 200	0.1397	Normal
24 hours	Control	N/A*	Not Applicable
	IFN- γ	0.1590	Normal
	MOI 10	0.9623	Normal
	MOI 50	0.4191	Normal
	MOI 100	0.7604	Normal
	MOI 200	0.6643	Normal
48 hours	Control	N/A*	Not Applicable
	IFN- γ	0.0852	Normal
	MOI 10	0.6901	Normal
	MOI 50	0.0517	Normal
	MOI 100	0.7151	Normal
	MOI 200	0.9454	Normal

* The control group was normalized (Mean = 1, SD = 0), making it ineligible for Shapiro-Wilk normality testing due to the absence of variability. Thus, P-values for the control group were not calculated.

Table S10. Homogeneity of Variance and Statistical Analysis Results for Protein Expression of PD-L1 in Response to Heat-Killed *F. nucleatum* ATCC 10953 Infection in CL-11 Cells

Time point	Homogeneity of Variance Test F-value	Homogeneity of Variance Test P-value	Test Type	F / H-value	P-value	Effect Size (η^2)
4 hours	0.9994	0.4585	ANOVA	1.064	0.427	0.307
8 hours	0.5497	0.7361	ANOVA	0.775	0.586	0.244
24 hours	1.408	0.2895	ANOVA	3.553	0.033	0.596
48 hours	0.8276	0.5538	ANOVA	3.124	0.049	0.565

Table S11. Normality and Homogeneity of Variance Test Results for PD-L1 Protein Expression in Response to Heat-Killed *F. nucleatum* ATCC 25586 Infection in CL-11 Cells

Time Point	Group	Shapiro-Wilk P-value	Normality Conclusion
4 hours	Control	N/A*	Not Applicable
	IFN- γ	0.3070	Normal
	MOI 10	0.2220	Normal
	MOI 50	0.4138	Normal
	MOI 100	0.2554	Normal
	MOI 200	0.7318	Normal
8 hours	Control	N/A*	Not Applicable
	IFN- γ	0.7879	Normal
	MOI 10	0.7723	Normal
	MOI 50	0.3649	Normal

	MOI 100	0.9391	Normal
	MOI 200	0.5897	Normal
24 hours	Control	N/A*	Not Applicable
	IFN- γ	0.3166	Normal
	MOI 10	0.5208	Normal
	MOI 50	0.3363	Normal
	MOI 100	0.9833	Normal
	MOI 200	0.7154	Normal
48 hours	Control	N/A*	Not Applicable
	IFN- γ	0.3359	Normal
	MOI 10	0.8155	Normal
	MOI 50	0.0124	Non-normal
	MOI 100	0.4220	Normal
	MOI 200	0.8066	Normal

* The control group was normalized (Mean = 1, SD = 0), making it ineligible for Shapiro-Wilk normality testing due to the absence of variability. Thus, P-values for the control group were not calculated.

Table S12. Homogeneity of Variance and Statistical Analysis Results for Protein Expression of PD-L1 in Response to Heat-Killed *F. nucleatum* ATCC 25586 Infection in CL-11 Cells

Time point	Homogeneity of Variance Test F-value	Homogeneity of Variance Test P-value	Test Type	F / H-value	P-value	Effect Size (η^2)
4 hours	0.7816	0.5791	ANOVA	0.850	0.541	0.2614

8 hours	1.178	0.3753	ANOVA	1.018	0.449	0.2979
24 hours	0.9461	0.4864	ANOVA	1.038	0.439	0.3018
48 hours	N/A	N/A	Kruskal-Wallis Test	9.460	0.092	0.556

Table S13. Normality and Homogeneity of Variance Test Results for PD-L1 Protein Expression in Response to Heat-Killed *F. nucleatum* ATCC 49256 Infection in PHGK.

Time Point	Group	Shapiro-Wilk P-value	Normality Conclusion
4 hours	Control	N/A*	Not Applicable
	IFN- γ	0.2634	Normal
	MOI 10	0.0409	Non-normal
	MOI 50	0.5086	Normal
	MOI 100	0.5833	Normal
	MOI 200	0.2490	Normal
8 hours	Control	N/A*	Not Applicable
	IFN- γ	0.0783	Normal
	MOI 10	0.8671	Normal
	MOI 50	0.6141	Normal
	MOI 100	0.3215	Normal
	MOI 200	0.5246	Normal

24 hours	Control	N/A*	Not Applicable
	IFN- γ	0.0646	Normal
	MOI 10	0.1495	Normal
	MOI 50	0.8287	Normal
	MOI 100	0.4305	Normal
	MOI 200	0.0650	Normal
48 hours	Control	N/A*	Not Applicable
	IFN- γ	0.9302	Normal
	MOI 10	0.0207	Non-normal
	MOI 50	0.5443	Normal
	MOI 100	0.1989	Normal
	MOI 200	0.3748	Normal

* The control group was normalized (Mean = 1, SD = 0), making it ineligible for Shapiro-Wilk normality testing due to the absence of variability. Thus, P-values for the control group were not calculated.

Table S14. Homogeneity of Variance and Statistical Analysis Results for Protein Expression of PD-L1 in Response to Heat-Killed *F. nucleatum* ATCC 49256 Infection in PHGK.

Time point	Homogeneity of Variance Test F-value	Homogeneity of Variance Test P-value	Test Type	F / H-value	P-value	Effect Size (η^2)
4 hours	N/A	N/A	Kruskal-Wallis Test	6.219	0.2855	0.3658
8 hours	0.6781	0.6484	ANOVA	1.133	0.395	0.321

24 hours	0.5540	0.7401	ANOVA	0.5797	0.7153	0.1945
48 hours	N/A	N/A	Kruskal-Wallis Test	7.792	0.1681	0.458

Table S15. Normality and Homogeneity of Variance Test Results for PD-L1 Protein Expression in Response to Heat-Killed *F. nucleatum* ATCC 10953 Infection in PHKG.

Time Point	Group	Shapiro-Wilk P-value	Normality Conclusion
4 hours	Control	N/A*	Not Applicable
	IFN- γ	0.0178	Non-normal
	MOI 10	0.3337	Normal
	MOI 50	0.3761	Normal
	MOI 100	0.1956	Normal
	MOI 200	0.3019	Normal
8 hours	Control	N/A*	Not Applicable
	IFN- γ	0.1358	Normal
	MOI 10	0.7259	Normal
	MOI 50	0.7549	Normal
	MOI 100	0.2989	Normal
	MOI 200	0.5649	Normal
24 hours	Control	N/A*	Not Applicable
	IFN- γ	0.3654	Normal

	MOI 10	0.8977	Normal
	MOI 50	0.0091	Non-normal
	MOI 100	0.6611	Normal
	MOI 200	0.7783	Non-normal
48 hours	Control	N/A*	Not Applicable
	IFN- γ	0.2726	Normal
	MOI 10	0.9465	Normal
	MOI 50	0.5381	Normal
	MOI 100	0.0272	Non-normal
	MOI 200	0.0317	Non-normal

* The control group was normalized (Mean = 1, SD = 0), making it ineligible for Shapiro-Wilk normality testing due to the absence of variability. Thus, P-values for the control group were not calculated.

Table S16. Homogeneity of Variance and Statistical Analysis Results for Protein Expression of PD-L1 in Response to Heat-Killed *F. nucleatum* ATCC 10953 Infection in PHKG.

Time point	Homogeneity of Variance Test F-value	Homogeneity of Variance Test P-value	Test Type	F / H-value	P-value	Effect Size (η^2)
4 hours	N/A	N/A	Kruskal-Wallis Test	8.380	0.1365	0.4929
8 hours	0.9047	0.5092	ANOVA	0.9730	0.4722	0.289
24 hours	N/A	N/A	Kruskal-Wallis Test	10.987	0.0516	0.646

48 hours	N/A	N/A	Kruskal-Wallis Test	10.705	0.0576	0.630

Table S17. Normality and Homogeneity of Variance Test Results for PD-L1 Protein Expression in Response to Heat-Killed *F. nucleatum* ATCC 25586 Infection in PHKG.

Time Point	Group	Shapiro-Wilk P-value	Normality Conclusion
4 hours	Control	N/A*	Not Applicable
	IFN- γ	0.4249	Normal
	MOI 10	0.3274	Normal
	MOI 50	0.0587	Normal
	MOI 100	0.8921	Normal
	MOI 200	0.0014	Non-normal
8 hours	Control	N/A*	Not Applicable
	IFN- γ	0.3716	Normal
	MOI 10	0.2340	Normal
	MOI 50	0.5662	Normal
	MOI 100	0.1974	Normal
	MOI 200	0.0329	Non-normal
24 hours	Control	N/A*	Not Applicable
	IFN- γ	0.8308	Normal
	MOI 10	0.6354	Normal

	MOI 50	0.5534	Normal
	MOI 100	0.7225	Normal
	MOI 200	0.1258	Normal
48 hours	Control	N/A*	Not Applicable
	IFN- γ	0.5800	Normal
	MOI 10	0.5691	Normal
	MOI 50	0.4241	Normal
	MOI 100	0.6075	Normal
	MOI 200	0.2685	Normal

* The control group was normalized (Mean = 1, SD = 0), making it ineligible for Shapiro-Wilk normality testing due to the absence of variability. Thus, P-values for the control group were not calculated.

Table S18. Homogeneity of Variance and Statistical Analysis Results for Protein Expression of PD-L1 in Response to Heat-Killed *F. nucleatum* ATCC 25586 Infection in PHKG.

Time point	Homogeneity of Variance Test F-value	Homogeneity of Variance Test P-value	Test Type	F / H-value	P-value	Effect Size (η^2)
4 hours	N/A	N/A	Kruskal-Wallis Test	10.212	0.069	0.601
8 hours	N/A	N/A	Kruskal-Wallis Test	11.128	0.049	0.655
24 hours	0.6539	0.6646	ANOVA	0.9282	0.4962	0.279
48 hours	0.8668	0.5307	ANOVA	0.882	0.1715	0.4396

Table S19. Normality and Homogeneity of Variance Test Results for PD-L1 mRNA Expression in Response to Heat-Killed *F. nucleatum* ATCC 49256 Infection in SCC-25.

Time Point	Group	Shapiro-Wilk P-value	Normality Conclusion
4 hours	Control	N/A*	Not Applicable
	IFN- γ	0.0378	Non-normal
	MOI 10	0.2804	Normal
	MOI 50	0.2319	Normal
	MOI 100	0.0969	Normal
	MOI 200	0.1407	Normal
8 hours	Control	N/A*	Not Applicable
	IFN- γ	0.1595	Normal
	MOI 10	0.0154	Non-normal
	MOI 50	0.3298	Normal
	MOI 100	0.0454	Non-normal
	MOI 200	0.6071	Normal
24 hours	Control	N/A*	Not Applicable
	IFN- γ	0.0068	Non-normal
	MOI 10	0.0644	Normal
	MOI 50	0.0724	Normal
	MOI 100	0.3021	Normal
	MOI 200	0.0168	Non-normal
48 hours	Control	N/A*	Not Applicable

IFN-γ	0.0487	Non-normal
MOI 10	0.8512	Normal
MOI 50	0.7490	Normal
MOI 100	0.0675	Normal
MOI 200	0.1742	Normal

* The control group was normalized (Mean = 1, SD = 0), making it ineligible for Shapiro-Wilk normality testing due to the absence of variability. Thus, P-values for the control group were not calculated.

Table S20. Homogeneity of Variance and Statistical Analysis Results for PD-L1 mRNA Expression in Response to Heat-Killed *F. nucleatum* ATCC 49256 Infection in SCC-25.

Time point	Homogeneity of Variance Test F-value	Homogeneity of Variance Test P-value	Test Type	F / H-value	P-value	Effect Size (η^2)
4 hours	N/A	N/A	Kruskal-Wallis Test	3.447	0.6314	0.2028
8 hours	N/A	N/A	Kruskal-Wallis Test	3.165	0.6745	0.1862
24 hours	N/A	N/A	Kruskal-Wallis Test	1.662	0.8937	0.0978
48 hours	N/A	N/A	Kruskal-Wallis Test	8.873	0.1142	0.5219

Table S21. Normality and Homogeneity of Variance Test Results for PD-L1 mRNA Expression in Response to Heat-Killed *F. nucleatum* ATCC 10953 Infection in SCC-25.

Time Point	Group	Shapiro-Wilk P-value	Normality Conclusion
4 hours	Control	N/A*	Not Applicable
	IFN- γ	0.5174	Normal
	MOI 10	0.1286	Normal
	MOI 50	0.3225	Normal
	MOI 100	0.2115	Normal
	MOI 200	0.0566	Normal
8 hours	Control	N/A*	Not Applicable
	IFN- γ	0.3611	Normal
	MOI 10	0.5701	Normal
	MOI 50	0.1331	Normal
	MOI 100	0.1514	Normal
	MOI 200	0.9066	Normal
24 hours	Control	N/A*	Not Applicable
	IFN- γ	0.0068	Non-normal
	MOI 10	0.5109	Normal
	MOI 50	0.2535	Normal
	MOI 100	0.8721	Normal
	MOI 200	0.6928	Normal
48 hours	Control	N/A*	Not Applicable

	IFN- γ	0.0487	Non-normal
	MOI 10	0.8079	Normal
	MOI 50	0.1836	Normal
	MOI 100	0.5963	Normal
	MOI 200	0.4176	Normal

* The control group was normalized (Mean = 1, SD = 0), making it ineligible for Shapiro-Wilk normality testing due to the absence of variability. Thus, P-values for the control group were not calculated.

Table S22. Homogeneity of Variance and Statistical Analysis Results for PD-L1 mRNA Expression in Response to Heat-Killed *F. nucleatum* ATCC 10953 Infection in SCC-25.

Time point	Homogeneity of Variance Test F-value	Homogeneity of Variance Test P-value	Test Type	F / H-value	P-value	Effect Size (η^2)
4 hours	0.4590	0.7993	ANOVA	0.6461	0.6698	0.2121
8 hours	0.4834	0.7823	ANOVA	0.1990	0.9568	0.0766
24 hours	N/A	N/A	Kruskal-Wallis Test	1.873	0.8664	0.1101
48 hours	N/A	N/A	Kruskal-Wallis Test	2.108	0.8340	0.124

Table S23. Normality and Homogeneity of Variance Test Results for PD-L1 mRNA Expression in Response to Heat-Killed *F. nucleatum* ATCC 25586 Infection in SCC-25.

Time Point	Group	Shapiro-Wilk P-value	Normality Conclusion
4 hours	Control	N/A*	Not Applicable
	IFN- γ	0.3937	Normal
	MOI 10	0.5081	Normal
	MOI 50	0.8863	Normal
	MOI 100	0.2917	Normal
	MOI 200	0.2612	Normal
8 hours	Control	N/A*	Not Applicable
	IFN- γ	0.2736	Normal
	MOI 10	0.5599	Normal
	MOI 50	0.9450	Normal
	MOI 100	0.7699	Normal
	MOI 200	0.1179	Normal
24 hours	Control	N/A*	Not Applicable
	IFN- γ	0.0696	Normal
	MOI 10	0.2740	Normal
	MOI 50	0.9236	Normal
	MOI 100	0.3182	Normal
	MOI 200	0.9217	Normal
48 hours	Control	N/A*	Not Applicable

	IFN-γ	0.2795	Normal
	MOI 10	0.1585	Normal
	MOI 50	0.4181	Normal
	MOI 100	0.2835	Normal
	MOI 200	0.3002	Normal

* The control group was normalized (Mean = 1, SD = 0), making it ineligible for Shapiro-Wilk normality testing due to the absence of variability. Thus, P-values for the control group were not calculated.

Table S24. Homogeneity of Variance and Statistical Analysis Results for PD-L1 mRNA Expression in Response to Heat-Killed *F. nucleatum* ATCC 25586 Infection in SCC-25.

Time point	Homogeneity of Variance Test F-value	Homogeneity of Variance Test P-value	Test Type	F / H-value	P-value	Effect Size (η^2)
4 hours	1.488	0.2646	ANOVA	6.205	0.0046	0.7211
8 hours	0.5215	0.7532	ANOVA	0.5316	0.7487	0.1813
24 hours	0.6260	0.6835	ANOVA	1.226	0.3554	0.3381
48 hours	0.6781	0.6484	ANOVA	0.5172	0.7588	0.1773

Table S25. Normality and Homogeneity of Variance Test Results for PD-L1 mRNA Expression in Response to Heat-Killed *F. nucleatum* ATCC 49256 Infection in CL-11.

Time Point	Group	Shapiro-Wilk P-value	Normality Conclusion
4 hours	Control	N/A*	Not Applicable
	IFN-γ	0.0360	Non-normal

	MOI 10	0.7580	Normal
	MOI 50	0.2073	Normal
	MOI 100	0.5979	Normal
	MOI 200	0.1507	Normal
8 hours	Control	N/A*	Not Applicable
	IFN- γ	0.0498	Non-normal
	MOI 10	0.6738	Normal
	MOI 50	0.9483	Normal
	MOI 100	0.5720	Nrmal
	MOI 200	0.7712	Normal
24 hours	Control	N/A*	Not Applicable
	IFN- γ	0.2610	Normal
	MOI 10	0.6860	Normal
	MOI 50	0.2499	Normal
	MOI 100	0.4107	Normal
	MOI 200	0.7842	Non-normal
48 hours	Control	N/A*	Not Applicable
	IFN- γ	0.8419	Normal
	MOI 10	0.0994	Normal
	MOI 50	0.4708	Normal
	MOI 100	0.6103	Normal
	MOI 200	0.1893	Normal

* The control group was normalized (Mean = 1, SD = 0), making it ineligible for Shapiro-Wilk normality testing due to the absence of variability. Thus, P-values for the control group were not calculated.

Table S26. Homogeneity of Variance and Statistical Analysis Results for PD-L1 mRNA Expression in Response to Heat-Killed *F. nucleatum* ATCC 49256 Infection in CL-11.

Time point	Homogeneity of Variance Test F-value	Homogeneity of Variance Test P-value	Test Type	F / H-value	P-value	Effect Size (η^2)
4 hours	N/A	N/A	Kruskal-Wallis Test	2.601	0.7612	0.153
8 hours	N/A	N/A	Kruskal-Wallis Test	1.309	0.9340	0.077
24 hours	1.136	0.3933	ANOVA	0.8913	0.5167	0.2866
48 hours	1.196	0.3677	ANOVA	0.8923	0.5161	0.2709

Table S27. Normality and Homogeneity of Variance Test Results for PD-L1 mRNA Expression in Response to Heat-Killed *F. nucleatum* ATCC 10953 Infection in CL-11.

Time Point	Group	Shapiro-Wilk P-value	Normality Conclusion
4 hours	Control	N/A*	Not Applicable
	IFN-γ	0.4379	Normal
	MOI 10	0.0757	Normal
	MOI 50	0.7454	Normal

	MOI 100	0.6516	Normal
	MOI 200	0.1888	Normal
8 hours	Control	N/A*	Not Applicable
	IFN- γ	0.7693	Normal
	MOI 10	0.3000	Normal
	MOI 50	0.3919	Normal
	MOI 100	0.9859	Normal
	MOI 200	0.0504	Normal
24 hours	Control	N/A*	Not Applicable
	IFN- γ	0.2610	Normal
	MOI 10	0.1046	Normal
	MOI 50	0.1346	Normal
	MOI 100	0.1508	Normal
	MOI 200	0.0293	Non-normal
48 hours	Control	N/A*	Not Applicable
	IFN- γ	0.3042	Normal
	MOI 10	0.0285	Non-normal
	MOI 50	0.3926	Normal
	MOI 100	0.0693	Normal
	MOI 200	0.0390	Non-normal

* The control group was normalized (Mean = 1, SD = 0), making it ineligible for Shapiro-Wilk normality testing due to the absence of variability. Thus, P-values for the control group were not calculated.

Table S28. Homogeneity of Variance and Statistical Analysis Results for PD-L1 mRNA Expression in Response to Heat-Killed *F. nucleatum* ATCC 10953 Infection in CL-11.

Time point	Homogeneity of Variance Test F-value	Homogeneity of Variance Test P-value	Test Type	F / H-value	P-value	Effect Size (η^2)
4 hours	0.8485	0.5414	ANOVA	0.6677	0.6553	0.2176
8 hours	2.338	0.1059	ANOVA	1.949	0.1594	0.4483
24 hours	N/A	N/A	Kruskal-Wallis Test	6.407	0.2686	0.3769
48 hours	N/A	N/A	Kruskal-Wallis Test	0.8162	0.9760	0.0480

Table S29. Normality and Homogeneity of Variance Test Results for PD-L1 mRNA Expression in Response to Heat-Killed *F. nucleatum* ATCC 25586 Infection in CL-11.

Time Point	Group	Shapiro-Wilk P-value	Normality Conclusion
4 hours	Control	N/A*	Not Applicable
	IFN- γ	0.7669	Normal
	MOI 10	0.0034	Non-normal
	MOI 50	0.0002	Non-normal
	MOI 100	0.5538	Normal
	MOI 200	0.0348	Non-normal
8 hours	Control	N/A*	Not Applicable
	IFN- γ	0.7047	Normal

	MOI 10	0.9760	Normal
	MOI 50	0.6015	Normal
	MOI 100	0.2084	Normal
	MOI 200	0.0857	Normal
24 hours	Control	N/A*	Not Applicable
	IFN- γ	0.6614	Normal
	MOI 10	0.9663	Normal
	MOI 50	0.2940	Normal
	MOI 100	0.6063	Normal
	MOI 200	0.3299	Normal
48 hours	Control	N/A*	Not Applicable
	IFN- γ	0.7666	Normal
	MOI 10	0.2431	Normal
	MOI 50	0.2812	Normal
	MOI 100	0.6877	Normal
	MOI 200	0.4018	Normal

* The control group was normalized (Mean = 1, SD = 0), making it ineligible for Shapiro-Wilk normality testing due to the absence of variability. Thus, P-values for the control group were not calculated.

Table S30. Homogeneity of Variance and Statistical Analysis Results for PD-L1 mRNA Expression in Response to Heat-Killed *F. nucleatum* ATCC 25586 Infection in CL-11.

Time point	Homogeneity of Variance Test F-value	Homogeneity of Variance Test P-value	Test Type	F / H-value	P-value	Effect Size (η²)
4 hours	N/A	N/A	Kruskal-Wallis Test	3.259	0.6601	0.1917
8 hours	2.248	0.1163	ANOVA	8.197	0.0014	0.7735
24 hours	0.8745	0.5263	ANOVA	0.6011	0.7005	0.2002
48 hours	0.6806	0.6468	ANOVA	0.4376	0.8140	0.1543

Table S31. Normality and Homogeneity of Variance Test Results for PD-L1 mRNA Expression in Response to Heat-Killed *F. nucleatum* ATCC 49256 Infection in PHGK.

Time Point	Group	Shapiro-Wilk P-value	Normality Conclusion
4 hours	Control	N/A*	Not Applicable
	IFN-γ	0.3872	Normal
	MOI 10	0.8756	Normal
	MOI 50	0.0236	Non-normal
	MOI 100	0.2329	Normal
	MOI 200	0.3170	Normal
8 hours	Control	N/A*	Not Applicable
	IFN-γ	0.2123	Normal
	MOI 10	0.2551	Normal

	MOI 50	0.5565	Normal
	MOI 100	0.0567	Normal
	MOI 200	0.3087	Normal
24 hours	Control	N/A*	Not Applicable
	IFN- γ	0.0934	Normal
	MOI 10	0.3861	Normal
	MOI 50	0.7874	Normal
	MOI 100	0.2241	Normal
	MOI 200	0.0278	Non-normal
48 hours	Control	N/A*	Not Applicable
	IFN- γ	0.2635	Normal
	MOI 10	0.5948	Normal
	MOI 50	0.8078	Normal
	MOI 100	0.8404	Normal
	MOI 200	0.8306	Normal

* The control group was normalized (Mean = 1, SD = 0), making it ineligible for Shapiro-Wilk normality testing due to the absence of variability. Thus, P-values for the control group were not calculated.

Table S32. Homogeneity of Variance and Statistical Analysis Results for PD-L1 mRNA Expression in Response to Heat-Killed *F. nucleatum* ATCC 49256 Infection in PHGK.

Time point	Homogeneity of Variance Test F-value	Homogeneity of Variance Test P-value	Test Type	F / H-value	P-value	Effect Size (η^2)
4 hours	N/A	N/A	Kruskal-Wallis Test	6.125	0.2943	0.3603
8 hours	0.8947	0.5148	ANOVA	0.6549	0.6639	0.2144
24 hours	N/A	N/A	Kruskal-Wallis Test	3.306	0.6529	0.1945
48 hours	1.161	0.3826	ANOVA	0.8500	0.5406	0.2615

Table S33. Normality and Homogeneity of Variance Test Results for PD-L1 mRNA Expression in Response to Heat-Killed *F. nucleatum* ATCC 10953 Infection in PHGK.

Time Point	Group	Shapiro-Wilk P-value	Normality Conclusion
4 hours	Control	N/A*	Not Applicable
	IFN- γ	0.3872	Normal
	MOI 10	0.0910	Normal
	MOI 50	0.2683	Normal
	MOI 100	0.1031	Normal
	MOI 200	0.7299	Normal
8 hours	Control	N/A*	Not Applicable

	IFN- γ	0.2123	Normal
	MOI 10	0.5018	Normal
	MOI 50	0.2223	Normal
	MOI 100	0.0628	Normal
	MOI 200	0.5772	Normal
24 hours	Control	N/A*	Not Applicable
	IFN- γ	0.0934	Normal
	MOI 10	0.1274	Normal
	MOI 50	0.5759	Normal
	MOI 100	0.0043	Non-normal
	MOI 200	0.6112	Normal
48 hours	Control	N/A*	Not Applicable
	IFN- γ	0.2635	Normal
	MOI 10	0.4002	Normal
	MOI 50	0.4811	Normal
	MOI 100	0.5059	Normal
	MOI 200	0.1696	Normal

* The control group was normalized (Mean = 1, SD = 0), making it ineligible for Shapiro-Wilk normality testing due to the absence of variability. Thus, P-values for the control group were not calculated.

Table S34. Homogeneity of Variance and Statistical Analysis Results for PD-L1 mRNA Expression in Response to Heat-Killed *F. nucleatum* ATCC 10953 Infection in PHGK.

Time point	Homogeneity of Variance Test F-value	Homogeneity of Variance Test P-value	Test Type	F / H-value	P-value	Effect Size (η^2)
4 hours	0.8985	0.5127	ANOVA	0.7342	0.6117	0.2344
8 hours	1.005	0.4554	ANOVA	0.8039	0.5682	0.2508
24 hours	N/A	N/A	Kruskal-Wallis Test	8.450	0.1331	0.4971
48 hours	0.7962	0.5729	ANOVA	0.8230	0.4990	0.2777

Table S35. Normality and Homogeneity of Variance Test Results for PD-L1 mRNA Expression in Response to Heat-Killed *F. nucleatum* ATCC 25586 Infection in PHGK.

Time Point	Group	Shapiro-Wilk P-value	Normality Conclusion
4 hours	Control	N/A*	Not Applicable
	IFN- γ	0.4934	Normal
	MOI 10	0.6284	Normal
	MOI 50	0.8498	Normal
	MOI 100	0.9176	Normal
	MOI 200	0.5909	Normal
8 hours	Control	N/A*	Not Applicable
	IFN- γ	0.0250	Non-normal
	MOI 10	0.107	Normal

	MOI 50	0.0758	Normal
	MOI 100	0.1683	Normal
	MOI 200	0.5900	Normal
24 hours	Control	N/A*	Not Applicable
	IFN- γ	0.6642	Normal
	MOI 10	0.5714	Normal
	MOI 50	0.5739	Normal
	MOI 100	0.0953	Normal
	MOI 200	0.7966	Normal
48 hours	Control	N/A*	Not Applicable
	IFN- γ	0.1013	Normal
	MOI 10	0.0989	Normal
	MOI 50	0.8843	Normal
	MOI 100	0.0492	Non-normal
	MOI 200	0.9380	Normal

* The control group was normalized (Mean = 1, SD = 0), making it ineligible for Shapiro-Wilk normality testing due to the absence of variability. Thus, P-values for the control group were not calculated.

Table S36. Homogeneity of Variance and Statistical Analysis Results for PD-L1 mRNA Expression in Response to Heat-Killed *F. nucleatum* ATCC 25586 Infection in PHGK.

Time point	Homogeneity of Variance Test F-value	Homogeneity of Variance Test P-value	Test Type	F / H-value	P-value	Effect Size (η^2)
4 hours	0.6651	0.6571	ANOVA	0.2683	0.9219	0.1005
8 hours	N/A	N/A	Kruskal-Wallis Test	1.591	0.9023	0.0936
24 hours	1.963	0.1570	ANOVA	8.276	0.0014	0.7531
48 hours	N/A	N/A	Kruskal-Wallis Test	3.165	0.6745	0.1862

Table S37. Shapiro-Wilk Test Results for Normality of SCC-25 Viability Data in Response to Heat-Killed *F. nucleatum* ATCC 49256 Across Time Points

Time Point	Group	Shapiro-Wilk P-value
4 hours	Control	0.9153
	IFN- γ	0.1436
	MOI 10	0.6369
	MOI 50	0.8776
	MOI 100	0.7017
	MOI 200	0.4072
8 hours	Control	0.3386
	IFN- γ	0.9532
	MOI 10	0.5634
	MOI 50	0.7554

	MOI 100	0.9592
	MOI 200	0.7121
24 hours	Control	0.1573
	IFN- γ	0.3748
	MOI 10	0.3976
	MOI 50	0.4678
	MOI 100	0.4271
	MOI 200	0.1939
48 hours	Control	0.5418
	IFN- γ	0.0694
	MOI 10	0.8032
	MOI 50	0.8428
	MOI 100	0.9884
	MOI 200	0.2333

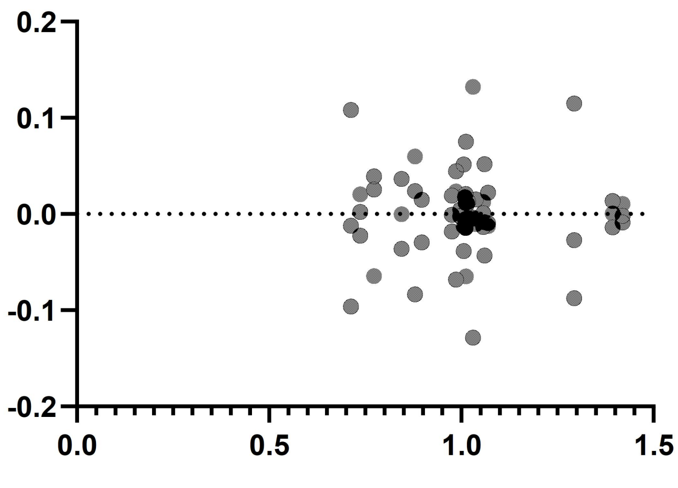

Figure S1. Residual Plots for Assessing Homogeneity of Variances in Two-Way ANOVA of SCC-25 Viability in Response to Heat-Killed *F. nucleatum* ATCC 49256

Table S38. Shapiro-Wilk Test Results for Normality of SCC-25 Viability Data in Response to Heat-Killed *F. nucleatum* ATCC 10953 Across Time Points

Time Point	Group	Shapiro-Wilk P-value
4 hours	Control	0.6435
	IFN- γ	0.3871
	MOI 10	0.0734
	MOI 50	0.2983
	MOI 100	0.6369
	MOI 200	0.2609
8 hours	Control	0.9420
	IFN- γ	0.4763
	MOI 10	0.2956
	MOI 50	0.7335
	MOI 100	0.7263
	MOI 200	0.1610
24 hours	Control	0.9312
	IFN- γ	0.2196
	MOI 10	0.6369
	MOI 50	0.2618
	MOI 100	0.2385
	MOI 200	0.2855
48 hours	Control	0.6764
	IFN- γ	0.8061

	MOI 10	0.6877
	MOI 50	0.4822
	MOI 100	0.1254
	MOI 200	0.9388

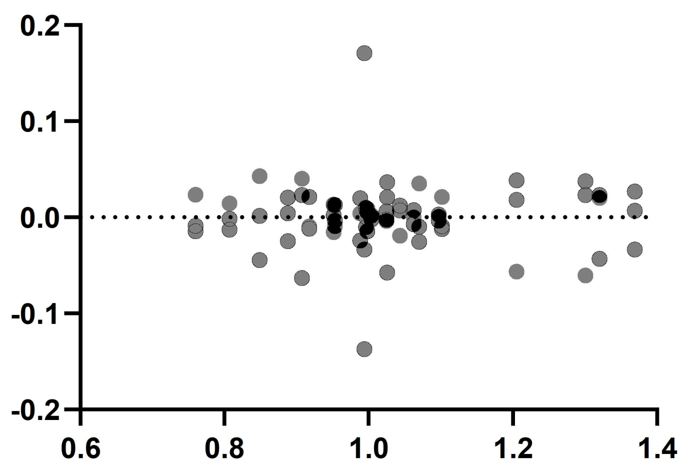

Figure S2. Residual Plots for Assessing Homogeneity of Variances in Two-Way ANOVA of SCC-25 Viability in Response to Heat-Killed *F. nucleatum* ATCC 10953

Table S39. Shapiro-Wilk Test Results for Normality of SCC-25 Viability Data in Response to Heat-Killed *F. nucleatum* ATCC 25586 Across Time Points

Time Point	Group	Shapiro-Wilk P-value
4 hours	Control	0.1223
	IFN- γ	0.6056
	MOI 10	0.0665
	MOI 50	0.7470
	MOI 100	0.7563

	MOI 200	0.7804
8 hours	Control	0.7017
	IFN- γ	0.2195
	MOI 10	0.5928
	MOI 50	0.2983
	MOI 100	0.0972
	MOI 200	1.0000
24 hours	Control	0.7941
	IFN- γ	0.1321
	MOI 10	0.0787
	MOI 50	0.6712
	MOI 100	0.7931
	MOI 200	0.6369
48 hours	Control	0.2018
	IFN- γ	0.0642
	MOI 10	0.7956
	MOI 50	0.3856
	MOI 100	0.0689
	MOI 200	0.3444

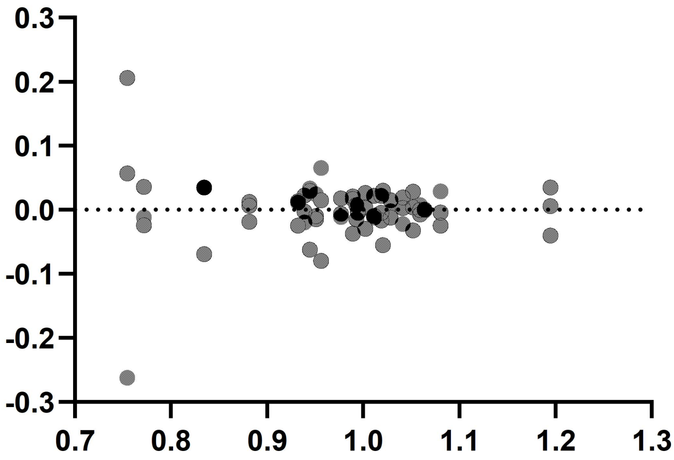

Figure S3. Residual Plots for Assessing Homogeneity of Variances in Two-Way ANOVA of SCC-25 Viability in Response to Heat-Killed *F. nucleatum* ATCC 25586

Table S40. Shapiro-Wilk Test Results for Normality of CL-11 Viability Data in Response to Heat-Killed *F. nucleatum* ATCC 49256 Across Time Points

Time Point	Group	Shapiro-Wilk P-value
4 hours	Control	0.1572
	IFN- γ	0.4633
	MOI 10	0.5827
	MOI 50	0.8999
	MOI 100	0.7019
	MOI 200	0.8428
8 hours	Control	0.6369
	IFN- γ	0.0612
	MOI 10	0.8105
	MOI 50	0.0601
	MOI 100	0.4822

	MOI 200	1.0000
24 hours	Control	0.639
	IFN- γ	0.4632
	MOI 10	0.6369
	MOI 50	0.5463
	MOI 100	0.4974
	MOI 200	0.0601
48 hours	Control	0.6788
	IFN- γ	0.0601
	MOI 10	0.4634
	MOI 50	0.1223
	MOI 100	0.5997
	MOI 200	0.1939

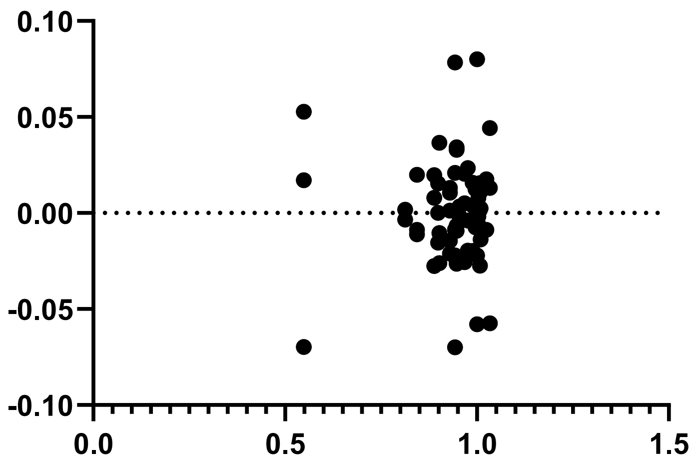

Figure S4. Residual Plots for Assessing Homogeneity of Variances in Two-Way ANOVA of CL-11 Viability in Response to Heat-Killed *F. nucleatum* ATCC 49256

Table S41. Shapiro-Wilk Test Results for Normality of CL-11 Viability Data in Response to Heat-Killed *F. nucleatum* ATCC 10953 Across Time Points

Time Point	Group	Shapiro-Wilk P-value
4 hours	Control	0.7082
	IFN- γ	0.5367
	MOI 10	0.6878
	MOI 50	0.1139
	MOI 100	0.0601
	MOI 200	0.0608
8 hours	Control	0.1436
	IFN- γ	0.8227
	MOI 10	0.1799
	MOI 50	0.4632
	MOI 100	0.1597
	MOI 200	0.2983
24 hours	Control	0.1939
	IFN- γ	0.7563
	MOI 10	0.9521
	MOI 50	0.7804
	MOI 100	0.4632
	MOI 200	0.8777
48 hours	Control	0.5666
	IFN- γ	0.1435

MOI 10	0.6678
MOI 50	0.1893
MOI 100	0.8998
MOI 200	0.8624

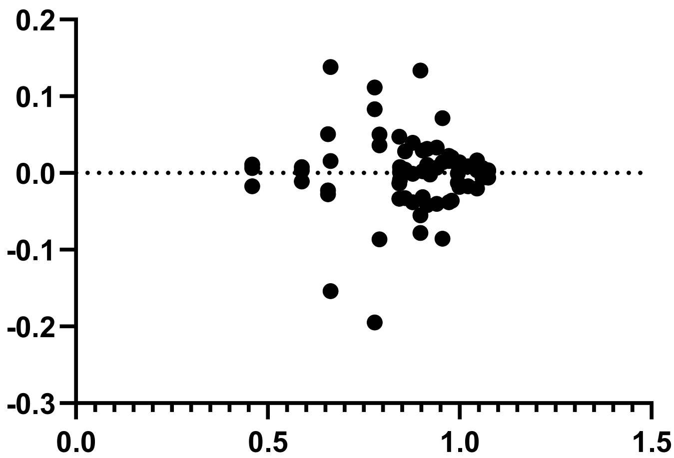

Figure S5. Residual Plots for Assessing Homogeneity of Variances in Two-Way ANOVA of CL-11 Viability in Response to Heat-Killed *F. nucleatum* ATCC 10953

Table S42. Shapiro-Wilk Test Results for Normality of CL-11 Viability Data in Response to Heat-Killed *F. nucleatum* ATCC 25586 Across Time Points

Time Point	Group	Shapiro-Wilk P-value
4 hours	Control	0.8998
	IFN- γ	0.0611
	MOI 10	0.5367
	MOI 50	0.2983
	MOI 100	0.2059
	MOI 200	0.8168

8 hours	Control	1.0000
	IFN- γ	0.1572
	MOI 10	0.2983
	MOI 50	0.0594
	MOI 100	0.7804
	MOI 200	0.0603
24 hours	Control	0.6369
	IFN- γ	1.0000
	MOI 10	0.3796
	MOI 50	0.5827
	MOI 100	0.8705
	MOI 200	0.1066
48 hours	Control	0.8998
	IFN- γ	0.1321
	MOI 10	0.7804
	MOI 50	0.1376
	MOI 100	0.3914
	MOI 200	0.4633

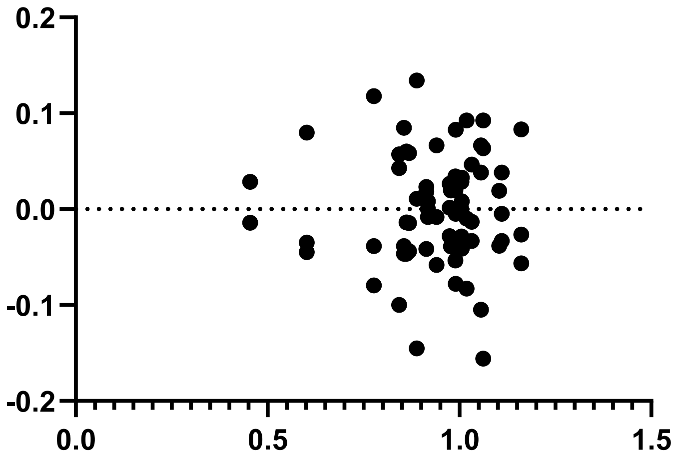

Figure S6. Residual Plots for Assessing Homogeneity of Variances in Two-Way ANOVA of CL-11 Viability in Response to Heat-Killed *F. nucleatum* ATCC 25586

Table S43. Shapiro-Wilk Test Results for Normality of PHGK Viability Data in Response to Heat-Killed *F. nucleatum* ATCC 49256 Across Time Points

Time Point	Group	Shapiro-Wilk P-value
4 hours	Control	0.7804
	IFN- γ	0.3747
	MOI 10	0.1736
	MOI 50	0.5463
	MOI 100	0.8533
	MOI 200	0.9399
8 hours	Control	0.3696
	IFN- γ	0.6627
	MOI 10	0.3444
	MOI 50	0.1939

	MOI 100	0.8241
	MOI 200	0.7421
24 hours	Control	0.8648
	IFN- γ	0.3230
	MOI 10	0.0735
	MOI 50	0.0601
	MOI 100	0.7365
	MOI 200	0.8123
48 hours	Control	0.9717
	IFN- γ	0.0806
	MOI 10	0.1321
	MOI 50	0.7563
	MOI 100	0.5808
	MOI 200	0.6659

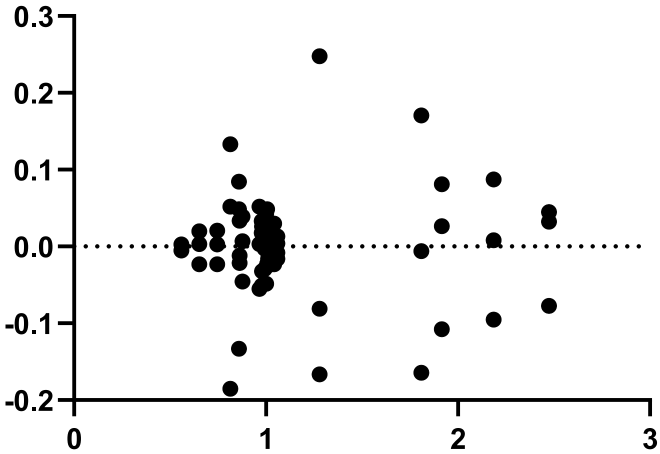

Figure S7. Residual Plots for Assessing Homogeneity of Variances in Two-Way ANOVA of PHGK Viability in Response to Heat-Killed *F. nucleatum* ATCC 49256

Table S44. Shapiro-Wilk Test Results for Normality of PHGK Viability Data in Response to Heat-Killed *F. nucleatum* ATCC 10953 Across Time Points

Time Point	Group	Shapiro-Wilk P-value
4 hours	Control	0.5588
	IFN- γ	0.9420
	MOI 10	0.3437
	MOI 50	0.3056
	MOI 100	0.1152
	MOI 200	0.1126
8 hours	Control	0.1832
	IFN- γ	0.4974
	MOI 10	0.9592
	MOI 50	0.6614
	MOI 100	0.5048

	MOI 200	0.5665
24 hours	Control	0.1066
	IFN- γ	0.0602
	MOI 10	0.7634
	MOI 50	0.4822
	MOI 100	0.1435
	MOI 200	0.0105
48 hours	Control	0.0882
	IFN- γ	0.5367
	MOI 10	0.6291
	MOI 50	0.1435
	MOI 100	0.0806
	MOI 200	0.1257

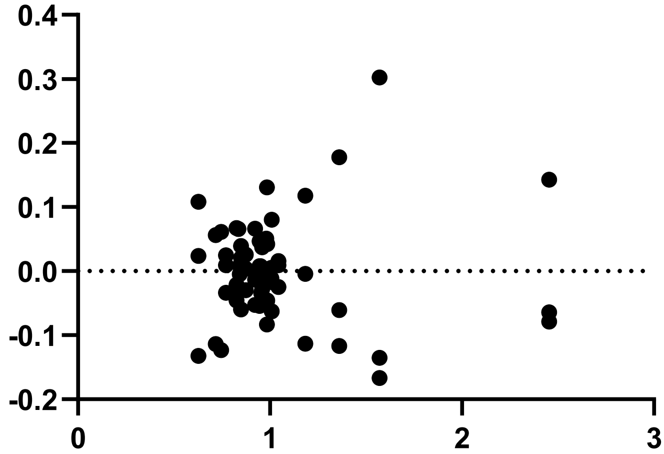

Figure S8. Residual Plots for Assessing Homogeneity of Variances in Two-Way ANOVA of PHGK Viability in Response to Heat-Killed *F. nucleatum* ATCC 10953

Table S45. Shapiro-Wilk Test Results for Normality of PHGK Viability Data in Response to Heat-Killed *F. nucleatum* ATCC 25586 Across Time Points

Time Point	Group	Shapiro-Wilk P-value
4 hours	Control	0.2006
	IFN- γ	0.7262
	MOI 10	0.8873
	MOI 50	0.5665
	MOI 100	0.8123
	MOI 200	0.8398
8 hours	Control	0.5367
	IFN- γ	0.0826
	MOI 10	0.0348
	MOI 50	0.4697
	MOI 100	0.5453
	MOI 200	0.2238
24 hours	Control	0.0704
	IFN- γ	0.3480
	MOI 10	0.7773
	MOI 50	0.3902
	MOI 100	0.0603
	MOI 200	0.4500
48 hours	Control	0.0147
	IFN- γ	0.0595

MOI 10	0.7470
MOI 50	0.7805
MOI 100	0.0751
MOI 200	0.7682

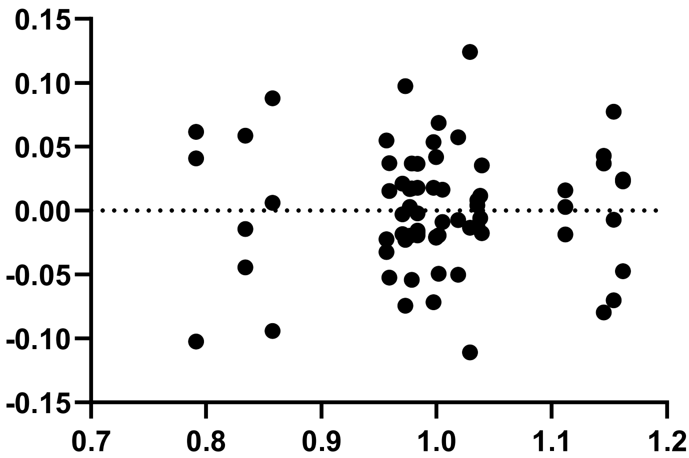

Figure S9. Residual Plots for Assessing Homogeneity of Variances in Two-Way ANOVA of PHGK Viability in Response to Heat-Killed *F. nucleatum* ATCC 25586

Contributions

Publications

Groeger S, **Zhou Y**, Ruf S, Meyle J. Pathogenic Mechanisms of Fusobacterium nucleatum on Oral Epithelial Cells. Front Oral Health. 2022 Apr 5;3:831607

Zhou Y, Meyle J, Groeger S. Periodontal pathogens and cancer development. Periodontol 2000. 2024 Oct;96(1):112-149.

Conferences

Zhou Y, Groeger S, Meyle J. Fusobacterium nucleatum induces PD-L1 Expression on Human Oral Squamous Carcinoma Cells, EuroPerio 10, 2022

Zhou Y, Groeger S, Meyle J. Fusobacterium nucleatum Inhibits Cell Proliferation and Induces PD-L1 Expression in Colon Cancer Cells, Deutsche Gesellschaft Für Parodontologie, 2022

Zhou Y, Groeger S, Meyle J. Fusobacterium nucleatum induces PD-L1 Expression in Colon Cancer Cells, International Association for Dental Research, 2022

Zhou Y, Groeger S, Meyle J. Immunosuppression by Fusobacterium nucleatum in vitro, Deutsche Gesellschaft Für Parodontologie, 2021

Zhou Y, Groeger S, Meyle J. Fusobacterium nucleatum induces PD-L1 Expression on Human Oral Squamous Carcinoma Cells, International Association for Dental Research, 2021

Declaration

I declare that I have completed this dissertation single-handedly without the unauthorized help of a second party and only with the assistance acknowledged therein. I have appropriately acknowledged and referenced all text passages that are derived literally from or are based on the content of published or unpublished work of others, and all information that relates to verbal communications. I have abided by the principles of good scientific conduct laid down in the charter of the Justus Liebig University of Giessen in carrying out the investigations described in the dissertation.

---------------------- ----------------------

Place, Date Original Signature

Ehrenwörtliche Erklärung

„Hiermit erkläre ich, dass ich die vorliegende Arbeit selbständig und ohne unzulässige Hilfe oder Benutzung anderer als der angegebenen Hilfsmittel angefertigt habe. Alle Textstellen, die wörtlich oder sinngemäß aus veröffentlichten oder nichtveröffentlichten Schriften entnommen sind, und alle Angaben, die auf mündlichen Auskünften beruhen, sind als solche kenntlich gemacht. Bei den von mir durchgeführten und in der Dissertation erwähnten Untersuchungen habe ich die Grundsätze guter wissenschaftlicher Praxis, wie sie in der „ Satzung der Justus-Liebig-Universität Gießen zur Sicherung guter wissenschaftlicher Praxis" niedergelegt sind, eingehalten sowie ethische, datenschutzrechtliche und tierschutzrechtliche Grundsätze befolgt. Ich versichere, dass Dritte von mir weder unmittelbar noch mittelbar geldwerte Leistungen für Arbeiten erhalten haben, die im Zusammenhang mit dem Inhalt der vorgelegten Dissertation stehen, und dass die vorgelegte Arbeit weder im Inland noch im Ausland in gleicher oder ähnlicher Form einer anderen Prüfungsbehörde zum Zweck einer Promotion oder eines anderen Prüfungsverfahrens vorgelegt wurde. Alles aus anderen Quellen und von anderen Personen übernommene Material, das in der Arbeit verwendet wurde oder auf das direkt Bezug genommen wird, wurde als solches kenntlich gemacht. Insbesondere wurden alle Personen genannt, die direkt und indirekt an der Entstehung der vorliegenden Arbeit beteiligt waren. Mit der Überprüfung meiner Arbeit durch eine Plagiatserkennungssoftware bzw. ein internetbasiertes Softwareprogramm erkläre ich mich einverstanden."

---------------------- ---------------------

Ort, Datum Unterschrift

Acknowledgments

I would like to express my sincere gratitude and appreciation to all those who have supported and contributed to the completion of this thesis.

First and foremost, I am deeply grateful to my supervisor, **Prof. Jörg Meyle** and **Dr. Sabine Gröger**, for your guidance, mentorship, and valuable insights throughout the entire research process. Your expertise and unwavering support have been instrumental in shaping this thesis. I have always appreciated the open door of your office and being extremely generous with you time and actionable advice. The trust, freedom, openness, and confidence you gave me were pivotal for my development as an independent scientist.

Prof. Meyle, I would like to express my sincere gratitude for your constant encouragement. Your acceptance into the program has been a pivotal moment in my academic career, and I am truly grateful for your belief in my potential. Your words of support have been a source of motivation and inspiration for me. Your guidance has played a pivotal role in shaping my academic pursuits, and I am immensely grateful for the opportunities you have provided me to expand my knowledge and skills. Your belief in my abilities has instilled confidence in me, and I am grateful for the trust you have placed in my work. I want to extend a heartfelt thank you for the meticulous attention and invaluable feedback you have provided on each of my research articles or abstracts. Your keen eye for detail and insightful suggestions have significantly improved the quality of my work. Your constructive criticism has challenged me to think critically and has guided me towards producing more rigorous and impactful research. I am immensely grateful for your dedication to refining my writing and helping me develop as a scholar. Lastly, I want to thank you for the invaluable experiences you have provided by exposing me to different parts of the world. Your leadership and guidance in arranging visits and collaborations have enabled me to gain a broader perspective and deepen my understanding of the global scientific landscape. These experiences have been transformative and have broadened my academic and cultural horizons.

Dr. Gröger, I want to extend a special thank you to you for your continuous help and clarifications. Your willingness to assist me at all times, whether it was answering my questions or offering explanations, has been incredibly beneficial. Your expertise and dedication have helped me overcome numerous challenges, and I am truly grateful for your guidance. Your patience and willingness to share your knowledge have made a significant impact on my learning experience. Your clear explanations and step-by-step guidance have not only helped me understand the intricacies of the experiments but have also improved my own technical capabilities. Your commitment to fostering a collaborative and supportive environment in the laboratory has made a significant impact on my overall learning experience. I would like to express my sincere gratitude to Dr. Gröger for invaluable assistance in meticulously reviewing and revising this thesis. Your unwavering dedication and expertise have greatly enriched the quality of my work, and I am sincerely thankful for your patience and thoroughness throughout these 5 years. Your insightful feedback and constructive criticism have undoubtedly helped me refine my ideas and sharpen my arguments. Working with you has been an enlightening and rewarding experience, and I feel fortunate to have had the opportunity to benefit from your guidance and expertise. Please accept my heartfelt appreciation for your invaluable contribution to my academic endeavors.

Furthermore, I would like to express my appreciation for the encouragement Prof. Meyle and Dr. Gröger have extended to me in participating in conferences. Your support and belief in my abilities have given me the confidence to present my work in front of esteemed professionals in the field. These opportunities have not only allowed me to showcase my research but have also broadened my horizons and expanded my network within the academic community. I am grateful for your guidance and for instilling in me the importance of sharing my findings with a wider audience.

Cynthia, thank you for the exceptional technical support you have provided me with during my time in the laboratory. Throughout my research endeavors, your knowledge and skills have been instrumental in the successful execution of various experiments. Your dedication to ensuring precision and accuracy in laboratory procedures has greatly contributed to the quality of my work. From troubleshooting complex equipment to offering insightful

suggestions, your technical support has been exceptional. Your meticulous attention to detail and commitment to maintaining a safe laboratory environment have been commendable.

Susanne, your encouragement, hospitality, and thoughtful gestures have made a significant impact on my life, and I am truly grateful for your kindness. I want to thank you for the continuous encouragement you have provided me with. Your words of support and belief in my abilities have motivated me during challenging times and have given me the confidence to pursue my goals. Your unwavering faith in me has been a source of strength, and I am deeply appreciative of your constant encouragement. I would also like to express my sincere gratitude for every invitation to your family party. The warmth and joy I experienced during that evening were truly remarkable. Your hospitality and generosity made me feel like part of your family, and I am thankful for the memories we created together.

I would like to express my heartfelt gratitude to **Prof. Chakraborty**, **Prof. Domann**, and **Ms. Hudel** for their invaluable assistance in cultivating bacteria for this research. Their unwavering support, guidance, and expertise have been instrumental in shaping the direction of this study. Without their help, my experiments would have faced significant challenges. I am truly thankful for their selfless dedication and mentorship throughout this endeavor.

I would like to extend my heartfelt thanks to the members of my **thesis committee**, for their time, expertise, and constructive feedback. Their valuable suggestions and recommendations have greatly enhanced the quality of this work.

I wanted to take a moment to express my heartfelt gratitude for the tremendous support and kindness my colleagues have extended to me. **Dr. Herrmann**, **Mr. Mahfoud**, **Stephanie**, **Kay**, **Sven**, **Lucia**, **Nathalie**, **Nina**, **Mariella**, **Petra**, your warm smiles, welcoming gestures, and genuine interest in my well-being have made me feel like a part of the team from day one. Your friendly interactions and willingness to offer assistance whenever needed have made the workplace a more enjoyable and supportive environment. I want to express my sincere appreciation for the help you have provided me with. Whether it was answering my questions,

sharing your expertise, or offering guidance on complex tasks, your support has been invaluable. Your willingness to lend a helping hand and your patience in explaining things have made my transition into the department much smoother. I am grateful for your generosity and willingness to go above and beyond to assist me. I am grateful for the opportunities to work alongside such talented and dedicated individuals like yourself.

Jiawen, **Yao**, **Lei, Xuesong**, **Wenjie**, and **Chaoyu**, I want to express my sincere appreciation for the help you have offered me in the lab. Your willingness to lend a hand, share your expertise, and brainstorm solutions to problems have been instrumental in overcoming challenges and achieving progress. Your support has not only enhanced the quality of my work but has also boosted my confidence in tackling complex experiments. I am grateful for your selflessness and dedication in assisting me. I would also like to extend my heartfelt gratitude to my friends, **Xiaoying**, **Yinfu**, **Xiao**, **Muyao**, **Junwen**, **Mengjiao** and **Wei** for their unwavering support and companionship throughout life's journey. Your presence has been a source of comfort and joy, and I am truly grateful for the moments we have shared together. Thank you for being there for me, for your kindness, and for the countless memories we have created together. Whether it was celebrating holidays, embarking on adventures, or simply being there for each other in times of need, your friendship has enriched my life in countless ways. Thank you for being the amazing friends that you are. I would like to extend my heartfelt gratitude to my friends of the **X Castle dance crew** for the joy, companionship, and support they have provided me throughout our journey together. Thank you for providing me with a platform to decompress and express myself. The dance crew has been my sanctuary, a space where I could channel my emotions, release stress, and find solace in the enchanting world of movement. Your unwavering support and understanding have created an environment where I felt free to express myself authentically and creatively.

I would also like to extend my heartfelt thanks to **China Scholarship Council** (No.201908450033) for the three years scholarship support I have received. This scholarship has not only provided me with the means to pursue my studies but has also opened doors to various academic and cultural experiences. The opportunities I have had, thanks to my country's sponsorship, have enriched my learning journey and broadened my horizons. I want to express my sincere appreciation to **Forschungsgemeinschaft Dental e.V.** (FGD)

(Nr.02/2022) for the one-year financial support you have extended to me. Your sponsorship has alleviated the financial burden of pursuing my education, allowing me to focus on my studies and research.

I would also like to thank my **parents**. From the very beginning, you have been my unwavering pillars of strength. You have showered me with unconditional love, guided me through both the smooth and challenging times, and taught me valuable life lessons that have shaped the person I am today. Our home has always been a sanctuary, filled with laughter, love, and a sense of belonging. The memories we have created together are cherished treasures that I will carry with me throughout my life. I would like to take this opportunity to express my heartfelt appreciation to my beloved husband **Zhicheng** for his unwavering support, companionship, understanding, and encouragement throughout the journey of completing my doctoral degree. His presence and unwavering belief in me have been instrumental in my success. I am also thankful for his endless patience and understanding. Balancing the demands of academics with personal life can be overwhelming, but my husband has been a constant source of support. To my dear husband, thank you for being my rock, my confidant, and my biggest supporter.

Lastly, I would like to express my appreciation to the academic and administrative staff at Justus-Liebig University Giessen for their assistance and the opportunities provided during my studies.

In conclusion, this thesis would not have been possible without the support and collaboration of all the individuals mentioned above. Their contributions have played an integral role in the successful completion of this research endeavor. Thank you all for your invaluable contributions and support.

Sincerely,

Yuxi